MODELING THE VASCULAR SYSTEM WITH MICROFLUIDIC TECHNOLOGY

Ву

Stephen T. Halpin

A DISSERTATION

Submitted to
Michigan State University
in partial fulfillment of the requirements
for the degree of

Doctor of Philosophy

Chemistry

2012

ABSTRACT

MODELING THE VASCULAR SYSTEM WITH MICROFLUIDIC TECHNOLOGY

By

Stephen T. Halpin

Here are presented several technologies advancing the state of microfluidic modeling of the vascular system through the integration of high throughput analysis equipment with microfluidic systems, allowing for the monitoring of cell-cell communication between the red blood cell (RBC) and endothelial cells. A review of the prior knowledge of the role of adenosine triphosphate (ATP) and nitric oxide (NO) release from the RBC is presented, along with the current understanding of the role these molecules play in vasodilation along with the endothelium. Here, this dissertation hypothesizes that hypoxic vasodilation of blood vessels requires ATP release from the RBC that stimulates NO synthesis in the endothelium, resulting in vasodilation.

To investigate this hypothesis, a microfluidic model capable of quantitatively determining NO and culturing endothelial cells near a flowing RBC channel is fabricated. Techniques for fabrication of microfluidic devices are reviewed, along with detection and cell culture systems integrated in microfluidic systems.

First presented is a novel system for analysis of NO released from RBCs under hypoxic conditions that uses a polydimethylsiloxane (PDMS) based microfluidic device incorporating a polycarbonate membrane. This membrane separates a flowing RBC sample from fluorogenic probe, DAF-FM, which when reacted with NO, has a larger fluorescence emission. This device was designed to be integrated into a fluorescence plate reader to obtain readout, which was a significant improvement over prior systems requiring custom

detection platforms or microscopes for readout. Using this technology, a significant increase in NO release from RBCs under hypoxic conditions was observed.

Next endothelial cell culture was incorporated onto the membrane of the device, and inhibition studies performed to investigate the origin of NO which reaches beyond an endothelial layer. In this model system, NO measured above an endothelial layer is representative of that available to the smooth muscle to induce vasodilation. Using this system, which integrated novel approaches of using the DAF-FM probe for NO in an extracellular manner and plate reader detection, it was shown that under hypoxic conditions, an increase in NO detected above the endothelium only is observed when RBC ATP release function and endothelial NO synthesis function is present, suggesting a pathway of hypoxic vasodilation requiring RBC ATP release and endothelial NO production

Also, technology was developed enabling electrochemical oxygen detection within a flowing channel on a microfluidic device using epoxy-immobilized gold and silver wires as working and reference electrodes, respectively. This presents an easily reusable and low cost platform to potentially vary then detect the oxygen concentration in a flowing cell sample prior to other analysis. This would allow the investigation of hypoxic systems at oxygen concentrations other than completely oxygenated, or completely deoxygenated.

Lastly, in efforts to explore other applications of the polycarbonate membrane based microfluidic devices, in particular their potential utility in drug screening and development. To this end, transport of several selected pharmaceutical molecules with the membrane based devices was investigated. In this process, it was discovered that some of the more hydrophilic molecules can absorb into PDMS based devices. To remove this limitation, techniques were developed which use the available fabrication equipment to produce PDMS devices to fabricate polystyrene devices. As polystyrene is frequently used in cell culture applications, this should allow for future work to more readily transfer cell culture protocols and techniques to microfluidic systems.

ACKNOWLEDGMENTS

I would first like to thank some organizations without whom this research would not be funded, and therefore impossible, including Michigan State University for research and travel funding on numerous occasions, the National Institutes of Health, and Merck. Furthermore I would like to thank the Michigan State University RTSF Mass Spectrometry Facility for their assistance in instrumentation usage when needed in this work.

Furthermore, I would like to thank the faculty of the chemistry department at MSU, whose willingness to offer assistance and the opportunity to borrow equipment was greatly appreciated. In particular I would like to thank Greg Swain whose assistance in electrochemistry early in my career was essential to some of the work in this dissertation. Furthermore, A. Daniel Jones was always helpful in discussing research ideas and in training to use the mass spectrometry facility in my research. Finally, Kathy Severin was always exceptionally willing to assist graduate students with the research through training and assistance in using instrumentation in the teaching laboratories, often at a significant time commitment on her part.

I would like to thank Dana M. Spence for his role as the advisor of this work. In particular, his commitment to training scientists through frequent presentation at conferences and desire to see the research group's work published in peer reviewed journals has enabled me to gain significant experience in essential communication skills needed as an independent investigator. Additionally, the structure in which the research group is organized is exceptionally fostering of creative work, and indeed much of the advances made within this work would not be possible without this structure or his guidance. Dana's unique treatment of his students as human beings with multiple life objectives made my

time in graduate school far more enjoyable, and therefore successful, than it would have been working for anyone else.

Additionally, due to the nature of the work in this dissertation, I would like to acknowledge the members of the Spence research group from 2007 through 2012. Much of this work required blood samples from either animals or humans, which take a significant amount of time to obtain and prepare. Also, some of the work utilized cultured cells which require attention at specific times. Without a research group to assist in these processes, this work would take much longer, and in some cases might not be possible.

I would also like to thank the people without whom the process of earning a doctoral degree would be significantly less enjoyable. Graduate school was not always smooth and predictable, and friends in particular have been essential in dealing with the hard times. Also, I would like to thank my family, in particular my parents. Without their commitment to my education throughout my life, it is unlikely I would have been prepared academically to complete this dissertation. Their sacrifice at times enabled me to learn what I needed to be prepared for this work.

Finally, I would like to thank my wife Rachel for her dedication to this work. Several years of a long-distance engagement followed by several years of putting her life on hold for me to finish this work represents a commitment more significant than mine to this dissertation. It is a difficult balancing act maintaining a relationship and a life while pursuing a graduate degree and Rachel's patience and tolerance in this regard has been much appreciated. Hopefully someday the benefits of this commitment can be realized by Rachel and I.

TABLE OF CONTENTS

LIST OF FIGURES		X
LIST OF TA	BLES	xi
CHAPTER	1: INTRODUCTION	1
1.1	The Vascular System, Red Cell and Vasodilation	1
	1.1.1 Red Blood Cell ATP	3
	1.1.2 Red Blood Cell NO	5
	1.1.3 Endothelial Cells	6
1.2	Current Hypothesis on Hypoxic Vasodilation	7
	1.2.1 Measurement Techniques	9
1.3 F	abrication and Detection in Microfluidic Devices	10
	1.3.1 Microfluidic Systems for Cellular Investigation	14
	1.3.2 Microfluidic Systems for Cell-Cell Communication	15
REFERENC	EES	18
CHAPTER :	2: Membrane based Separations on Microfluidic Devices for	
	Analysis of Compounds in RBC Solution	28
2.1 P	olycarbonate Membrane Based Devices	28
2.2 Γ	Petection of Nitric Oxide	31
2.3 N	Methods	31
	2.3.1 Device Fabrication	31
	2.3.2 Master fabrication	32
	2.3.3 Pumping System	36
	2.3.4 Alignment in Plate Reader	37
	2.3.5 DAF-FM as a NO probe, Tank NO, NO Donors	
	(NONOates)	37
	2.3.6 Nitrite Determination with Griess Reaction	39
	2.3.7 Isolation and Preparation of RBCs, Hypoxic RBCs	41
2.4 R	esults	41
	2.4.1 Images of Devices and Characterizing Channel	
	Structure	41
	2.4.2 Selection of Pumping System for Chip-to-world	
	Interfaces	42
	2.4.3 Fluorescein Transport	42
	2.4.5 DAF FM as a Fluorogenic Probe for NO	46
	2.4.6 Selection of Membrane Pore Diameter, DAF FM	
	Concentration	46
	2.4.7 NO release from Hypoxic RBCs	51
2.5 D	Discussion	51

2.5.1 Engineering Changes to Polycarbonate Membrane	
Device to Enable Plate Reader Detection	51
2.5.2: Alignment in the Plate Reader	53
2.5.3: Detection of NO	54
2.5.3: Preparation of NO standards	55
2.5.4: Microfluidic Fabrication Enhancements	57
2.5.5 NO Measurements on Microfluidic Device	59
REFERENCES	63
CHAPTER 3: Membrane Based Devices for Monitoring Cell-Cell	
Communication: Elucidating a Mechanism of Hypoxic	
Vasodilation	66
3.1 Introduction	66
3.1.1 Intracellular NO Measurements Using Microfluidic	
Devices	66
3.1.2 A Proposed Role for RBC-derived ATP in Hypoxic	
Vasodilation	67
3.1.3 Need for Confluent Cells	68
3.1.4 Basis of Trans-endothelium Electrical Resistance (TEER)	
Measurements	68
3.2 Methods	69
3.2.1 Microfluidic Device Fabrication	69
3.2.2 Culture of Endothelial Cells onto Microfluidic Device	70
3.2.3 Verification of Use of 1/8" Wells	70
3.2.4 Optimization of DAF FM for Extracellular Measurement	71
3.2.5 Analysis of NO Release	71
3.2.6 Development of Software for Real-time TEER	
Measurements	71
3.2.7 Detection of RBC ATP	72
3.3 Results	73
3.3.1 Quality of Cell Culture	73
3.3.2 NO Standards in 1/4" Versus 1/8" Wells	75
3.3.3 DAF-FM Optimization with Acetocholine and ATP	75
3.3.4 Endothelial Cells Block NO Transport	78
3.3.5 ATP Release from Hypoxic RBCs	78
3.3.6 TEER Data Processing	80
3.3.7 NO Above Endothelial Layer Measurement	82
3.4 Conclusions	84
3.4.1 Cell Culture and NO detection on Microfluidic Devices	84
3.4.2: Inhibition Studies of ATP Release and eNOS-derived NO	85
3.4.3 TEER Measurements on a Microfluidic Device	86
3.4.4: NO Available to the Smooth Muscle Requires RBC ATP	
Release and eNOS Function	86

REFERENCES	
CHAPTER 4: Improved Control of Hypoxic Environments in	
Microfluidic Models	93
4.1 Introduction	93
4.1.1 Methods of Achieving Hypoxia and Applications to	
Sickle Cell Anemia	93
4.1.2 Classical Electrochemical Detection of Oxygen	94
4.2 Methods	98
4.2.1 Verification of Oxyrase Function with Commercial	
Clark Electrode	98
4.2.2 Deoxygenation with Sodium Sulfite, Argon and Oxyrase	98
4.2.3 Fabrication of Epoxy Enclosed Disk Electrodes	99
4.2.4 Flow Injection System for Oxygen Detection	101
4.2.5 Validation of Flow Injection System with Fluorescence	
Microscopy	103
4.2.6 PDMS Membrane Fabrication	104
4.2.7 Operation of Electrochemical Oxygen Detection Device	106
4.2.8 Observation of Linear Response of Microfluidic Device	100
to Oxygen	106
4.2.9 Assembly of Device to Control Oxygen in Channel	108
4.3 Results	108
4.3.1 Deoxygenation Methods with Commercial Electrode	108
4.3.2 Validation of Flow Injection System	110
4.3.3 Validation of Microfluidic Electrochemical System	110
4.3.4 Reproducibility/function of Oxygen Sensor	119
4.3.5 Linear Response of Oxygen Sensor to Commercial	117
Sensor	119
4.3.6 Device Design for Oxygen Control	120
4.4 Conclusions	120
4.4.1: Selection of a deoxygenating system	122
4.4.2: Flow Injection Systems for Microfluidic Sample	122
Introduction	122
4.4.3: Electrochemistry in the Microfluidic Device	123
4.4.4 Control of Oxygen Concentration within the Channel	125
REFERENCES	128
REI EREIVOES	120
CHAPTER 5: Conclusions/Future Directions	130
5.1 Conclusions on Nitric Oxide (NO) Detection from the Red Blood	
Cell (RBC)	130
5.2 Conclusions on ATP-NO Investigations	131
5.3 Conclusions on Electrochemical Detection of Oxygen	132

5.4 Future Directions for Microfluidic Models	134
5.4.1 Improving Reliability: Polystyrene Devices	136
5.4.1.1 Motivation	136
5.4.1.2 Methods of Polystyrene Fabrication	136
5.4.1.3 Current State/Progress	138
5.4.2 PK/PD studies	141
5.4.2.2 Methods	142
5.4.2.3 Results	145
REFERENCES	155

LIST OF TABLES

Table 2.1: Determination of Optimum Pore Size for NO Analysis: Calibration curves of DEANO (1-9 μ M) were analyzed with n=3 microfluidic devices, and the resulting parameters shown here. A pore diameter of 0.2 μ m was chosen for future work as devices fabricated with these showed best reproducibility and correlation coefficients. Errors indicated as standard deviation.
Table 2.2: Optimization of DAF-FM Concentration for Determination of RBC NO Release: To determine the optimum DAF-FM probe concentration, DEANO standards (1-9 μ M) were analyzed on n=3 microfluidic devices, and the calibration curve parameters in addition to the reproducibility of the 1 μ M and 9 μ M standard determined. 20 μ M was chosen as the optimal concentration because of the lower detection limit and sufficient reproducibility at the higher standard.
Table 5.1: Retention Time and Target Ions for MS/MS Analysis: Shown above are the target ions for analysis and the retention times on the described chromatographic system. Each compound is ionized and injected to the collision cell with an optimized ESI cone voltage and collisional energy. Internal standard calibration is performed to obtain concentrations in the wells.

LIST OF FIGURES

Figure 1.1: Cross section of a resistance vessel. The inner core of the vessel is where the blood components, such as RBCs, flow. The next layer out from the center of the resistance vessel is the endothelium, which confluently lines the inner layer of the vessel. Finally, the smooth muscle layer is on the outside, and it is this muscle that is responsible for the expansion and contraction of the vessel. For interpretation of the references to color in this and all other figures, the reader is referred to the electronic version of this dissertation.
Figure 1.2: eNOS catalyzed reaction to form NO, and inhibitors for eNOS: Shown above is the reaction catalyzed by eNOS to form nitric oxide and citrulline. Shown below are the arginine analogues which competitively inhibit the enzyme
Figure 1.3: Proposed mechanism by which RBC mediated hypoxic vasodilation occurs: Shown in (a) is the cross section of a blood vessel, through which RBCs and other blood components flow. Panel (b) summarizes the mechanism headed by Stamler et al. showing that as hemoglobin deoxygenates, it is able to release the NO bound to a cysteine residue. Panel (c) shows the mechanism proposed by Gladwin et al. in which hemoglobin acts as a nitrite reductase, reducing nitrite to NO, making it available in the bloodstream. Panel (d) shows the mechanism proposed in this dissertation in addition to others shown above in which ATP released from the RBC activates eNOS production of NO, which is then available for vasodilation
Figure 2.1: Fabrication of the Microfluidic Device for RBC NO Detection – As shown, this device consists of two layers of PDMS, the bottom containing L-shaped channels 200 µm wide by 100 µm tall. Between this layer and the "well" layer on top, are polycarbonate track-etched membranes allowing for transport of cellular components (such as NO), but not the cells themselves, where these components can interact with a fluorogenic probe, such as DAF-FM
Figure 2.2: Fabrication of a Master: Masters for microfluidic devices are fabricated using lithographic techniques developed in the microelectronics industry. Briefly, a cleaned silicon wafer is spin-coated with SU-8 photoresist, a mask is placed over the photoresist, and exposed to UV light. The photoresist exposed to light cross links, forming a rigid structure. The remaining polymer is dissolved away, resulting in a master or mold with raised features.
Figure 2.3: Reaction between DAF-FM and NO: Shown in the upper left is one of the earliest probes for NO, diaminofluorescein. In order to reduce the background fluorescence, and improve selectivity of NO over nitrite, two fluoro groups were added in addition to the methyl group in the active area of the probe. Shown below is a potential mechanism by which the fluorescent DAF-FM-NO is formed, with a peroxynitrite intermediate. While this mechanism is debated, DAF-FM fluorescence in the presence of NO is significantly reduced in the absence of oxygen, suggesting this mechanism. DAF-FM-NO fluorescence could be observed using the fluorescence microscopes, fluorometer or plate reader at wave-

lengths similar to fluorescein, with a peak excitation wavelength of 485 nm and a peak emission of 515 nm
Figure 2.4: Griess Reaction for Nitrite Determination - Under acidic conditions, the sulfanilamide reacts with nitrite, and then with N-(1-naphthalenediamine) to produce the colored diazonium, which absorbs light at a maximum of 543 nm
Figure 2.5: Cross Section of a Microfluidic Channel and Completed Device: The top image shows a cross section of a channel as described in 2.4.1. To determine approximate channel measurements, the images can be measured. Some distortion is present as a result of preparing the cross section, but there is minimal evidence of t-topping, which can be indicative of overexposure in the master fabricating process. The bottom image is a picture of an array microfluidic device prior to use, taken from the bottom, where the inlets and associated stainless steel tubes can be observed
Figure 2.6: Reliability of Different Syringe Types: Hamilton Gastight (500 µL) and BD 1 mL syringes were used to pump a 5 ppm fluorescein standard through a long, serpentine channel, and the time to displace buffer from the channel was measured. While these two syringes did not produce a statistically significant different flow rate at 95% confidence (n=9 syringes), the disposable syringes flow rate precision was less desirable44
Figure 2.7: Shown in (a) is the arrangement of fluorescein standards spatially in the devices investigated to monitor fluorescein standards. This arrangement allows for the monitoring of crosstalk in the devices, as the no analyte standards are adjacent to the highest concentration standards, showing minimal crosstalk. Panel (b) shows signals typically obtained from such a measurement
Figure 2.8: DAF-FM as a fluorogenic probe for NO: A fluorescein based probe, DAF-FM has a large background signal (shown in black), but the fluorescence increases significantly with addition of 20 μ M NO as shown here. The emission maximum occurs at 505 nm with an excitation of 485 nm
Figure 2.9 DAF-FM limitations with calcium and glucose: DAF-FM signal is significantly different dependent upon calcium concentration in the buffer (n=3 samples, 95% confidence).
Figure 2.10: NO Release from Hypoxic RBCs: In n=4 rabbits, statistically more NO was released from hypoxic RBCs than from normoxic RBCs (p < 0.01). The NO concentration is calibrated to DEANO standards.
Figure 3.1: bPAECs in Culture Flask: Shown here are endothelial cells that exhibit the cobblestone appearance and high confluency often expected with endothelial cells. Cells

were not used in microfluidic analyses unless this appearance was present. Furthermore, the absence of large vacuoles, which store excess waste products in the cell, in these cells suggest healthy cells.
Figure 3.2: Sample calibration for NO release above membrane: Standards for these experiments were mixed with DAF-FM at a final concentration of 5 μ M and incubated at 37 °C. Shown here are n=4 samples in a single microfluidic device with error bars as standard deviations. A detection limit around 200 nM, with standards placed above the membrane, was common for these assays in the plate reader
Figure 3.3: Endothelial Cells Decrease NO Transport Across Barrier: Shown here in $n=4$ devices, the presence of endothelial cells significantly reduces ($p < 0.01$) the amount of NO standard which is able to cross a polycarbonate membrane.
Figure 3.4: ATP Release and Inhibition from Hypoxic RBCs: As shown in figure 3.4, ATP release is significantly greater (n=3 human samples) under hypoxic conditions (*p < 0.03). Furthermore, this ATP release is inhibited, or significantly reduced in the presence of 100 μM or 200 μM diamide (*p < 0.03).
Figure 3.5: TEER system for determining endothelial cell confluency: (Top) is the perturbation used in the system, a square wave at 20 Hz. (Bottom) The resulting current through the electrodes was then measured, and an example output is shown in the bottom. These current versus time curves were then integrated, and the resulting charge values averaged for a set of 40 decays to produce a TEER signal, in units of charge
Figure 3.6: NO Past Endothelial Barrier is Endothelial-Derived. Calibrated to NO standards above the membrane, significantly more NO (p < 0.05) is detected in the presence of hypoxic RBCs, but not when endothelial NO is inhibited with L-NAME. Furthermore, incubation of RBCs with diamide prior to inducing hypoxia and flowing under the microfluidic device, no difference is observed, suggesting the NO which is detected requires both eNOS function and ATP release from the RBCs
Figure 4.1: A Commercial Clark Electrode: Commercially available from VWR, this electrode has a coaxial electrode system with a silver chloride outer layer with a platinum disk inside. This disk is polished before use (not the reference portion). The cap is filled with the electrolyte solution prior to sealing. The cap contains a nylon membrane which, when screwed tightly to the body, seals over the electrode. The handheld portion of the meter contains a potential source and a means for measuring the current, along with software to perform calibrations.
Figure 4.2: Fabrication of epoxy disk encapsulating disk electrodes: In fabricating the epoxy disk containing the electrodes, wires are placed into uncured epoxy, and the epoxy is cured. The resulting disk is then sanded until exposed wires are evident. Lastly, a channel

is cut into the epoxy disk using a rotary tool, and a 1/16 inch fitting secured to the opposite side with JB Weld, producing the final electrode disk
Figure 4.3: Flow injection system used for oxygen detection. Figure location: Shown above is the flow injection system used to inject samples of oxygenated or deoxygenated buffer onto the microfluidic device. Shown in the bottom is the method for changing the solution in the oxygenation/deoxygenation region from oxygenated to deoxygenated buffer. A switching valve is used between two pumps, and all connections made by quartz capillary tubing, allowing for minimal off-chip dead volumes in changing the solutions 102
Figure 4.4: Fabrication of PDMS membranes: As shown above, a master is prepared with two layers of SU-8, the top layer containing a square feature which will hold the electrolyte solution above the working electrodes. Below is shown the process of casting a PDMS membrane and subsequent sealing of the channel above the membrane
Figure 4.5: Final Device for Measuring and Controlling Oxygen Concentration: Shown in the left portion of the device is a region where a flowing sample can equilibrate oxygen concentration with a larger lower channel. The resulting change will then be measured in the right portion of the device at the Clark electrode fabricated within the epoxy. The waste would then be available for integration into other devices
Figure 4.6: Deoxygenation rates of methods used in hypoxic investigations: Three methods of deoxygenation were investigated; first addition of sodium sulfite to solution caused a rapid and sustained deoxygenation. Argon purging resulted in deoxygenation, but this was susceptible to reoxygenation. All methods resulted in deoxygenation in 800 seconds.109
Figure 4.7: Validation of Injection System with Fluorescence as a Function of Time: Shown here is fluorescence as a function of time data validating the use of a large injection loop. Such an experiment was periodically necessary to verify a lack of clogging in the flow injection system, and also to determine the time from injection to detection independent of the membrane limited mass transport in the electrochemical system
Figure 4.8: Validation of Seal Between Epoxy and PDMS: To verify no solution leaking from the channel, or along the length of the electrode into the epoxy, a picture was taken before and after flowing fluorescein over the electrodes in two hours. In the first picture, we see some autofluorescence around the working electrode that is present in the final image as well.
Figure 4.9: Cyclic Voltammetry of Potassium Ferricyanide on Microfluidic Device: Shown here is a voltammogram of 5 mM ferricyanide for the particular Ag/AgCl quasi reference electrode, indicating the potential of the quasi-reference relative to a standard redox system.

Figure 4.10: Reliability of electrode system verified with ferricyanide injections: As shown in this example, current resulting from injections of 1 mM potassium ferricyanide show peak area reproducibility of less than 5% RSD over the course of three hours (x-axis shortened here so peak detail can be seen). This shows the reliability in both the flow injection system and electrochemical systems for a reliable redox system
Figure 4.11: Cyclic Voltammetry of an Oxygenated and Deoxygenated Solution: Shown here in grey is the cyclic voltammogram of an oxygen-saturated solution at the gold working electrode, and that of a purged solution in black. Note that a diffusion limited region for oxygen appears beyond about -775 mV, suggesting its use as an amperometric potential for the investigation of oxygen concentration.
Figure 4.12: Repeated injections of oxygen rich solutions into oxygen poor buffer: Shown here is a series of injections of oxygen rich solution into a deoxygenated solution. Peak area RSD was less than 7% RSD over the course of two hours
Figure 4.13: Linear Response of Microfluidic Sensor to Oxygen: source: Shown here is the response in peak current of the microfluidic oxygen system as a function of the response of the commercially available sensor for a series of sodium sulfite solutions. Similar linearity was observed for $n = 4$ devices. (R2 = 0.97 +/- 0.02). Note that at low oxygen concentrations, linearity is lost, as the commercial sensor is not sensitive to these low concentrations
Figure 5.1: Rapid Prototyping in Polystyrene: A master is prepared with a recessed feature in SU-8 photoresist using the lithography techniques described in chapter 2. A PDMS replicate of this is made, and then modified as shown. Polystyrene is then melted into this mold, and removed. Using this technique, a polystyrene device can be fabricated from master to completion in one day
Figure 5.2: Surface Modification Eliminates Bubbles from Replicate: Shown above, is a polystyrene replicate fabricated from an unmodified PDMS mold. Shown below is a different replicate formed from a PDMS mold modified with 0.1 M (3-mercaptopropyl) trimethylsiloxane, which improves the interaction between the melted polystyrene and the PDMS mold.
Figure 5.3: Endothelial Cell Culture in Polystyrene Device: A polystyrene device containing serpentine features is fabricated as described above. The channels are treated with $100 \mu \text{g/mL}$ fibronectin for 3 hours, and then a cell solution obtained in the same manner as described in chapter 3 is pumped into the channels. The channels are re-seeded with the cell solution after 1 hour, and then media changed every hour for six hours
Figure 5.4: LC Gradient for LC-MS Analysis: This gradient was used in the chromatographic separation of the pharmaceutical compounds in the analysis investigating the com-

pound transport across the polycarbonate membrane in the microfluidic device144
Figure 5.6: Efavirenz Absorbs Completely into PDMS: Shown here, Efavirenz absorbs completely into PDMS as none is detected in the wells after an incubation time of one hour (n=4 devices, error bars area SD)
Figure 5.7: Linezolid Does Not Absorb Into PDMS. Shown here, linezolid does not absorb into PDMS. (n=4 devices, error bars area SD)
Figure 5.8: Levofloxacin Absorption into PDMS: Shown here, levofloxacin partitions minimally into PDMS. (n=4 devices, error bars area SD)
Figure 5.9: Linezolid Transport Across Membrane: As flow time increases, a greater concentration of linezolid can be detected above the membrane. (n=4 devices, error bars are standard deviation)
Figure 5.10: Raltegravir Transport Across Membrane: As flow time increases, a greater concentration of Raltegravir can be detected above the membrane. (n=4 devices, error bars are standard deviation)
Figure 5.11: Raltegravir Transport Across Membrane: As flow time increases, a greater concentration of raltegravir can be detected above the membrane. (n=4 devices, error bars are standard deviation)
Figure 5.12: Clopidogrel Transport Across Membrane: Little transport of clopidogrel is observed until higher concentrations are pumped underneath the membrane, or longer flow times are used. This suggests the PDMS becomes saturated with clopidogrel, allowing it to flow through the membrane instead of absorbing. (n=4 devices, error bars are standard deviation)

Chapter 1 - Introduction

1.1 The Vascular System, Red Cell and Vasodilation

The human vascular system consists of the circulatory network of blood vessels that distribute blood components such as red blood cells (RBCs), platelets and plasma to tissue throughout the body. The blood is pumped through this system by the heart, starting with the largest oxygenated vessels, arteries, and then decreasing in diameter through arterioles, and ultimately capillaries, where exchange of oxygen, carbon dioxide, and other nutrients provided by the bloodstream occurs. The arterioles and capillaries are classified as resistance vessels, typically between 20 and 250 µm in diameter, provide resistance to flow. In these resistance vessels, blood hematocrit, or the volume percentage of the blood occupied by RBCs, can be reduced to less than 10%. After exchanging oxygen and other nutrients, the vessel diameter then become progressively larger as the deoxygenated blood is circulated through veins back up to the heart, where the cycle begins again.

Resistance vessels make up the majority of the surface area of the circulatory system, as they are often found within 100 µm of tissue, to allow for rapid diffusion of nutrients to that tissue.² These blood vessels are characterized as an open tube, through which the blood components flow. As shown in figure 1.1, the inside of this vessel is lined with endothelial cells, which act as a semi-permeable barrier between the blood and tissue. Beyond the endothelial layer is the smooth muscle, which by expansion and contraction controls the blood vessel diameter, and ultimately blood pressure as a whole.

It was discovered in the late 1980's that nitric oxide (NO) plays a role in inducing vasodilation, or the expansion of these blood vessels³ in work that would ultimately result in the Nobel Prize in Medicine in 1998. NO participates in vasodilation by inducing intracellular increases in cyclic guanine monophosphate (cGMP)^{4, 5} in the smooth muscle, which as a regulator of ion channel conductance, results in smooth muscle relaxation.⁶

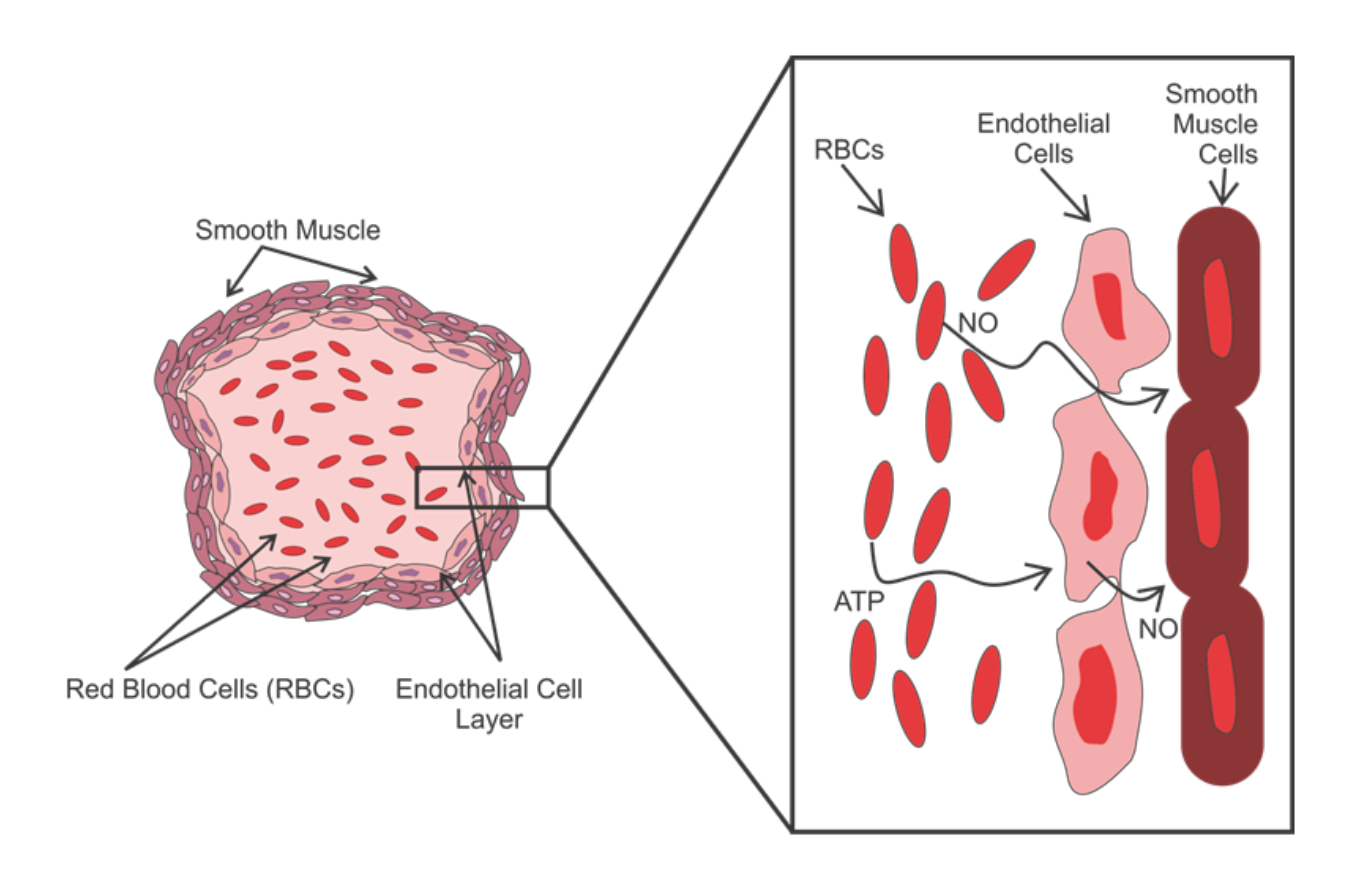


Figure 1.1: Cross section of a resistance vessel. The inner core of the vessel is where the blood components, such as RBCs, flow. The next layer out from the center of the resistance vessel is the endothelium, which confluently lines the inner layer of the vessel. Finally, the smooth muscle layer is on the outside, and it is this muscle that is responsible for the expansion and contraction of the vessel. For interpretation of the references to color in this and all other figures, the reader is referred to the electronic version of this dissertation.

There is considerable debate in the literature, described below, concerning the source of this NO.

The RBC itself is the significant carrier of oxygen in the bloodstream through its binding to hemoglobin, some of which is membrane bound.^{7, 8} Hemoglobin, a protein with four subunits, changes conformation upon binding or releasing oxygen. These confirmations are referred to as the relaxed or tense states, respectively.^{9, 10} Hemoglobin makes up the majority of the mass of the RBC after water, can also bind NO as a S-nitrosothiol at a cysteine residue. This NO is readily released when hemoglobin is in the tense, or deoxygenated, state.¹¹ While the RBC contains no internal nucleus or mitochondria, and is therefore unable to undergo oxidative glycolysis, the RBC does contain millimolar concentrations of adenosine triphosphate (ATP) inside the cell membrane,¹² that can be actively released as discussed below.

1.1.1 Red Blood Cell ATP

RBCs release ATP in response to a number of stimuli, including shear stress, ¹³ hypoxia, (the absence of oxygen)^{14, 15} pharmaceutical agents such as pentoxyfilline or iloprost, ¹⁶ hydroxyurea, ¹⁷ or small peptides such as metal-activated C-peptide. ¹⁸ The pathway for the release of this ATP from RBCs is known to be an active process and not due to cellular lysis, as shown by Sprague. ^{19, 20} Furthermore, this release mechanism can be pharmacologically inhibited using diamide, ²¹ or glibenclamide, ¹⁹ further validating it is an active process. As shown in figure 1.2, ATP is proposed to be an important controller of vascular tone, by activating the P2Y purinergic receptor ²² on the endothelial cells which

$$H_2N$$
 H_2N
 H_2N

Inhibitors:

1-arginine

Figure 1.2: eNOS catalyzed reaction to form NO, and inhibitors for eNOS: Shown above is the reaction catalyzed by eNOS to form nitric oxide and citrulline. Shown below are the arginine analogues which competitively inhibit the enzyme.

results in a calcium influx into the cell, activating endothelial nitric oxide synthase, and subsequent production of NO.^{23, 24}

1.1.2 Red Blood Cell NO

It is also known that RBCs release NO a short-lived free radical molecule, ²⁵ in response to hypoxia. ²⁶ In vivo, the source of the NO is debatable; one hypothesis by Stamler states that NO is carried as a s-nitrosothiol on a cysteine residue on hemoglobin, ²⁷⁻²⁹ and under hypoxic conditions, as oxygen is released from the heme, the hemoglobin molecule changes conformation, which induces the release of the NO. By storing the NO as a s-nitrosothiol, it is protected from species in the bloodstream such as oxygen, glutathione, or albumin that may react with it.

Gladwin has proposed an alternative mechanism that is based upon activity of deoxygenated hemoglobin as a nitrite reductase, reducing nitrite to NO. First observed in the
1980's, 30 this hypothesis proposed that nitrite is the molecule through which NO is stored
in the plasma, and then is reduced to NO under hypoxic conditions. This is supported
since plasma contains 500-1000 nM nitrite, 31 and a gradient of nitrite concentrations was
observed between venous and arterial blood, as perhaps nitrite is reacting with hemoglobin
in the absence of oxygen. 32 One of the strongest pieces of evidence supporting this hypothesis, however, is that when nitrite is added to the bloodstream *in vivo*, an increase in blood
flow is observed. 33

One thing that is clear from both of these hypothesis is that NO is released by RBCs under hypoxic conditions, but in order to participate in vasodilation, it must diffuse through

the oxidizing environment of the blood and plasma, through an endothelial layer, and to the smooth muscle where it can participate in vasodilation.

1.1.3 Endothelial Cells

As shown in figure 1.1, the endothelium lines the inside of a blood vessel, between the flowing blood components and the smooth muscle surrounding the vessel. The cells form a confluent layer, which in the brain, as the blood brain barrier; can be as resistive as $150\text{-}200~\Omega/\text{cm-}2$ as measured by trans-endothelium electrical resistance measurements. ^{34, 35} Importantly for this work, as shown in figure 1.2, these cells contain the NO producing enzyme endothelial nitric oxide synthase (eNOS), which converts L-arginine to L- citrulline, requiring NADPH, oxygen and calcium as cofactors, producing NO, which then is available to diffuse to the smooth muscle. The role of the enzyme in vasodilation is supported *in vivo* by examples where the absence of eNOS under stroke conditions increases the risk of reperfusion injury. ³⁶ Furthermore, like RBCs, it has been shown that in culture, endothelial cells up-regulate endothelial nitric oxide synthase under shear stress. ³⁷

The eNOS function is important to the hypothesis of the role of the RBC in controlling vascular tone. In the hypothesis proposed below, ATP binds to the P2Y receptor on the endothelium, stimulating a calcium influx into the cell.²³ Calcium, a required cofactor for eNOS, then increases the NO synthesis in the endothelium.³⁸ The role of calcium is well-established as other agonists that induce calcium flux into the endothelium, such as bradykinin²³ or acetylcholine⁵ and are known to stimulate NO production.

Furthermore, when administered *in vivo*, eNOS inhibitors reduce blood flow increases during exercise.³⁹ These NOS inhibitors are important tools that facilitate the determination of the source of NO detected. Most of the eNOS inhibitors are analogues of L-arginine and are therefore competitive inhibitors for eNOS. There are three commonly used inhibitors of the NOS family of enzymes, with varying degrees of sensitivity to vari-

ous NOS isoforms, but are broadly active at high concentrations. These inhibitors include L-NG-nitroarginine methyl ester (L-NAME), N-iminoethyl-L-ornithine (L-NIO), and NG-monomethyl-L-arginine (L-NMMA)⁴⁰ as shown in figure 1.2.

1.2 Current Hypothesis on Hypoxic Vasodilation

There are currently two hypothesis of RBC mediated vasodilation under hypoxia: one states that NO released from the RBC, diffuses across the endothelial barrier to the smooth muscle, where vasodilation is induced. The other is that the RBC releases ATP, which activates eNOS in the endothelium, producing NO, which is then able to diffuse to the smooth muscle. Both mechanisms are plausible and are supported by a wide body of literature, stating that ATP and NO are released from RBCs upon exposure to hypoxic conditions. However, in this dissertation, evidence is shown that the ATP dependent mechanism is more plausible, as it does not require the short-lived free radical molecule NO to diffuse through the bloodstream, across a cell layer, and to the smooth muscle where it can stimulate vasodilation. Instead, the more stable ATP molecule can diffuse through the bloodstream, and stimulating endothelial production of NO, which can then participate in vasodilation.

The two mechanisms by which NO is thought to be released as discussed above and, both are summarized in figure 1.3. It is known that NO is released from hypoxic RBCs, however the exact mechanism is not known, even though mechanisms have been proposed. 41, 42 Most interestingly, in support of these mechanisms, nitrite has been infused into human forearms, and a reduction in blood pressure was observed. However, other researchers have shown that nitrite (and other vasodilators such as nitroglycerin) can induce release of ATP from RBCs, 43, 44 which could possibly explain these effects.

Considering these findings, microfluidic technologies were employed herein to fabricated a blood vessel mimic as an effective model to elucidate these mechanisms. The

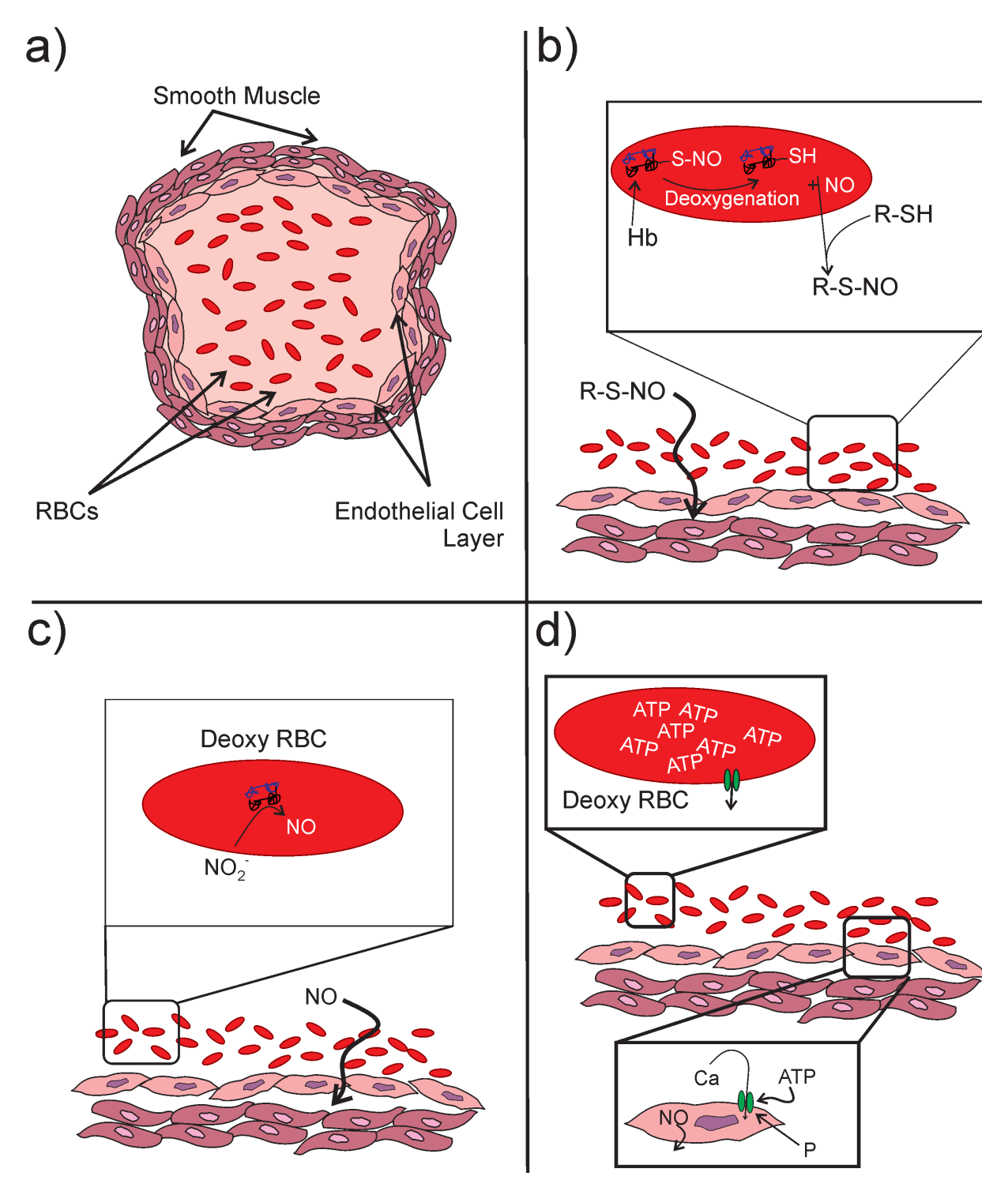


Figure 1.3: Proposed mechanism by which RBC mediated hypoxic vasodilation occurs: Shown in (a) is the cross section of a blood vessel, through which RBCs and other blood components flow. Panel (b) summarizes the mechanism headed by Stamler et al. showing that as hemoglobin deoxygenates, it is able to release the NO bound to a cysteine residue. Panel (c) shows the mechanism proposed by Gladwin et al. in which hemoglobin acts as a nitrite reductase, reducing nitrite to NO, making it available in the bloodstream. Panel (d) shows the mechanism proposed in this dissertation in addition to others shown above in which ATP released from the RBC activates eNOS production of NO, which is then available for vasodilation.

ideal microfluidic system would be able to model the important fluid dynamics including shear stress and flow present *in vivo*, and more importantly, allow for NO release in a physiologically relevant distance from the endothelium, which considering the short half life of NO, will be essential to modeling its *in vivo* effects.

1.2.1 Measurement Techniques

Measurement of cell excretion and cell-cell interactions can be performed using a variety of techniques including fluorescence staining, electrochemical techniques, chemiluminescence, or mass spectrometry. Furthermore, various investigative models can be utilized, from *in vivo* human investigation, through animal models and primary cell investigations to perpetual cell line investigations *in vitro*, each offering value at different stages of an investigation.

The selection of an investigative model often limits the analytical techniques available to interrogate the system, a need that is to be balanced with the accuracy of the model. For example, if a human model is selected, the analytical techniques used must typically be non-invasive, generally requiring imaging techniques such as magnetic resonance imaging (MRI) to investigate things like pulmonary blood flow, ⁴⁵ neurotransmitter function, ⁴⁶⁻⁴⁸ or cancer detection. ^{49, 50}

By moving to animal models however, more invasive tools can be used to monitor *in vivo* systems. For example, rather than using the noninvasive techniques such as MRI as shown above, microdialysis sampling^{51, 52} or implanted electrodes⁵³ can be used to measure neurotransmitter function^{54, 55} or blood vessel permeability.⁵⁶ Furthermore, blood vessel extraction and investigation, such as in the aortic ring assay^{57, 58} for vessel dilation, or insertion of pressure transducers into vessels, is possible with animal models.

Cell culture systems, or systems which extract primary cells from an organism, like RBCs, may be used in order to achieve finer control over a system, and reduce vari-

ability from animal to animal, in addition to reducing the cost per analysis. These are particularly useful when screening drug libraries⁵⁹ and are amenable to automation.⁶⁰ In these systems, virtually any analytical technique can be used from electrochemistry⁶¹⁻⁶³ to chemiluminescence^{13, 64} to fluorescence staining⁶⁵⁻⁶⁷ and antibody capture techniques such as ELISA.^{68, 69}

One limitation to the above described techniques is that they do not allow for several key components required to investigate interactions between blood components and the endothelium. Firstly, they do not allow for flow adjacent to a cultured layer of endothelial cells. While attempts have been made to culture endothelial cells in capillary tubes, 70 culture is easier to perform on a flat surface. 71 This flow component is necessary because it is known the RBCs release more ATP under flowing conditions. 21, 72, 73 Also, since we are interested in investigating the role of NO release from RBCs, it is important to have a system which mimics the dimensions which exist *in vivo* as NO is a short lived free radical molecule. 25, 74 For example, in a well plate, endothelial cells may be cultured on the bottom of a well. If 150 µL of RBCs were then placed in this plate, some of the RBCs would be several millimeters from the endothelial cells. Given the short half life of NO (reported to be less than 5 seconds), this NO may not diffuse to the endothelium. In the microfluidic system described here, channel heights are 100 microns, which allow the NO sufficient time to diffuse to the endothelial barrier.

1.3 Fabrication and Detection in Microfluidic Devices

Early development of microfluidic systems for chemical analysis began using technology from the microelectronics industry, and therefore started using materials familiar to that industry, such as silicon.⁷⁵ One of the earliest publications in the area was a microfluidic gas chromatograph,⁷⁶ developed in 1979. While the device was contained on a single 4" diameter wafer, its performance was comparable in terms of performance to

standard instrumentation, however because of the larger mass of the silicon wafer relative to capillary columns, took longer to heat and cool. Furthermore, while the small size may help multiplexing by having many of these devices in a single oven, they were still plagued by the problem of a chip-to-world interface. More specifically, there was no effective way to inject microliter volumes from an autosampler onto a series of these devices, which was superior to using columns in parallel in a traditional GC oven. Nonetheless, this first application sparked significant interest in using microelectronic technologies as fluidic handling tools in analytical chemistry.

Future work in silicon often took advantage of the electrical properties of the material, as conductivity sensors and accompanying electronics can be fabricated alongside fluidic features. An early example in 1985 integrated a coulometric sensor for on-device titrations, 77 and with the addition of pumping systems onto silicon in 1988, 78 the reality of lab-on-a-chip, where a total analysis could be integrated onto a microfluidic device was approaching reality, with the first issue of the Royal Society of Chemistry's journal, *Lab on A Chip*, appearing in 2001. 79 This lab-on-a-chip concept helped develop technologies 80 that contributed substantially to the sequencing of the human genome. 81-83

Many of these technologies and techniques were implemented in either silicon or glass, largely due to the durability of these materials. While some work investigating biochemical systems was performed using these materials,⁸⁴ the use of microfluidic systems for biochemical analysis on cellular systems largely required polymeric materials to which less non-specific binding would occur, and materials enabling easier fabrication. In the late 1990's the Whitesides group largely started this with the development of soft lithography,⁸⁵,

⁸⁶ where silicon masters were patterned with raised features fabricated from photoresists, that could be used as a mold for polydimethylsiloxane (PDMS) devices.

While PDMS has many disadvantages as a material for fabricating microfluidics, ⁸⁷ such as hydrophobicity, ⁸⁸ the tendency to absorb compounds as shown in chapter 5, and flexibility, it has several advantages for use in biochemical analysis. It is optically transparent to visible light, readily enabling cell visualization and optical analysis, ⁸⁹, ⁹⁰ and it is gas permeable, which allows for carbon dioxide and oxygen exchange in cell culture. ⁹¹⁻⁹³ Considering some of the disadvantages of PDMS, other materials are frequently used in fabricating microfluidic devices, often with more complicated fabrication techniques. ⁹⁴ For example, polystyrene has been used, ⁹⁵ offering the advantage of being the same material as traditional culture flasks, allowing easy adaptation of existing cell culture techniques to microfluidic technology. Other polymeric materials which have been employed for microfluidic fabrication include polymethyl methacrylate (PMMA), ⁹⁶ polycarbonate, ⁹⁷, ⁹⁸ and even epoxy materials. ⁹⁹

In addition to material selection, detection is a formidable challenge in microfluidic systems due to the small volume of sample involved, and therefore small number of molecules available for detection. While advances have been made recently, ¹⁰⁰ absorbance techniques are typically not successful due to the short pathlengths associated with microfluidic channels. Fluorescence techniques are popular, due to low detection limits. Laser induced fluorescence is exceptionally popular, being used to detect genetic material and amino acids, ¹⁰¹, ¹⁰² labeled proteins, ¹⁰³, ¹⁰⁴ cells, ¹⁰⁵, ¹⁰⁶ and cellular components. ⁶⁵, ¹⁰⁷, ¹⁰⁸ Many of these systems utilizing fluorescence detection also implement electrophoretic separations to improve selectivity, as these separations are rapid and can operate under lower pressures in comparison to traditional chromatography. Fluorescence staining of live cells ¹⁰⁹⁻¹¹¹ and the use of fluorogenic probes ¹¹⁰ are also popular detection schemes,

achieving readout with optical microscopes for similar reasons; acceptable detection limits in small volumes.

Electrochemical techniques are also very popular, having the distinct advantage that as electrode size decreases, background current decreases linearly, offering signal-to-noise ratio enhancement. Furthermore, the low cost of most electrochemical sensors makes them popular to a wide range of researchers. A wide variety of electrode materials have been integrated into microfluidic systems^{112, 113} to detect many analytes. For example, by using bound antibody techniques, electrochemical sensors can be used as a readout mechanism for ELISA in a microfluidic system.^{112, 114, 115} Of note, carbon ink electrodes have been used for NO detection from immobilized endothelial cells,¹¹⁶ while other electrode systems have been used for detection of neurotransmitters in vesicles¹¹⁷ or glutamate release from cells.¹¹⁸ Microfluidic technologies offer a significant advantage for monitoring single cell release events as they restrict the volume around the cell, allowing for detection of a larger portion of the released components. Furthermore, they could be potentially multiplexed around microfabricated electrodes, allowing for many single cells to be investigated at once.

Finally, applications integrating microfluidic systems and mass spectrometry are becoming more popular as the lower volumes used in the microfluidic systems are inherently compatible with solvent evaporation prior to introduction of a sample into a mass spectrometer. Furthermore, microfabrication techniques can be used to reproducibly fabricate small tips for electrospray ionization. Devices that perform electrophoretic separation prior to analysis for proteomic samples have also been developed, enabling faster separation times relative to liquid chromatography. More recently, micro-

fluidic technologies have been used to perform on-chip derivatization of small molecules before analysis¹²³, and for drug metabolite investigations.^{124, 125}

1.3.1 Microfluidic Systems for Cellular Investigation

While there is a wide variety of research involving detection methods for microfluidic technologies, there are fewer works investigating biochemical mechanisms with these systems. A popular trend at the current time is the investigation of microfluidic technologies to replace flow cytometry systems for cell sorting. First begun in the late 1990's with electrophoretic techniques, 127 and ultimately moving towards laminar flow systems similar to commercially available cytometers, 128 these technologies would be essential to integrating a total analysis of a biological sample onto a device. In such an analysis, frequently one cell type, such as a red blood cell, needs to be separated from others, such as platelets. Such sorting systems can also collect and interrogate cells 128 in a smaller volume, potentially allowing for the discovery of rare cells.

While in some cases, such as cancer detection, the simple identification of a cell is sufficient to complete an analysis, the majority of analyses require detection of some property of the cell, such as a synthesized protein, an active receptor, or the quantitative determination of some released analyte from the cell. Microfluidic technologies used to interrogate physiological problems were first used in the early to mid 2000's with investigations into the impact of pathogens on blood cells, ¹²⁹ fluorescence investigations of intracellular dyes, ¹³⁰ chemiluminescence determination of extracellular ATP, ¹³¹ and nitric oxide. ²⁶ Furthermore, the technologies have been used to investigate peptide secretion, such as insulin from Islet cells. ¹³² Microfluidic systems have also been used to investigate

cellular release of electrochemically active compounds such as nitric oxide¹³³ and catecholamines. 134-137

1.3.2 Microfluidic Systems for Cell-Cell Communication

A significant advantage to microfluidic technologies that cannot be readily attained in other manners is the ability to culture and flow different cell types in close proximity to each other, so that distances between cell types can mimic those present *in vivo*. ¹³⁸ Furthermore, the flow channels allow for the mimicking of shear forces present in vivo. ¹³⁹ Early work in this area by the Spence group involved platelet and red blood cell interactions, ¹⁴⁰ monitoring platelets adhering to cultured endothelial cells, in which the platelets were pumped over the endothelium, ⁹⁰ and later work investigated the role of ATP released from flowing red blood cells inducing nitric oxide production in endothelial cells. ¹¹¹, ¹⁴¹- ¹⁴³ Other early work in the use of microfluidic systems to monitor cell-cell interaction was used in pharmacodymanic investigations, ¹⁴⁴ whereas more recent work has investigated other cell adhesion to endothelial layers, ¹⁴⁵ or so called "organ-on-a-chip¹⁴⁶" and tissue engineering technologies ¹⁴⁷ which seek to culture multiple cell types in three dimensional arrangements in similar geometries to those observed in vivo.

Considering the advantages described above, microfluidic technologies provide an excellent model for investigating the mechanisms of hypoxic vasodilation in an *in vitro* model that offers enhanced opportunities for system validation. Herein the following were employed: first, a microfluidic device was utilized to detect nitric oxide release from red blood cells in response to hypoxia.²⁶ Next, reproducibly confluent endothelial cell cultures¹⁴³ were integrated into the device, forming our vascular mimic that allows for blood flow in proximity to a cultured endothelial layer. Using this device, enabled the ability to elicit the role of red blood cell derived ATP¹⁴, red blood cell derived nitric oxide,²⁶ and ATP-stimulated endothelial nitric oxide¹⁴⁸ release in hypoxic vasodilation. This device

will allow for NO release from the RBCs to occur in close proximity to the endothelium, allowing determination of the role of this short-lived molecule. Inhibition studies of ATP release 149 and endothelium nitric oxide production, 150 further enabled us to investigate the hypothesis 151 that nitric oxide production during hypoxic vasodilation is endothelium derived, and stimulated by red blood cell ATP release.

REFERENCES

REFERENCES

- 1. Pries, A. R.; Secomb, T. W., *American Journal of Physiology-Heart and Circulatory Physiology* **2005**, *289* (6), H2657-H2664.
- 2. Oleinick, A. I.; Amatore, C.; Guille, M.; Arbault, S.; Klymenko, O. V.; Svir, I., *Mathematical Medicine and Biology-a Journal of the Ima* **2006**, *23* (1), 27-44.
- 3. Ignarro, L. J.; Buga, G. M.; Wood, K. S.; Byrns, R. E.; Chaudhuri, G., *Proc. Natl. Acad. Sci. U. S. A.* **1987**, *84* (24), 9265-9.
- 4. Duszyk, M.; Radomski, M. W., Free Radic Res 2000, 33 (5), 449-59.
- 5. Ignarro, L. J.; Byrns, R. E.; Buga, G. M.; Wood, K. S., *Circulation Research* **1987**, *61* (6), 866-79.
- 6. Sprague, R. S.; Stephenson, A. H.; Bowles, E. A.; Stumpf, M. S.; Lonigro, A. J., *Diabetes* **2006**, *55* (12), 3588-3593.
- 7. Mi, X. Q.; Chen, J. Y.; Zhou, L. W., *Journal of photochemistry and photobiology*. *B, Biology* **2006**, *83* (2), 146-50.
- 8. Friederichs, E.; Farley, R. A.; Meiselman, H. J., *Am J Hematol* **1992,** *41* (3), 170-7.
- 9. Jensen, F. B., *Acta Physiol Scand* **2004**, *182* (3), 215-27.
- 10. Perutz, M. F.; Wilkinson, A. J.; Paoli, M.; Dodson, G. G., *Annual Review of Biophysics and Biomolecular Structure* **1998,** 27, 1-34.
- 11. Stamler, J. S.; Jia, L.; Eu, J. P.; McMahon, T. J.; Demchenko, I. T.; Bonaventura, J.; Gernert, K.; Piantadosi, C. A., *Science* **1997**, *276* (5321), 2034-2037.
- 12. Beutler, E., *Experientia* **1969**, *25* (5), 470-3.
- 13. Edwards, J., Sprung, Robert, Sprague, Randy, Spence Dana M., *Analyst* **2001**, *126*, 1257-1260.
- 14. Faris, A.; Spence, D. M., *Analyst (Cambridge, U. K.)* **2008,** *133* (5), 678-682.
- 15. Bergfeld, G. R.; Forrester, T., Cardiovascular Research 1992, 26 (1), 40-7.
- 16. Carroll, J. S.; Ku, C.-J.; Karunarathne, W.; Spence, D. M., *Anal. Chem. (Washington, DC, U. S.)* **2007,** *79* (14), 5133-5138.
- 17. Raththagala, M.; Karunarathne, W.; Kryziniak, M.; McCracken, J.; Spence, D. M., *European Journal of Pharmacology* **2010**, *645* (1-3), 32-38.
- 18. Meyer, J. A.; Froelich, J. M.; Reid, G. E.; Karunarathne, W. K. A.; Spence, D. M.,

- Diabetologia 2008, 51 (1), 175-82.
- 19. Sprague, R. S.; Ellsworth, M. L.; Stephenson, A. H.; Kleinhenz, M. E.; Lonigro, A. J., *Am. J. Physiol.* **1998,** *275* (5, Pt. 2), H1726-H1732.
- 20. Sprague, R. S.; Ellsworth, M. L.; Stephenson, A. H.; Lonigro, A. J., *Am. J. Physiol.* **2001**, *281* (4, Pt. 1), C1158-C1164.
- 21. Price, A., K.; Fischer David, J.; Martin, R. S.; Spence Dana, M., *Analytical Chemistry* **2004**, *76* (16), 4849-55.
- 22. Allsup, D. J.; Boarder, M. R., *Mol. Pharm.* **1990,** *38*, 84-91.
- 23. Bogle, R. G.; Coade, S. B.; Moncada, S.; Pearson, J. D.; Mann, G. E., *Biochemical and Biophysical Research Communications* **1991**, *180* (2), 926-932.
- 24. Dull, R. O.; Tarbell, J. M.; Davies, P. F., *Journal of vascular research* **1992**, *29* (6), 410-9.
- 25. Hakim, T. S.; Sugimori, K.; Camporesi, E. M.; Anderson, G., *Physiological Measurement* **1996**, *17* (4), 267-277.
- 26. Halpin, S. T.; Spence, D. M., *Analytical Chemistry* **2010**, *82* (17), 7492-7497.
- 27. Jia, L.; Bonaventura, C.; Bonaventura, J.; Stamler, J. S., *Nature* **1996**, *380* (6571), 221-226.
- 28. Gow, A. J.; Luchsinger, B. P.; Pawloski, J. R.; Singel, D. J.; Stamler, J. S., *Proceedings of the National Academy of Sciences of the United States of America* **1999**, 96 (16), 9027-9032.
- 29. Gow, A. J.; Stamler, J. S., *Nature* **1998**, *391*, 169-173.
- 30. Doyle, M. P.; Pickering, R. A.; Deweert, T. M.; Hoekstra, J. W.; Pater, D., *Journal of Biological Chemistry* **1981**, *256* (23), 2393-2398.
- 31. Gladwin, M. T.; Shelhamer, J. H.; Schechter, A. N.; Pease-Fye, M. E.; Waclawiw, M. A.; Panza, J. A.; Ognibene, F. P.; Cannon, R. O., *Proceedings of the National Academy of Sciences of the United States of America* **2000**, *97* (21), 11482-11487.
- 32. Lauer, T.; Preik, M.; Rassaf, T.; Strauer, B. E.; Deussen, A.; Feelisch, M.; Kelm, M., *Proceedings of the National Academy of Sciences of the United States of America* **2001**, *98* (22), 12814-12819.
- 33. Cosby, K.; Partovi, K. S.; Crawford, J. H.; Patel, R. P.; Reiter, C. D.; Martyr, S.; Yang, B. K.; Waclawiw, M. A.; Zalos, G.; Xu, X. L.; Huang, K. T.; Shields, H.; Kim-Shapiro, D. B.; Schechter, A. N.; Cannon, R. O.; Gladwin, M. T., *Nature Medicine* **2003**, *9* (12), 1498-1505.
- 34. Douville, N. J.; Tung, Y.-C.; Li, R.; Wang, J. D.; El-Sayed, M. E. H.; Takayama, S.,

- Anal. Chem. (Washington, DC, U. S.) 82 (6), 2505-2511.
- 35. Stanness, K. A.; Westrum, L. E.; Fornaciari, E.; Mascagni, P.; Nelson, J. A.; Stenglein, S. G.; Myers, T.; Janigro, D., *Brain Res. FIELD Full Journal Title:Brain Research* **1997**, 771 (2), 329-342.
- 36. Jones, S. P.; Girod, W. G.; Palazzo, A. J.; Granger, D. N.; Grisham, M. B.; Jourd'heuil, D.; Huang, P. L.; Lefer, D. J., *American Journal of Physiology-Heart and Circulatory Physiology* **1999**, *276* (5), H1567-H1573.
- 37. Topper, J. N.; Cai, J. X.; Falb, D.; Gimbrone, M. A., *Proceedings of the National Academy of Sciences of the United States of America* **1996**, *93* (19), 10417-10422.
- 38. Arnal, J. F.; Dinh-Xuan, A. T.; Pueyo, M.; Darblade, B.; Rami, J., Cellular and molecular life sciences: CMLS 1999, 55 (8-9), 1078-87.
- 39. Ishibashi, Y.; Duncker, D. J.; Zhang, J. Y.; Bache, R. J., *Circulation Research* **1998**, 82 (3), 346-359.
- 40. Rees, D. D.; Palmer, R. M.; Schulz, R.; Hodson, H. F.; Moncada, S., *Br J Pharmacol* **1990**, *101* (3), 746-52.
- 41. Stamler, J. S.; Simon, D. I.; Osborne, J. A.; Mullins, M. E.; Jaraki, O.; Michel, T.; Singel, D. J.; Loscalzo, J., *Proceedings of the National Academy of Sciences of the United States of America* **1992**, *89* (1), 444-448.
- 42. Crawford, J. H.; Isbell, T. S.; Huang, Z.; Shiva, S.; Chacko, B. K.; Schechter, A. N.; Darley-Usmar, V. M.; Kerby, J. D.; Lang, J. D.; Kraus, D.; Ho, C.; Gladwin, M. T.; Patel, R. P., *Blood* **2006**, *107* (2), 566-574.
- 43. Garcia, J. I.; Seabra, A. B.; Kennedy, R.; English, A. M., *Journal of Inorganic Biochemistry* **2010**, *104* (3), 289-296.
- 44. Cao, Z. L.; Bell, J. B.; Mohanty, J. G.; Nagababu, E.; Rifkind, J. M., *American Journal of Physiology-Heart and Circulatory Physiology* **2009**, *297* (4), H1494-H1503.
- 45. Fratz, S.; Hess, J.; Schwaiger, M.; Martinoff, S.; Stern, H. C., *Circulation* **2002**, *106* (12), 1510-3.
- 46. Chen, Y. C. I.; Galpern, W. R.; Brownell, A. L.; Matthews, R. T.; Bogdanov, M.; Isacson, O.; Keltner, J. R.; Beal, M. F.; Rosen, B. R.; Jenkins, B. G., *Magnet Reson Med* **1997**, *38* (3), 389-398.
- 47. McGuire, P.; Howes, O. D.; Stone, J.; Fusar-Poli, P., *Trends Pharmacol Sci* **2008**, 29 (2), 91-98.
- 48. Lingford-Hughes, A., *Curr Opin Pharmacol* **2005**, *5* (1), 42-46.
- 49. Weissleder, R., *Science* **2006**, *312* (5777), 1168-1171.

- 50. Weissleder, R., *Nature Reviews Cancer* **2002**, *2* (1), 11-18.
- 51. Justice, J. B., *Journal of Neuroscience Methods* **1993**, 48 (3), 263-276.
- 52. Close, G. L.; Jackson, M. J., *Methods Mol. Biol. (Totowa, NJ, U. S.)* **2008,** 477 (Advanced Protocols in Oxidative Stress I), 123-136.
- 53. Garris, P. A.; Kilpatrick, M.; Bunin, M. A.; Michael, D.; Walker, Q. D.; Wightman, R. M., *Nature* **1999**, *398* (6722), 67-69.
- 54. Wightman, R. M.; Robinson, D. L., *Journal of Neurochemistry* **2002**, *82* (4), 721-735.
- 55. Venton, B. J.; Wightman, R. M., *Analytical Chemistry* **2003**, *75* (19), 414a-421a.
- 56. Hansen, D. K.; Scott, D. O.; Otis, K. W.; Lunte, S. M., *J. Pharm. Biomed. Anal.* **2002,** *27* (6), 945-958.
- 57. Nicosia, R. F.; Ottinetti, A., *Laboratory investigation; a journal of technical methods and pathology* **1990**, *63* (1), 115-22.
- 58. Kruger, E. A.; Duray, P. H.; Tsokos, M. G.; Venzon, D. J.; Libutti, S. K.; Dixon, S. C.; Rudek, M. A.; Pluda, J.; Allegra, C.; Figg, W. D., *Biochem Biophys Res Commun* **2000**, *268* (1), 183-91.
- 59. Monks, A.; Scudiero, D.; Skehan, P.; Shoemaker, R.; Paull, K.; Vistica, D.; Hose, C.; Langley, J.; Cronise, P.; Vaigrowolff, A.; Graygoodrich, M.; Campbell, H.; Mayo, J.; Boyd, M., *J Natl Cancer I* **1991**, *83* (11), 757-766.
- 60. Finlay, G. J.; Baguley, B. C.; Wilson, W. R., *Analytical Biochemistry* **1984**, *139* (2), 272-277.
- 61. Kumar, G. K.; Overholt, J. L.; Bright, G. R.; Hui, K. Y.; Lu, H.; Gratzl, M.; Prabhakar, N. R., *Am J Physiol* **1998**, *274* (6 Pt 1), C1592-600.
- 62. Sombers, L.; Ewing, A. G., Electrochemical Monitoring of Exocytosis from Individual PC12 Cells in Cultures. In *Electroanalytical Methods for Biological Materials*, Brajter-Toth, A. C.; James, Q., Eds. Marcel Dekker: New York City, 2002; p 540.
- 63. Amatore, C.; Arbault, S.; Chen, Y.; Crozatier, C.; Tapsoba, I., *Lab on a Chip* **2007**, 7 (2), 233-238.
- 64. Hendgen-Cotta, U.; Grau, M.; Rassaf, T.; Gharini, P.; Kelm, M.; Kleinbongard, P., *Methods Enzymol* **2008**, *441*, 295-315.
- 65. Mainz, E. R.; Gunasekara, D. B.; Caruso, G.; Jensen, D. T.; Hulvey, M. K.; da Silva, J. A. F.; Metto, E. C.; Culbertson, A. H.; Culbertson, C. T.; Lunte, S. M., *Anal Methods-Uk* **2012**, *4* (2), 414-420.

- 66. Hartell, N. A.; Archer, H. E.; Bailey, C. J., *Biochem. Pharmacol.* **2005**, *69* (5), 781-790.
- 67. Anderson, K. B.; Karunarathne, W.; Spence, D. M., *Anal Methods-Uk* **2012**, *4* (1), 101-105.
- 68. Medawala, W.; McCahill, P.; Giebink, A.; Meyer, J.; Ku, C. J.; Spence, D. M., *The review of diabetic studies : RDS* **2009**, *6* (3), 148-58.
- 69. Nousia-Arvanitakis, S.; Galli-Tsinopoulou, A.; Dracoulacos, D.; Karamouzis, M.; Demitriadou, A., *J Pediatr Endocrinol Metab* **2000**, *13* (3), 319-24.
- 70. Kotsis, D. H.; Spence, D. M., *Analytical Chemistry* **2003**, *75* (1), 145-151.
- 71. Spence, D., M.; Torrence Nicholas, J.; Kovarik Michelle, L.; Martin, R. S., *The Analyst* **2004**, *129* (11), 995-1000.
- 72. Sprung, R.; Sprague, R.; Spence, D., *Analytical Chemistry* **2002**, 74 (10), 2274-2278.
- 73. Sprague, R. S.; Ellsworth, M. L.; Stephenson, A. H.; Lonigro, A. J., *Exp Clin Cardiol* **1998**, *3*, 73-77.
- 74. Kelm, M.; Feelisch, M.; Deussen, A.; Schrader, J.; Strauer, B. E., *Journal of Cardiovascular Pharmacology* **1991**, *17*, S95-S99.
- 75. Petersen, K. E., *Proceedings of the IEEE* **1982**, *70* (5), 420-457.
- 76. Terry, S. C.; Jerman, J. H.; Angell, J. B., *Trans. electron Devices* **1979**, *26*, 1880-1886.
- 77. Vanderschoot, B.; Bergveld, P., Sensors and Actuators 1985, 8 (1), 11-22.
- 78. Vanlintel, H. T. G.; Vandepol, F. C. M.; Bouwstra, S., *Sensors and Actuators* **1988**, *15* (2), 153-167.
- 79. *Lab on a Chip* **2001,** *I* (1), 1N-2N.
- 80. Ye, M. L.; Hu, S.; Schoenherr, R. M.; Dovichi, N. J., *Electrophoresis* **2004**, *25* (9), 1319-1326.
- 81. Dovichi, N. J.; Zhang, J. Z., *Angewandte Chemie-International Edition* **2000**, *39* (24), 4463-+.
- 82. Kidd, J. M.; Cooper, G. M.; Donahue, W. F.; Hayden, H. S.; Sampas, N.; Graves, T.; Hansen, N.; Teague, B.; Alkan, C.; Antonacci, F.; Haugen, E.; Zerr, T.; Yamada, N. A.; Tsang, P.; Newman, T. L.; Tuzun, E.; Cheng, Z.; Ebling, H. M.; Tusneem, N.; David, R.; Gillett, W.; Phelps, K. A.; Weaver, M.; Saranga, D.; Brand, A.; Tao, W.; Gustafson, E.; McKernan, K.; Chen, L.; Malig, M.; Smith, J. D.; Korn, J. M.; McCarroll, S. A.; Altshuler, D. A.; Peiffer, D. A.; Dorschner, M.; Stamatoyannopoulos,

- J.; Schwartz, D.; Nickerson, D. A.; Mullikin, J. C.; Wilson, R. K.; Bruhn, L.; Olson, M. V.; Kaul, R.; Smith, D. R.; Eichler, E. E., *Nature* **2008**, *453* (7191), 56-64.
- 83. Easley, C. J.; Karlinsey, J. M.; Bienvenue, J. M.; Legendre, L. A.; Roper, M. G.; Feldman, S. H.; Hughes, M. A.; Hewlett, E. L.; Merkel, T. J.; Ferrance, J. P.; Landers, J. P., *Proceedings of the National Academy of Sciences of the United States of America* **2006**, *103* (51), 19272-19277.
- 84. Weigl, B. H.; Hixson, G. T.; Kenny, M.; Zebert, D.; Dwinnell, S.; Buj, T.; Yager, P., *Proceedings of SPIE-The International Society for Optical Engineering* **1997**, *2980* (Advances in Fluorescence Sensing Technology III), 171-181.
- 85. Duffy, D. C.; McDonald, J. C.; Schueller, O. J. A.; Whitesides, G. M., *Analytical Chemistry* **1998**, *70* (23), 4974-4984.
- 86. McDonald, J. C.; Duffy, D. C.; Anderson, J. R.; Chiu, D. T.; Wu, H.; Schueller, O. J.; Whitesides, G. M., *Electrophoresis* **2000**, *21* (1), 27-40.
- 87. Regehr, K. J.; Domenech, M.; Koepsel, J. T.; Carver, K. C.; Ellison-Zelski, S. J.; Murphy, W. L.; Schuler, L. A.; Alarid, E. T.; Beebe, D. J., *Lab on a Chip* **2009**, *9* (15), 2132-2139.
- 88. Hillborg, H.; Gedde, U. W., *Polymer* **1998**, *39* (10), 1991-1998.
- 89. Hu, S.; Zhang, L.; Krylov, S.; Dovichi, N. J., *Analytical Chemistry* **2003**, 75 (14), 3495-3501.
- 90. Ku, C. J.; Oblak, T. D.; Spence, D. M., *Analytical Chemistry* **2008**, *80* (19), 7543-7548.
- 91. Leclerc, E.; Sakai, Y.; Fujii, T., *Biotechnology Progress* **2004**, *20* (3), 750-755.
- 92. Mehta, G.; Mehta, K.; Sud, D.; Song, J. W.; Bersano-Begey, T.; Futai, N.; Heo, Y. S.; Mycek, M. A.; Linderman, J. J.; Takayama, S., *Biomedical Microdevices* **2007**, 9 (2), 123-134.
- 93. Mizutani, F.; Yabuki, S.; Sawaguchi, T.; Hirata, Y.; Sato, Y.; Iijima, S., Sensors and Actuators B-Chemical 2001, 76 (1-3), 489-493.
- 94. Soper, S. A.; Ford, S. M.; Qi, S.; McCarley, R. L.; Kelly, K.; Murphy, M. C., *Anal Chem* **2000**, *72* (19), 642A-651A.
- 95. Young, E. W. K.; Berthier, E.; Guckenberger, D. J.; Sackmann, E.; Lamers, C.; Meyvantsson, I.; Huttenocher, A.; Beebe, D. J., *Analytical Chemistry* **2011**, *83* (4), 1408-1417.
- 96. Henry, A. C.; Tutt, T. J.; Galloway, M.; Davidson, Y. Y.; McWhorter, C. S.; Soper, S. A.; McCarley, R. L., *Analytical Chemistry* **2000**, *72* (21), 5331-5337.
- 97. van Midwoud, P. M.; Janse, A.; Merema, M. T.; Groothuis, G. M.; Verpoorte, E. M.,

- Anal Chem 2012.
- 98. Witek, M. A.; Hupert, M. L.; Park, D. S. W.; Fears, K.; Murphy, M. C.; Soper, S. A., *Analytical Chemistry* **2008**, *80* (9), 3483-3491.
- 99. Selimovic, A.; Johnson, A. S.; Kiss, I. Z.; Martin, R. S., *Electrophoresis* **2011**, *32* (8), 822-31.
- 100. Deal, K. S.; Easley, C. J., Analytical Chemistry 2012, 84 (3), 1510-1516.
- 101. Matsunaga, H.; Anazawa, T.; Yeung, E. S., *Electrophoresis* **2003**, *24* (3), 458-465.
- 102. Ocvirk, G.; Salimi-Moosavi, H.; Szarka, R. J.; Arriaga, E. A.; Andersson, P. E.; Smith, R.; Dovichi, N. J.; Harrison, D. J., *Proceedings of the IEEE* **2004**, *92* (1), 115-125.
- 103. Cai, L.; Friedman, N.; Xie, X. S., *Nature* **2006**, *440* (7082), 358-362.
- 104. Huang, B.; Wu, H. K.; Bhaya, D.; Grossman, A.; Granier, S.; Kobilka, B. K.; Zare, R. N., *Science* **2007**, *315* (5808), 81-84.
- 105. Wu, H. K.; Wheeler, A.; Zare, R. N., *Proceedings of the National Academy of Sciences of the United States of America* **2004**, *101* (35), 12809-12813.
- 106. Hellmich, W.; Pelargus, C.; Leffhalm, K.; Ros, A.; Anselmetti, D., *Electrophoresis* **2005**, *26* (19), 3689-3696.
- 107. Gunasekara, D. B.; Hulvey, M. K.; Jensen, D. T.; Mainz, E. R.; Caruso, G.; Lunte, S. M.; Culbertson, C. T., *Abstracts*, *45th Midwest Regional Meeting of the American Chemical Society, Wichita, KS, United States, October 27-30* **2010**, MWRM-405.
- 108. Gao, J.; Yin, X. F.; Fang, Z. L., *Lab on a Chip* **2004**, *4* (1), 47-52.
- 109. Cate, D. M.; Sip, C. G.; Folch, A., *Biomicrofluidics* **2010**, *4* (4).
- 110. Tolan, N. V.; Genes, L. I.; Spence, D. M., *Analytical Chemistry* **2009**, *81* (8), 3102-3108.
- 111. Oblak, T. D.; Root, P.; Spence, D. M., *Analytical Chemistry* **2006**, 78 (9), 3193-3197.
- 112. Rossier, J.; Reymond, F.; Michel, P. E., *Electrophoresis* **2002**, *23* (6), 858-867.
- 113. Yi, C. Q.; Zhang, Q.; Li, C. W.; Yang, J.; Zhao, J. L.; Yang, M. S., *Analytical and Bioanalytical Chemistry* **2006**, *384* (6), 1259-1268.
- 114. Choi, J. W.; Oh, K. W.; Thomas, J. H.; Heineman, W. R.; Halsall, H. B.; Nevin, J. H.; Helmicki, A. J.; Henderson, H. T.; Ahn, C. H., *Lab on a Chip* **2002**, *2* (1), 27-30.
- 115. Wang, J.; Ibanez, A.; Chatrathi, M. P.; Escarpa, A., Analytical Chemistry 2001, 73

- (21), 5323-5327.
- 116. Hulvey, M. K.; Genes, L. I.; Spence, D. M.; Martin, R. S., *Analyst* **2007**, *132* (12), 1246-1253.
- 117. Omiatek, D. M.; Santillo, M. F.; Heien, M. L.; Ewing, A. G., *Analytical Chemistry* **2009**, *81* (6), 2294-2302.
- 118. Mourzina, Y.; Kaliaguine, D.; Schulte, P.; Offenhausser, A., *Analytica Chimica Acta* **2006**, *575* (2), 281-289.
- 119. Ahonen, L.; Keski-Rahkonen, P.; Saarelainen, T.; Paviala, J.; Ketola, R. A.; Auriola, S.; Poutanen, M.; Kostianen, R., *Anal Chim Acta* **2012**, *721*, 115-21.
- 120. Schultz, G. A.; Corso, T. N.; Prosser, S. J.; Zhang, S., *Analytical Chemistry* **2000**, 72 (17), 4058-4063.
- 121. Wang, C.; Oleschuk, R.; Ouchen, F.; Li, J. J.; Thibault, P.; Harrison, D. J., *Rapid Commun Mass Sp* **2000**, *14* (15), 1377-1383.
- 122. Gao, J.; Xu, J.; Locascio, L. E.; Lee, C. S., Anal Chem **2001**, 73 (11), 2648-55.
- 123. Duong, C. T.; Roper, M. G., *Analyst* **2012**, *137* (4), 840-6.
- 124. Mao, S. F.; Gao, D.; Liu, W.; Wei, H. B.; Lin, J. M., Lab on a Chip **2012**, *12* (1), 219-226.
- 125. Baker, C. A.; Roper, M. G., Anal Chem **2012**, 84 (6), 2955-60.
- 126. Fu, A. Y.; Spence, C.; Scherer, A.; Arnold, F. H.; Quake, S. R., *Nature Biotechnology* **1999**, *17* (11), 1109-1111.
- 127. De Gasperis, G.; Yang, J.; Becker, F. F.; Gascoyne, P. R. C.; Wang, X.-B., *Biomedical Microdevices* **1999**, *2* (1), 41-49.
- 128. Oakey, J.; Allely, J.; Marr, D. W. M., *Biotechnology Progress* **2002**, *18* (6), 1439-1442.
- 129. Shelby, J. P.; White, J.; Ganesan, K.; Rathod, P. K.; Chiu, D. T., *Proceedings of the National Academy of Sciences of the United States of America* **2003**, *100* (25), 14618-14622.
- 130. McClain, M. A.; Culbertson, C. T.; Jacobson, S. C.; Allbritton, N. L.; Sims, C. E.; Ramsey, J. M., *Analytical Chemistry* **2003**, *75* (21), 5646-5655.
- 131. Kotsis, D., H.; Spence, D. M., Analytical Chemistry 2003, 75 (1), 145-51.
- 132. Roper, M. G.; Shackman, J. G.; Dahlgren, G. M.; Kennedy, R. T., *Analytical Chemistry* **2003**, *75* (18), 4711-4717.

- 133. Spence, D. M.; Torrence, N. J.; Kovarik, M. L.; Martin, R. S., *Analyst* **2004**, *129* (11), 995-1000.
- 134. Li, M.; Spence, D. M.; Martin, R. S., *Electroanal.* **2005**, *17*, 1171-1180.
- 135. Li, M. W.; Martin, R. S., Analyst **2008**, 133, 1358-1366.
- 136. Mecker, L. C.; Martin, R. S., *Analytical Chemistry* **2008**, *80* (23), 9257-9264.
- 137. Wang, Y.; Chen, Z. Z.; Li, Q. L., *Microchimica Acta* **2010**, *168* (3-4), 177-195.
- 138. Khademhosseini, A.; Langer, R.; Borenstein, J.; Vacanti, J. P., *Proceedings of the National Academy of Sciences of the United States of America* **2006**, *103* (8), 2480-2487.
- 139. Young, E. W. K.; Wheeler, A. R.; Simmons, C. A., *Lab on a Chip* **2007**, *7* (12), 1759-1766.
- 140. Carroll, J. S.; Ku, C.-J.; Karunarathne, W.; Spence Dana, M., *Analytical Chemistry* **2007**, *79* (14), 5133-8.
- 141. Genes, L., I.; Tolan, N., V.; Hulvey, M., K.; Martin, R. S.; Spence, D., M., *Lab on a Chip* **2007**, *7* (10), 1256-1259.
- 142. Letourneau, S.; Hernandez, L.; Faris, A. N.; Spence, D. M., *Anal. Bioanal. Chem.*, No pp yet given.
- 143. Vogel, P. A.; Halpin, S. T.; Martin, R. S.; Spence, D. M., *Analytical Chemistry* **2011**, 83 (11), 4296-4301.
- 144. Shuler, M. L.; Ghanem, A.; Quick, D.; Wong, M. C.; Miller, P., *Biotechnology and Bioengineering* **1996**, *52* (1), 45-60.
- 145. Srigunapalan, S.; Eydelnant, I. A.; Simmons, C. A.; Wheeler, A. R., *Lab on a Chip* **2012**, *12* (2), 369-375.
- 146. Huh, D.; Matthews, B. D.; Mammoto, A.; Montoya-Zavala, M.; Hsin, H. Y.; Ingber, D. E., *Science* **2010**, *328* (5986), 1662-1668.
- 147. Kaihara, S.; Borenstein, J.; Koka, R.; Lalan, S.; Ochoa, E. R.; Ravens, M.; Pien, H.; Cunningham, B.; Vacanti, J. P., *Tissue Eng* **2000**, *6* (2), 105-117.
- 148. Genes, L. I.; Nicole, V. T.; Hulvey Matthew, K.; Martin, R. S.; Spence Dana, M., *Lab on a Chip* **2007**, *7* (10), 1256-9.
- 149. Kosower, N.; Kosower, E.; Wertheim, B.; Correa, W., *Biochem Biophys Res Commun* **1969**, *37*, 593-596.
- 150. Sprague, R. S.; Stephenson, A. H.; Dimmit, R. A.; Weintraub, N. A.; Branch, C. A.; McMurdo, L.; Lonigro, A. J., *Am. J. Physiol* **1995**, *296*, H1941-H1948.

151. Halpin, S. T.; Anderson, K. B.; Vogel, P. A.; Spence, D. M., *Open Nitric Oxide Journal* **2011**, *3*, 8-15.

Chapter 2: Membrane based Separations on Microfluidic Devices for Analysis of NO in RBC Solution

2.1 Polycarbonate Membrane Based Devices

Polycarbonate membranes have been used occasionally in cell-interfaced microfluidic technologies. As early as 2001, a microfluidic system was used to determine the potentiometric resistance of a cell culture on a polycarbonate membrane, but this system was meant to take potentiometric measurements on small cell cultures, and did not allow for other readout mechanisms or flow. Other work has focused on the ability to use the membrane as a separation mechanism prior to analysis by electrospray ionization-mass spectrometry, as an introduction method to interface micro-scale devices to the nanoscale, or in the Spence group, as a sample cleanup method prior to fluorescence analysis in the presence of an RBC matrix, or sample cleanup prior to electrochemical measurements. These membranes have also been used as a cell scaffold, allowing endothelial cells, for example, to be cultured near a channel containing flowing blood components.

None of these examples, while offering the ability to perform sample cleanup or interface microfluidic channels with cell culture, have been integrated into mainstream biochemical laboratory infrastructure. This is because they require custom detection systems that are generally unique to each lab performing the analysis. The cost and complexity of these newer systems prevent their implementation in other labs because the benefits do not justify purchasing and maintaining additional equipment. To further improve the utilization of our devices, the work presented in this dissertation will focus on using off-the-shelf equipment for readout, such as a fluorescence plate reader. This will help to overcome one of the major limitations to wide scale implementation of microfluidic technologies.

2.2 Detection of Nitric Oxide

Ever since the discovery of NO as the endothelium derived relaxation factor by Ignarro and coworkers^{9,10} in the late 1980's and subsequent Nobel Prize in 1998, there has

been a large community interested in measuring NO in challenging biological matrices. These attempts are complicated by the fact that NO has a short half-life *in vivo*, reported to be on the order of seconds, ^{11, 12} as it is a free-radical which reacts with oxygen or thiols in plasma. This short half-life dictates that many of the detection techniques for NO are indirect, subsequently requiring reaction of the NO with some other molecule, and subsequent detection of a property of the product molecule after reaction. There are generally four ways of detecting NO in a sample, one of which, electrochemical techniques, do not require the NO to react with another species, and is therefore a direct technique. NO detection by chemiluminescence required reaction with ozone, while fluorogenic or absorbance options observing a reaction between a fluorescent or absorbing dye, and by downstream measurement of analytes that react with NO.

The electrochemical techniques, with the advantage of being able to directly detect NO, have employed a variety of electrode materials, such as platinum, ^{13, 14} carbon ink, ^{5, 15} gold/indium tin oxide ¹⁶ and carbon nanotubes. ¹⁷ As the samples of interest often foul electrode surfaces, and because extreme oxidizing potentials are often required, polymeric coatings such as Nafion are used frequently with electrochemical sensors to prevent fouling and maintain selectivity. Polymeric coatings, while gas permeable, can reduce the sensitivity of electrochemical sensors by adding a layer to the electrode surface, which is most often less permeable than solution. While many of these systems can achieve sufficient detection limits in ideal situations, they often lack robustness in terms of extended measurements, and would require significant engineering in order to be implemented in a high throughput setting. Furthermore, electrochemical sensors are not selective for NO. In most cases, they can also detect nitrite and peroxynitrite, both of which are degradation

products of NO. While attempts have been made to perform electrophoretic separation of NO degradation products in some cases, ^{18, 19} this is not the norm.

The most popular method of detecting NO, particularly in clinical investigations. 20-23 involves commercially available "nitric oxide analyzers" such as the Sievers Nitric Oxide Analyzer by GE. These techniques are based on the chemiluminescence reaction between NO and ozone. The light produced by the chemiluminescence reaction in the presence of excess ozone is proportional to the NO concentration in a method that is selective for NO over nitrite, nitrate and peroxynitrite, ^{24, 25} but typically requires larger samples than would be available in the microfluidic cell-cell communication to be monitored in chapter 3. Furthermore, these methods can measure NO byproducts (such as nitrite) if desired by reaction with reducing agents.²⁴ Chemiluminescence techniques are certainly capable of the needed detection limits, and the commercially available instruments are very reliable, as indicated by their prevalence. While chemiluminescence analyzers are not capable of simultaneous measurement of samples in parallel, they could likely be integrated with a flow injection system to improve their throughput. The primary limitation to the chemiluminescence system is that it requires a stand-alone system to produced ozone and the accompanying instrumentation to measure the chemiluminescence. It has not been integrated into already existing high throughput analysis solutions, and requires larger sample volumes than typical electrochemical or fluorogenic techniques.

Another reliable method for analyzing NO is through reaction with a molecule such as a fluorogenic probe like DAF-FM^{26, 27} as shown in figure 2.3, or through Griess reaction,²⁸ as shown in figure 2.4, and subsequent detection by absorbance. Both of these systems have the advantage of potential integration into high throughput screening, as they both utilize optical detection. However, the Griess reaction is limited because it detects nitrite, thus requiring NO oxidation prior to detection. Furthermore, as an absorbance

technique, the Griess reaction has detection limits of around 1 μM, reducing its utility for many NO producing systems. Alternatively, reaction of NO with DAF-FM, has had low nanomolar detection limits reported, ²⁶ but its selectivity is not certain, as it has been reported to react with peroxynitrite and ascorbic acid. ²⁹ These selectivity problems could potentially be mediated by performing an electrophoretic separation prior to laser-induced-fluorescence detection. ^{30, 31} As optical techniques, the primary limitation to these systems will be their performance in the presence of a RBC matrix, which due to the intense absorbance of hemoglobin, can interfere with optical measurements. This can be avoided using a separation technique, such as an electrophoretic separation, or using a polycarbonate membrane to separate the NO from the flowing RBC solutions ^{4, 32}.

Considering the capabilities of each of these available NO detection methods, and the goals of this investigation: to measure NO from hypoxic RBCs in a high throughput manner, the DAF-FM probe and subsequent fluorogenic reaction has been selected to detect NO. It offers compatibility with small sample volumes, easy integration into the flowing microfluidic systems, and the potential for high throughput readout using existing infrastructure without any need for gas generation as in the chemiluminescence method.

2.3 Methods

2.3.1 Device Fabrication

General fabrication of PDMS slabs is in Dow Corning's Sylgard 184 Elastomer (Ellsworth Adhesives, Germantown WI), which is sold as a 10:1 PDMS (w/w) to curing agent kit. For most work, a 20:1 mixture is prepared for surfaces requiring sealing, and 5:1 for portions that need to be more rigid. For a slab of PDMS on a 4 in. wafer, using 20:1 over channels and 5:1 over the entire slab for ease in punching inlets, 5 g of each 20:1 and 5:1 PDMS are mixed, and degassed under vacuum. The 20:1 PDMS is then poured over the channels or flat surface of the master, and cured at 75 °C for 13 minutes. The master is then

removed from the oven and immediately the 5:1 is poured onto it, particularly on surfaces requiring rigidity, and heated for 14 minutes.

The resulting PDMS coated master is allowed to cool to room temperature and the PDMS released from master by prying the edge off with a scalpel, then bulk removal by hand. Inlets are punched in the ends of the channels using 20 gauge steel tubing, and the resulting plug of PDMS removed using forceps under a stereomicroscope.

For the top, channel-free well layer, wells were punched using a ¼ inch hollow punch, with the resulting plugs removed with forceps. The final device, as shown in figure 2.1 is assembled by placing glass slides cut in half by the MSU glass shop underneath the channel layer (channels face up), then placing the polycarbonate membrane (Steriltech Inc.) over the channels, and finally the well layer over the membranes. The completed device is then heated for 15 minutes at 75 °C to reversibly seal the layers together.

2.3.2 Master fabrication

First, a mask or negative must be prepared containing the desired features. A vector drawing of the desired features is prepared using CorelDraw, Adobe Illustrator, or Macromedia Freehand. The computer drawing can then either be printed at 1000 DPI on a conventional transparency if the features to be printed are larger than 200 µm, or sent out to a high resolution printer if higher resolution is required. If the mask is printed using a conventional printer, during development prior to rinsing with acetone and isopropanol as a final step, the features should be rinsed with gamma-butyrolactone (the solvent in the SU-8-50 photoresist), then gently rubbed to clean up the features.

If thin features are desired (height less than 40 μ m), the SU-8-50 photoresist (MicroChem Inc.) can be thinned with gamma-butyrolactone at roughly a 1:10 ratio of solvent to photoresist to achieve significantly thinner features (5-40 μ m), but height must be determined empirically, as there is no table available to estimate spin speeds. If the normal

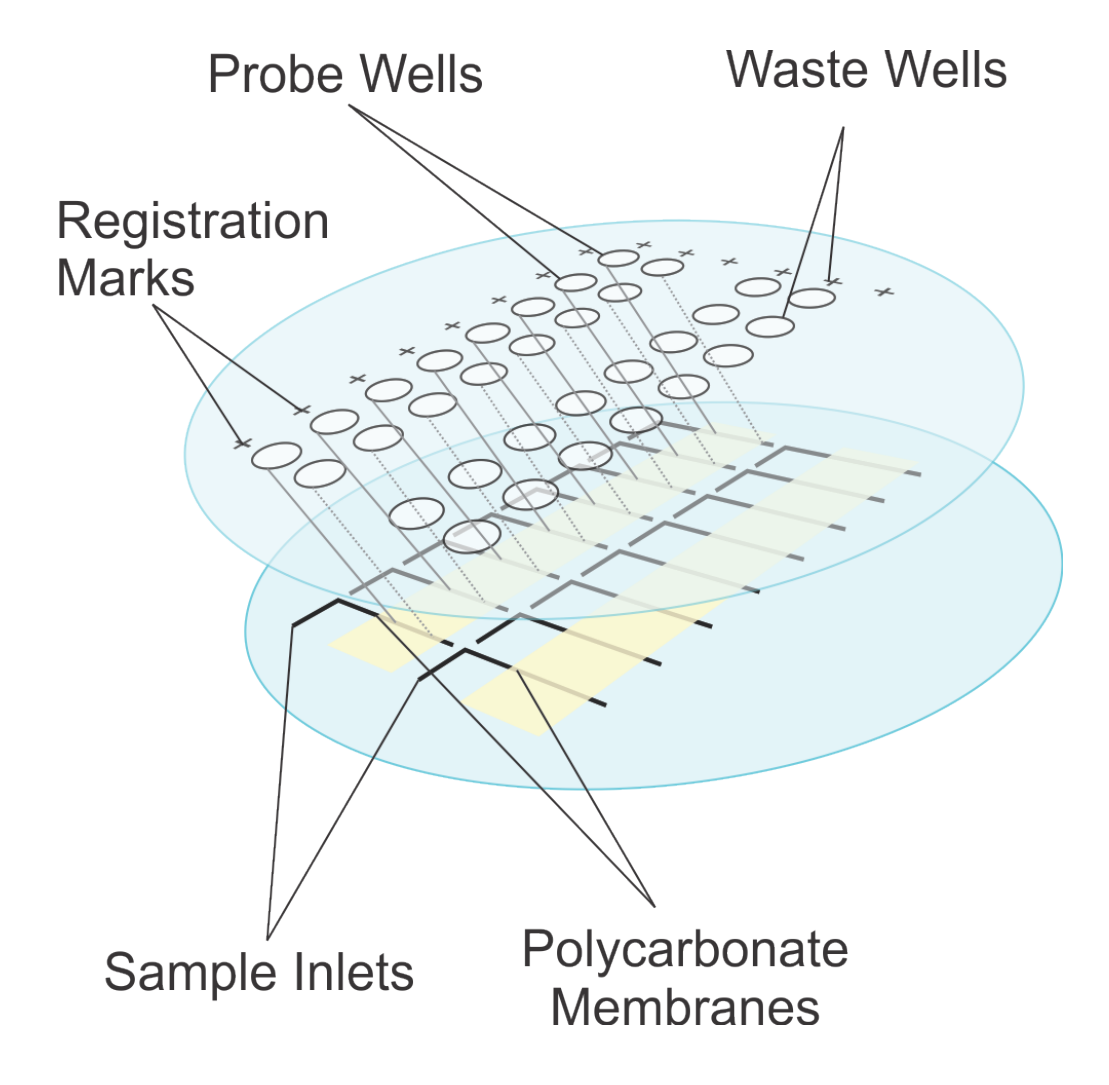


Figure 2.1: Fabrication of the Microfluidic Device for RBC NO Detection – As shown, this device consists of two layers of PDMS, the bottom containing L-shaped channels 200 μ m wide by 100 μ m tall. Between this layer and the "well" layer on top, are polycarbonate track-etched membranes allowing for transport of cellular components (such as NO), but not the cells themselves, where these components can interact with a fluorogenic probe, such as DAF-FM.

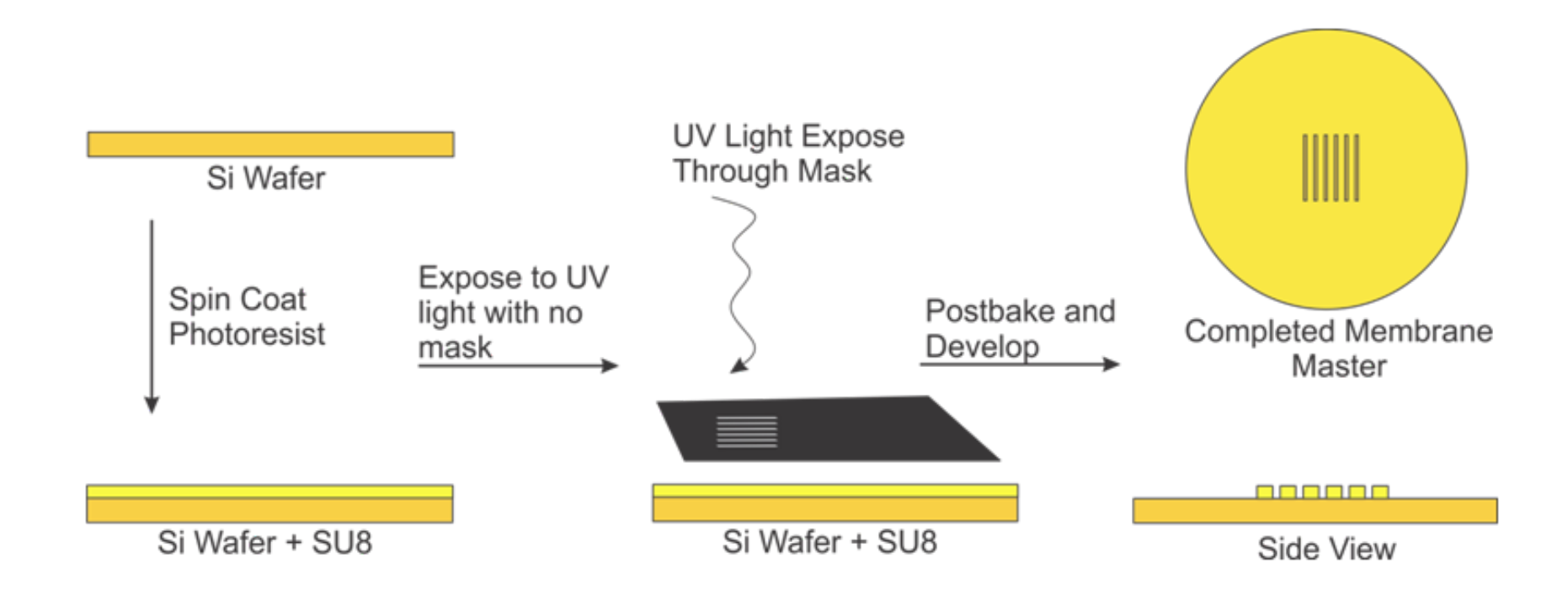


Figure 2.2: Fabrication of a Master: Masters for microfluidic devices are fabricated using lithographic techniques developed in the microelectronics industry. Briefly, a cleaned silicon wafer is spin-coated with SU-8 photoresist, a mask is placed over the photoresist, and exposed to UV light. The photoresist exposed to light cross links, forming a rigid structure. The remaining polymer is dissolved away, resulting in a master or mold with raised features.

SU-8-50 is to be used, it should be dispensed by pouring into a 50 mL syringe the night before use to allow bubbles to settle.

The light source for activating the crosslinking process consists of a mercury arc lamp with a dichroic mirror reflecting short wavelengths of light (<375 nm) to the focusing lens, that does not allow transmission of low wavelength UV light. The exposure control system also contains a detector mounted perpendicular to the light path, allowing for precise dosing as the mercury arc lamp ages. This detector is not calibrated, so calibration must be performed with a handheld light meter. In this process, UV opaque glasses should be used and direct exposure to the light source minimized. Prior to calibration, the lamp and all detectors are warmed up for 15 minutes. The dosing system is configured to display the output of the perpendicularly mounted detector in microamps, and the shutter manually opened. After verifying uniformity across the exposed surface, which may require bulb alignment, the values from the calibrated handheld meter and dosing system are recorded, and assumed to be equivalent. The dose can then be calculated using the product guide for the photoresist, which contains a table describing the light energy per unit area (mJ/ cm²). To determine time of exposure, the desired energy density is divided by the reading of the handheld meter (in units of mW/cm²). This exposure time, multiplied by the dosing system's readout in microamps, is the value to be programmed into the system for "dose."

As summarized in figure 2.2, previously used silicon wafers are scraped clean of any pre-existing photoresist or PDMS and washed with acetone, then isopropanol, and then water. Wafers are stacked into slotted glass rods and then into an evaporation dish for cleaning with piranha solution (2:1 sulfuric acid, 30% (w/w) hydrogen peroxide) (Caution, piranha solutions are very corrosive, use proper protocol and personal protective equipment), and heated to 95 °C for 12 hours. The solution and wafers are then allowed to cool to room temperature, and the piranha solution drained off to waste. Wafers are washed several

times with deionized water. If needed, wafers can be rinsed with isopropanol and rubbed with a lint free wipe to remove any remaining residue.

After wafers are cleaned, they are heated to 200 °C for one hour to dehydrate the silicon surface. The wafer is then cooled to room temperature, and spin coated with SU-8-50. While a table describing spin speeds is included with the product guide, as a starting point a spin program of accelerating at 100 rpm/s to 500 rpm for 15 seconds then accelerating at 300 rpm/s to 1000 rpm for 30 seconds will produce features that are 100 µm tall. The wafer and photoresist are then contact heated on a hot plate to 95 °C for 15 minutes. A mask is then aligned over the wafer, and the SU-8 exposed to UV light for approximately 30 seconds or a properly dosed amount of light. The wafer is then heated at 95 °C for 5 minutes to finish the curing process, and then developed in propylene glycol monomethyl ether acetate until the excess photoresist is washed away. The final master is washed followed by acetone then isopropanol.

2.3.3 Pumping System

Syringe pumps driving 500 µL Hamilton Gastight syringes were used in all flow studies. Syringes were connected to Tygon tubing through an adapter connecting a male luer syringe to a female 10-32 compression fitting (Upchurch/IDEX scientific). Tygon tubes were interfaced with the microfluidic device through 20 gauge stainless steel tubing (New England Small Tube Company), whose outer diameter fit tightly into the Tygon tubing and the microfluidic inlets described in 2.3.1. For studies requiring tubing that was not oxygen permeable, polymer sleeves designed to adapt 360 µm OD capillary tubing to 10-32 fittings were used to attach quartz capillaries to syringes. The same 20 gauge stainless tubes were used to connect to the microfluidic inlet, but they were attached to the capillary by removing 1 cm of the polyimide coating from the capillary through combustion, then securing with JB Weld. For microfluidic parallel arrays, such as the NO detection described here,

flow rates of 1.0 μ L/min were used. For other studies not requiring parallel channels, either NanoPorts (Upchurch Scientific) or female 10-32 fittings were secured to the devices with JB Weld, and plumbed with compression fittings.

2.3.4 Alignment in Plate Reader

As shown in figure 2.7, a Molecular Devices M4 plate reader was used for fluorescence readout. To properly align the chip, a 1/8" glass plate, with a notch cut out of the bottom left corner by the MSU glass shop, and a transparency with a plate printed onto it was taped onto the glass plate in a way that it aligned with a microplate when placed into the reader. The glass plate was placed into the plate reader, and the glass plate placed in tight contact with the upper right corner of the sample tray, as the instrument assumes the top and right edges of the plate are flush against the tray. The microfluidic device (cut to an appropriate size) was then aligned over the transparency, and the top-read mode was used to analyze solutions on the device. It is imperative that no shaking of the plate occur during measurement.

2.3.5 DAF-FM as a NO probe, Tank NO, NO Donors (NONOates)

Two methods were used to prepare NO standards, namely, preparation from tank NO or through the use of a class of NO donor molecules, NONOates. Tank NO standards were prepared in buffer purged with nitrogen for 5 minutes, then sealed into pear bottom flasks with septa. The purged flasks were then placed on a vacuum line until small bubbles ceased to form, and then purged again with inert gas. This cycle was performed three times. A NO stock solution was then prepared by purging with NO gas (after allowing all NOx to be purged from the lines as evidenced by brown gas) for three minutes, leaving a headspace of NO in the flask at approximately one atmosphere pressure, controlled with an oil bubbler. The flask was then sealed, allowed to reach room temperature, and then equilibrated for 30 minutes. The NO concentration should then be 1.5 mM. Serial dilutions

Figure 2.3: Reaction between DAF-FM and NO: Shown in the upper left is one of the earliest probes for NO, diaminofluorescein. In order to reduce the background fluorescence, and improve selectivity of NO over nitrite, two fluoro groups were added in addition to the methyl group in the active area of the probe. Shown below is a potential mechanism by which the fluorescent DAF-FM-NO is formed, with a peroxynitrite intermediate. While this mechanism is debated, DAF-FM fluorescence in the presence of NO is significantly reduced in the absence of oxygen, suggesting this mechanism. DAF-FM-NO fluorescence could be observed using the fluorescence microscopes, fluorometer or plate reader at wavelengths similar to fluorescein, with a peak excitation wavelength of 485 nm and a peak emission of 515 nm.

were performed with a Gastight syringe having a fixed needle into flasks purged of oxygen as described above.

NONOate solutions, both the spermine and diethylamine forms were first prepared by dissolving 10 mg of the NONOate compound in 0.01 M NaOH. These donor molecules are stable for several hours at high pH. Subsequent dilution was then made by adding donors to physiological buffers and the NONOate standards used shortly thereafter.

DAF-FM (4-amino-5-methylamino- 2',7'-difluorofluorescein, Invitrogen Inc.) was used as received. To prepare working solutions, 1 mg was dissolved in high purity, water free DMSO to make a 5 mM solution. This solution was separated into 7 µL aliquots, and stored at -20 °C in the absence of light, as freeze-thaw cycles and light reduce the fluorogenic behavior. Solutions of the desired concentration were then prepared immediately before use in Hank's Balanced Salt Solution or water, and care was taken to keep the solutions away from light, as they photobleach rapidly.

2.3.6 Nitrite Determination with Griess Reaction

As an alternative to the DAF FM probes, the Griess reaction (summarized in figure 2.4) was occasionally used to validate NO measurements. The particular Griess reaction used in this work did not include any means of reducing nitrate back to nitrite. Nitrite standards were prepared from sodium nitrite, and the two Griess reagents prepared as stock solutions, one a 0.1% naphthalenediamine solution in water, and the other 1% sulfanilamide in 5% (v/v) phosphoric acid.

Equal volumes of sample and each solution were mixed and then analyzed by monitoring absorbance at 543 nm using either a UV-Vis spectrometer or plate reader. Analysis

Figure 2.4: Griess Reaction for Nitrite Determination - Under acidic conditions, the sulfanilamide reacts with nitrite, and then with N-(1-naphthalenediamine) to produce the colored diazonium, which absorbs light at a maximum of 543 nm.

should occur rapidly (within 15 minutes) of sample preparation, as the absorbing compound can degrade over time.

2.3.7 Isolation and Preparation of RBCs, Hypoxic RBCs

Rabbit RBCs were obtained from healthy male New Zealand White rabbits between 2.0 and 2.5 kg in body mass. The animals were initially anesthetized with ketamine (8 mg/kg) and xylazine (1 mg/kg) followed by sodium pentobarbital (15 mg/kg). Rabbits were ventilated after tracheotomy, heparin administered, and exsanguinated through the carotid artery into polypropylene tubes. Whole blood was centrifuged at 500 g for 10 minutes then washed three times in a physiological salt solution (PSS) containing 4.7 mM KCl, 2.0 mM CaCl₂ 140.5 mM NaCl, 12 mM MgSO₄, 21 mM tris(hydroxymethyl)aminomethane, 11.1 mM glucose with 5% w/v bovine serum albumin at pH 7.4.

For use in microfluidic analysis, 7% hematocrit solutions of RBCs were prepared in either normal PSS or hypoxic PSS. The PSS was made hypoxic through the Oxyrase system by making a 1:10 solution of Oxyrase to PSS and allowing it to incubate for 30 minutes. For the measurement of NO release from RBCs, samples were analyzed within eight hours of removal from the animal.

2.4 Results

2.4.1 Images of Devices and Characterizing Channel Structure

In the development of proper protocols for lithography techniques, it was important to confirm the dimensions of structures fabricated on the microfluidic masters. Dimensions can be determined using instrumentation such as a profilometer, but it was desirable to have a technique that could be used on a day-to-day basis. To do this, a 10:1 PDMS replicate of the master was fabricated, and a slice 1 mm in length perpendicular to a channel was obtained and imaged under our inverted microscope. As shown in figure 2.5, this allows for a cross section of the channel to be obtained. The aspect ratio of the channel can then

be determined through direct measurement enabling a comparison between the expected width and height. Furthermore, the absence of artifacts can be confirmed, such as t-topping, where overexposure results in broadening of the top of the feature.

2.4.2 Selection of Pumping System for Chip-to-world Interfaces

While configurations involving the attachment of NanoPorts or other threaded fittings to a glass plate offer the most reliable interface between a sample and a microfluidic device, their high cost (\$60 per NanoPort in early 2012) and fragile nature motivate the search for alternative methods. For several years our group has been using^{4, 32-34} an approach that incorporates a stainless steel tube connecting to Tygon tubing. The Tygon tubing attaches to a Hamilton Gastight syringe, as shown in figure 2.5. To further reduce this cost, substitution of disposable 1 mL (BD, Franklin Lakes NJ) was investigated. A long serpentine channel microfluidic device was fabricated, and the time required for a fluorescein solution to displace a buffer solution from start to finish was determined to evaluate flow rate precision. The results of these times are summarized in figure 2.6.

2.4.3 Fluorescein Transport

Fluorescein was used as a test compound before working with NO in order to more easily characterize the process of aligning the microfluidic device in the plate reader, and improve our understanding of compounds crossing the polycarbonate membranes. Fluorescein standards were selected that would yield similar signals to the DAF-FM-NO of similar concentrations to investigate issues such as crosstalk, unwanted signal from an adjacent well via accidental coupling between wells.

An example standard curve is shown in figure 2.7 showing the process of how these devices are analyzed. Standards between 0 μ M and 3.0 μ M fluorescein were selected because the numerical values obtained for fluorescence after transport across the membrane in the microfluidic device were similar to those obtained from NO standards. Also shown

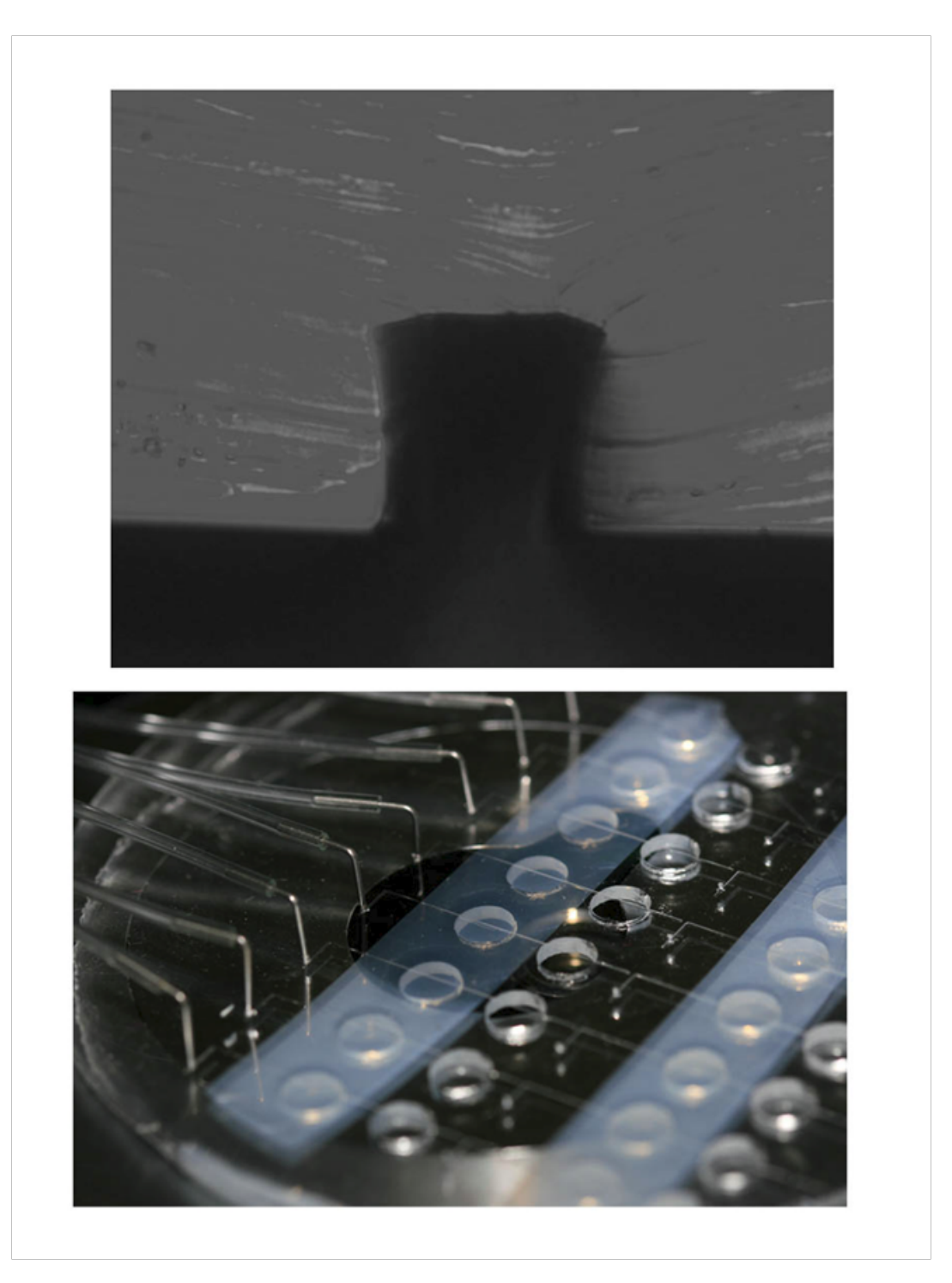


Figure 2.5: Cross Section of a Microfluidic Channel and Completed Device: The top image shows a cross section of a channel as described in 2.4.1. To determine approximate channel measurements, the images can be measured. Some distortion is present as a result of preparing the cross section, but there is minimal evidence of t-topping, which can be indicative of overexposure in the master fabricating process. The bottom image is a picture of an array microfluidic device prior to use, taken from the bottom, where the inlets and associated stainless steel tubes can be observed.

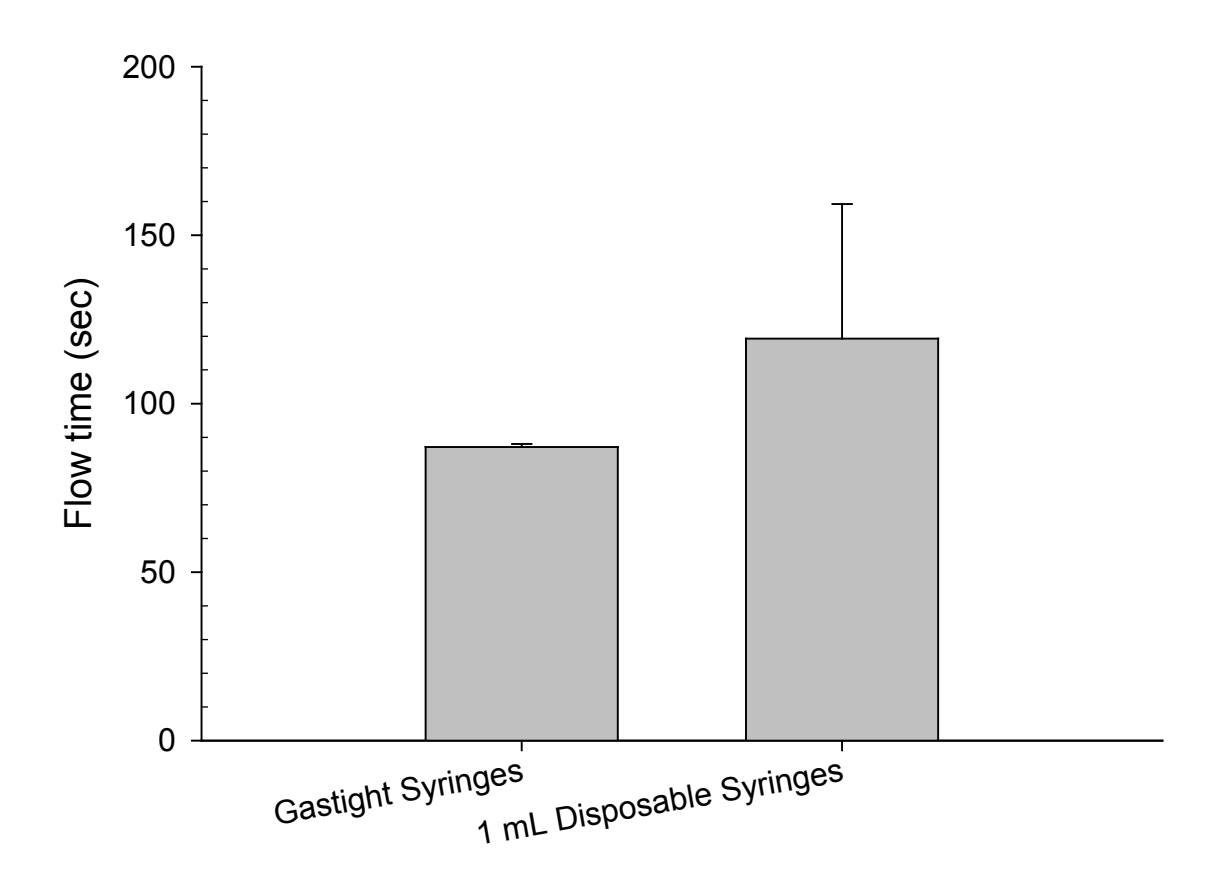


Figure 2.6: Reliability of Different Syringe Types: Hamilton Gastight (500 μ L) and BD 1 mL syringes were used to pump a 5 ppm fluorescein standard through a long, serpentine channel, and the time to displace buffer from the channel was measured. While these two syringes did not produce a statistically significant different flow rate at 95% confidence (n=9 syringes), the disposable syringes flow rate precision was less desirable.

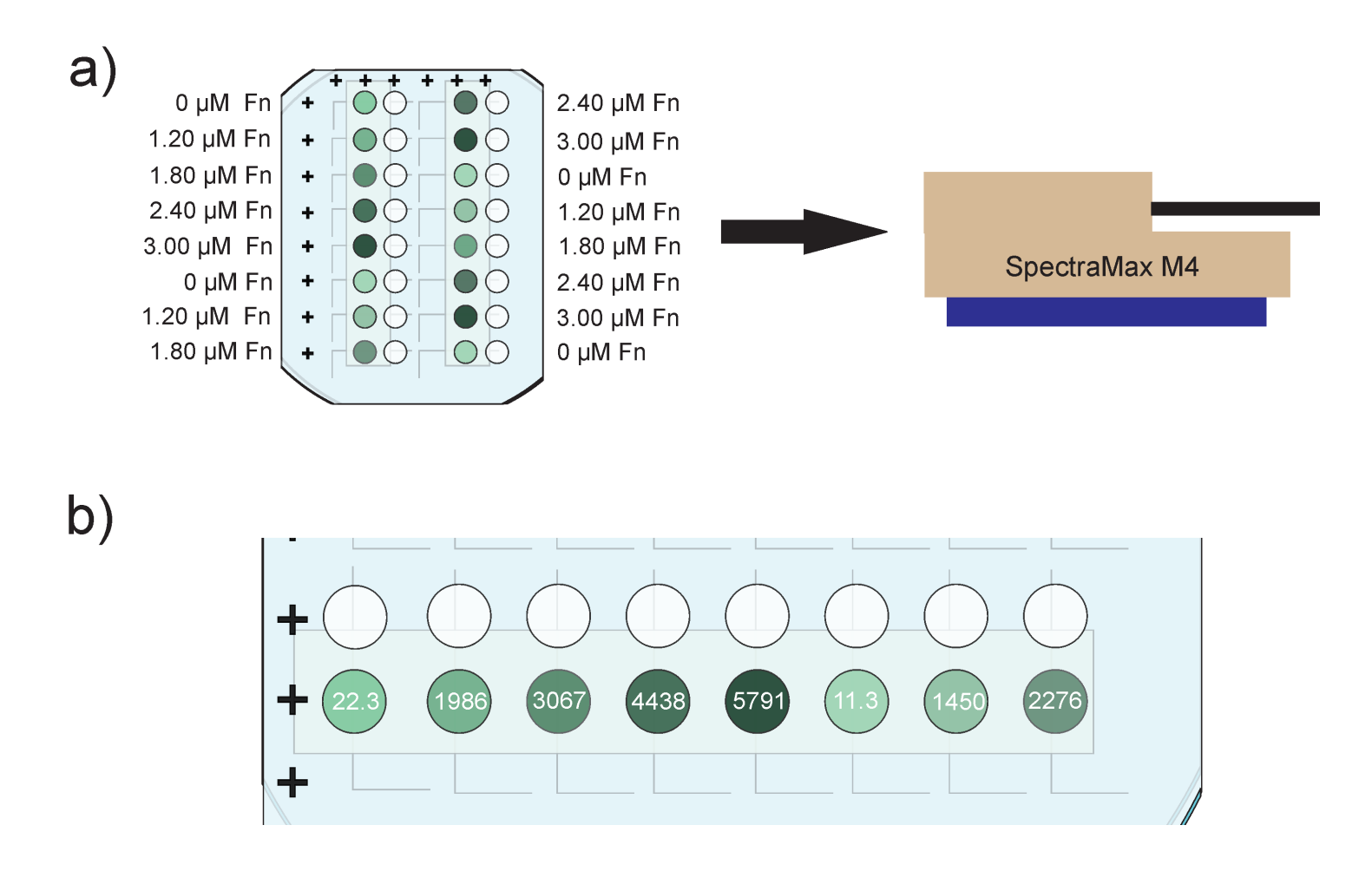


Figure 2.7: Shown in (a) is the arrangement of fluorescein standards spatially in the devices investigated to monitor fluorescein standards. This arrangement allows for the monitoring of crosstalk in the devices, as the no analyte standards are adjacent to the highest concentration standards, showing minimal crosstalk. Panel (b) shows signals typically obtained from such a measurement.

also in figure 2.7 is an example of how crosstalk is minimized, as the highest concentration standard adjacent to an analyte-free well shows minimal signal in the analyte free well.

2.4.5 DAF FM as a Fluorogenic Probe for NO

As shown in figure 2.8, DAF-FM, a fluorescein based probe, yields a large background fluorescence, relative to the signal obtained from a 20 µM DAF-FM-NO solution. This large background is common in fluorescein based probes. Furthermore, the excitation and emission maxima vary slightly from fluorescein, with an excitation maximum at 485 nM and an emission minimum around 505 nm. For analysis in the plate reader however, an emission wavelength of 515 nm was used because the larger fixed slit widths in the monochromators in the plate reader allowed for too much excitation light to pass to the detector, resulting in a larger background signal.

While the DAF-FM probe is an effective tool in quantifying NO, there are several limitations to its usefulness in solutions of varying conditions. Firstly, while a mechanism is not quite clear, the probe signal is diminished in calcium free buffers, as shown in figure 2.9. One potential explanation is that calcium interacts with the negatively charged groups on the DAF-FM probe, stabilizing the fluorescence signal

2.4.6 Selection of Membrane Pore Diameter, DAF FM Concentration

In using the microfluidic devices containing a membrane for separation of blood components from a fluorogenic probe, it is desirable to use a membrane pore size that allows for the highest flux of analyte, but does not allow for bulk transport of solution, which reduces the reproducibility of the device. Polycarbonate track etched membranes were used with pore sizes varying from 0.1 µm to 0.6 µm in diameter were used in devices

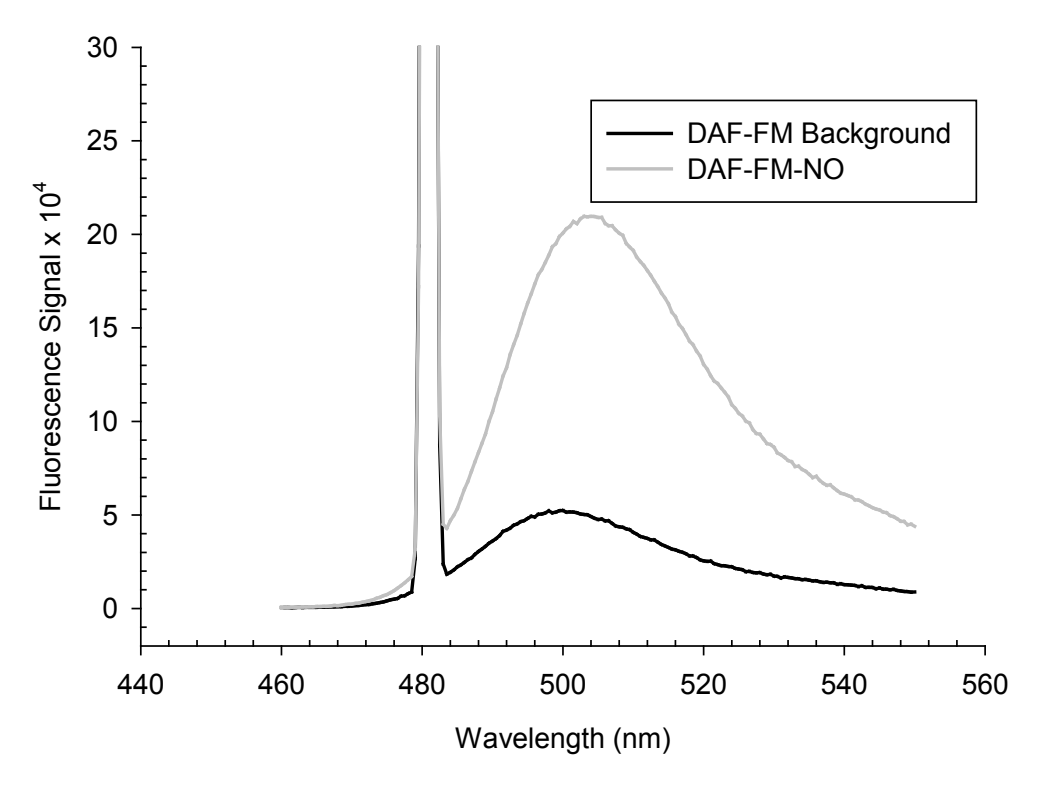


Figure 2.8: DAF-FM as a fluorogenic probe for NO: A fluorescein based probe, DAF-FM has a large background signal (shown in black), but the fluorescence increases significantly with addition of 20 μ M NO as shown here. The emission maximum occurs at 505 nm with an excitation of 485 nm.

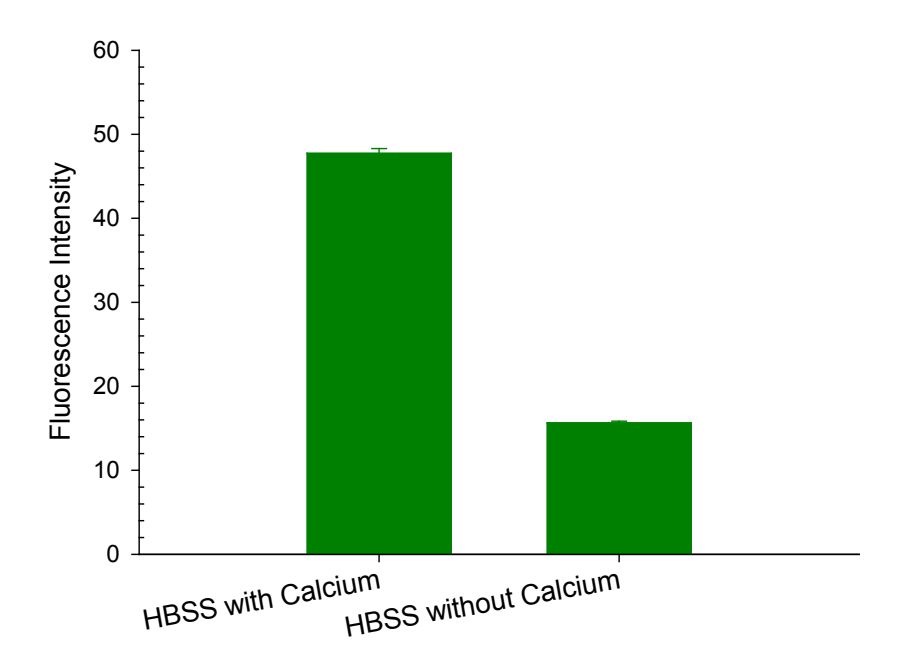


Figure 2.9 DAF-FM limitations with calcium and glucose: DAF-FM signal is significantly different dependent upon calcium concentration in the buffer (n=3 samples, 95% confidence).

Membrane Pore Size (μm)	y-intercept (Fl. U)	slope (μM/Fl U)	R ²	RSD of 5 µM standard (%)
0.6	6100 +/- 120	110 +/- 40	0.67 +/- 0.13	21+/- 8
0.4	5800 +/- 370	82 +/- 13	0.88 +/- 0.01	11.0 +/- 1.0
0.2	6240 +/- 490	113 +/- 23	0.98 +/- 0.01	3.0 +/- 0.70
0.1	7340 +/- 410	173 +/- 21	0.90 +/- 0.02	9.0 +/- 0.91

Table 2.1: Determination of Optimum Pore Size for NO Analysis: Calibration curves of DEANO (1-9 $\mu M)$ were analyzed with n=3 microfluidic devices, and the resulting parameters shown here. A pore diameter of 0.2 μm was chosen for future work as devices fabricated with these showed best reproducibility and correlation coefficients. Errors indicated as standard deviation.

DAF-FM Concentration (μM)	Detection Limit (μΜ)	R ²	RSD of 1 µM std	RSD of 9 µM std
10	1.32 +/- 0.18	0.96 +/- 0.04	3.1 +/- 0.9	7.2 +/- 1.3
20	0.51 +/- 0.08	0.97 +/- 0.02	3.6 +/- 0.3	0.6 +/- 0.21
30	1.82 +/- 0.13	0.92 +/- 0.03	7.9+/- 1.3	4 +/- 0.8
40	28 +/- 13	0.77 +/- 0.14	8.0 +/- 1.5	6 +/- 1.1

Table 2.2: Optimization of DAF-FM Concentration for Determination of RBC NO Release: To determine the optimum DAF-FM probe concentration, DEANO standards (1-9 μM) were analyzed on n=3 microfluidic devices, and the calibration curve parameters in addition to the reproducibility of the 1 μM and 9 μM standard determined. 20 μM was chosen as the optimal concentration because of the lower detection limit and sufficient reproducibility at the higher standard.

in which DEANO standards were pumped, and the resulting calibration curve parameters shown in table 2.1

Due to the DAF-FM probe having high background fluorescence in the absence of NO, it is desirable to use as little probe as needed to reduce the background. However, enough must be used to maintain linearity for a large dynamic range, as the probe can become the limiting reagent. Therefore, an optimum concentration of probe must be determined for each experiment to be performed. In the case of monitoring RBC NO release under hypoxic conditions, optimizations were performed and the results shown in table 2.2. DEANO standards were prepared and analyzed on three microfluidic devices at DAF-FM concentrations ranging from 10 to 40 μ M.

2.4.7 NO release from Hypoxic RBCs

7% solutions of normoxic and hypoxic RBCs were prepared as described above, and then pumped through the microfluidic device at 1 μ L per minute for 30 minutes underneath a membrane with pore diameters of 0.2 μ m and a DAF-FM concentration of 20 μ M, with standards being pumped simultaneously. The resulting microfluidic devices were then analyzed in the plate reader, and the NO release from the hypoxic and normoxic cells determined. As shown in figure 2.10, more NO was released from hypoxic RBCs than from normoxic RBCs.

2.5 Discussion

2.5.1 Engineering Changes to Polycarbonate Membrane Device to Enable Plate Reader Detection

Previous polycarbonate membrane based devices for analysis of cellular components in the Spence group have used multiple 1/8 inch wells over a channel,⁴ although this approach was not used in the fabrication of this device for two reasons. First, larger wells were selected to more closely match the diameter of a well in a microtiter plate. The primary advantage of larger wells was they minimized crosstalk such that a 3 µM solution

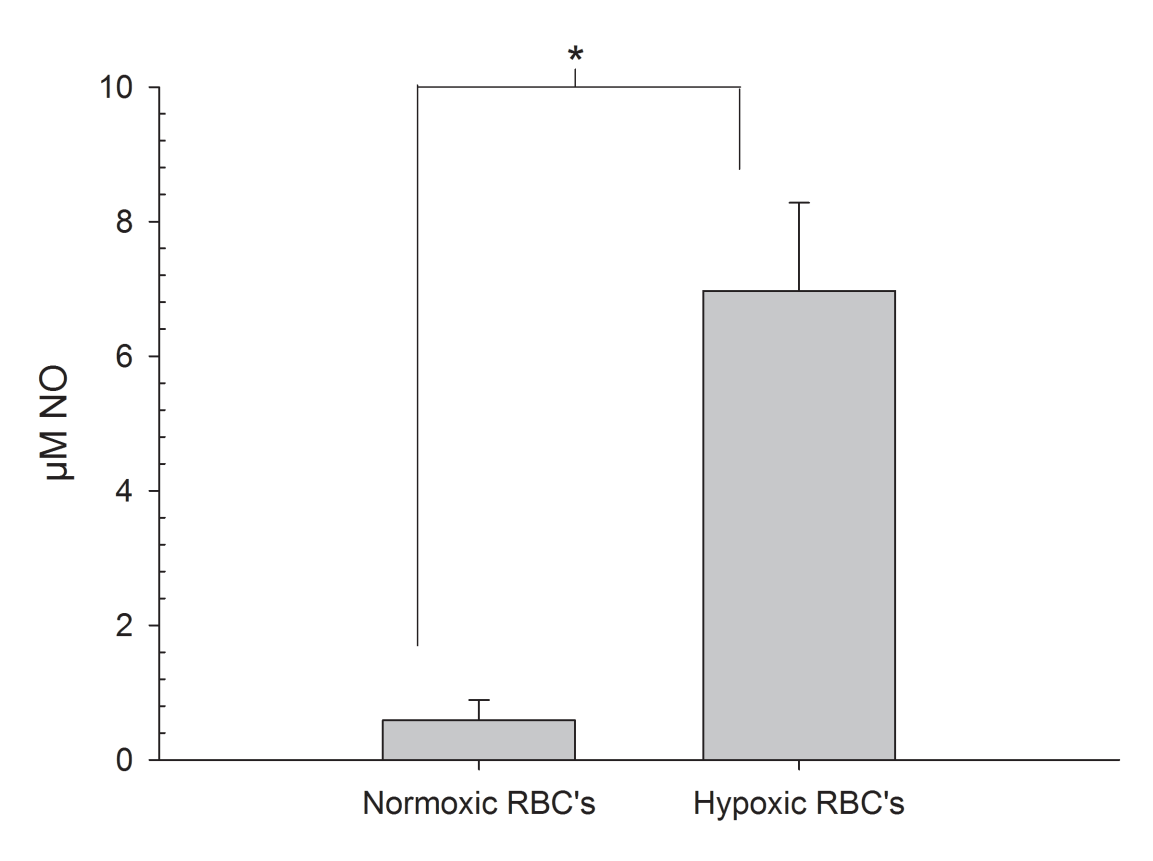


Figure 2.10: NO Release from Hypoxic RBCs: In n=4 rabbits, statistically more NO was released from hypoxic RBCs than from normoxic RBCs (p < 0.01). The NO concentration is calibrated to DEANO standards.

of fluorescein next to a buffer solution would yield a minimal signal in the buffer well. A resolution to this problem, which will be discussed in chapter three, was later developed, allowing for use of smaller wells. The second engineering change was moving to only one well per channel, this change was made because consistent signal was not observed across multiple wells in the same channel, the signal decreased as more wells were added further along the channel, suggesting there was depletion at the top of the channel of the analyte of interest, causing the local concentration at downstream wells to be reduced. The decreased signal in downstream wells is likely due to the increase in interaction area between the wells and channel with the larger well diameter. Alternatively, past work had utilized multiple smaller wells within a channel to signal average fluorescence signals within a channel, offering improved reproducibility. With different signals in downstream wells, this was no longer reasonable, so the additional wells were eliminated.

In order to reduce strain on the inlets at the bottom of the device, improving their reliability, the device was placed on a table of perforated stainless steel with holes 2.5 mm in diameter, through which the tubing addressing the chip could be run, placing most of the weight of the tubing on the stainless steel shelf. This allowed for the tubing to be level from the syringe outlet, through the stainless steel table, to the chip, preventing the RBCs from pooling anywhere in the tubing. If the RBCs pool in the tubing, they never reach the microfluidic device, and NO release is not observed. Furthermore, it was discovered the Tygon tubing must be replaced periodically, particularly as it loses its flexibility, as the NO signal from standards would be significantly reduced. Tubing was replaced approximately every 30 cleaning cycles.

2.5.2: Alignment in the Plate Reader

The most significant novel contribution of this work is alignment (and subsequent readout) of the device in the plate reader. To accomplish this, a glass template was fabri-

cated by the glass shop to be within 2 mm in each direction of the dimensions of a standard plate. A transparency, prepared in CorelDraw, was then printed with wells on it, with the same geometry of a well plate, and taped to the glass plate in the same position a plate would be. Once this alignment was confirmed, the microfluidic device could be placed in such a way that the wells overlapped the template, assuring alignment.

Alignment can be verified by pipetting in alternating order fluorescein standards and buffer. Alignment is accomplished when the buffer wells show a minimum signal, suggesting there is not a portion of a standard well under the reading head when only buffer should be present. Using fluorescein standards in this manner offers a convenient way to verify alignment of the transparency to the glass plate.

2.5.3: Detection of NO

After successfully achieving a reliable mechanism for aligning microfluidic devices in the plate reader, NO detection with the microfluidic system was investigated. There are four ways NO is usually detected: electrochemically by oxidation, through chemiluminescence reaction with ozone in the gas phase, through analysis of some reacted product such as nitrosylated protein or nitrite/nitrate, and by fluorogenic reaction. While the electrochemical techniques offer an affordable approach, challenges with detection limits and biofouling of any proteins at the electrode make these approaches challenging. Chemiluminescence reaction with ozone is one of the most popular ways of detecting NO, but is challenging to do in a high throughput manner. Analysis of downstream products, such as nitrite, nitrate, or nitrosylated protein/glutathione by mass spectrometry is also popular, but these approaches do not measure NO directly, and since nitrosylated products could result from other physiological processes, their specificity towards the process of interest is not clear. Considering these, the fluorogenic probes (specifically DAF-FM) were chosen

because of previous work using intracellular probes, offering sufficient detection limits, and their ease of use.

The DAF-FM probe is a selective probe for NO, showing no increase in fluorescence emission with nitrite or nitrate. It has a low detection limit in solution of around 5 nM NO, and sufficient sensitivity to be used in the manner shown in this dissertation. DAF-FM does have some disadvantages. For example, there is a debate in the literature whether or not the probe is sensitive to calcium concentration in solution. This is an important consideration as the probe is used *in vivo*, where calcium is often required for NO synthesis. As removing calcium from solution is commonly used to inhibit NO synthesis, the source of the lower fluorescence emission is not clear. Using NO standards in our laboratory, in HBSS with or without calcium, as shown in figure 2.9, higher fluorescence emission was observed when calcium was present, suggesting a calcium dependence. This was not a major concern for the work shown here or in subsequent work because calcium is always in the buffers used. This could be a concern for workers who use the absence of calcium as a way to negatively control NO synthesis, as they could just be suppressing probe sensitivity, instead of NO synthesis.

2.5.3: Preparation of NO standards

Another challenge in studying systems involving NO is determining how to make standard NO solutions. As NO is a free radical molecule that is reactive with oxygen, one might consider working under anoxic conditions. However, with the desire to work in living aerobic systems, it is not practical to always work under anoxic conditions such as those found on a vacuum line or glove box. Initial studies investigating the efficacy of DAF-FM as a probe for NO nonetheless were performed using oxygen free samples, prepared on a vacuum line from tank NO, to validate the use of simpler methods, namely the NONOate donor compounds. A class of compound which will spontaneously release NO

under physiological conditions, NONOates can be initially diluted under basic conditions (0.01 M NaOH), and transferred to buffers with a neutral pH where they will release NO at a known rate with first order kinetics. Two compounds were investigated in this work, first spermine NONOate with a half life of 37 minutes, and diethylamine NONOate (DEANO), with a half life of 3 minutes. The faster reacting DEANO was preferred because then by the time the compound reached the microfluidic device, it had already reacted to form NO. With the slower reacting spermine NONOate, it is possible to be observing the NONOate crossing the polycarbonate membrane, instead of NO. Therefore, DEANO was used as the NO source for the standards mentioned here.

In verifying the function of the NONOate compounds, it was desired to have a method that was independent of the DAF-FM probe system. While electrochemical approaches were attempted, a good method to determine whether NO or the NONOate compounds themselves were being analyzed was not realized electrochemically. Therefore, the Griess reaction, as described above, was used to verify there were no problems with the function of the NONOates. The Griess reaction could not be used however for the regular analysis of RBC components because as an absorbance based assay, it had a detection limit of approximately 1 μ M, and has been reported to have interference issues with bovine serum albumin, which is present in our PSS solution.

While methods of producing hypoxic solutions are discussed at length in chapter 4, briefly, the Oxyrase system was chosen because it does not require purging of protein rich solutions with noble gases, which results in foaming, and risks dispersing biohazard-ous materials. Additionally, a solution deoxygenated with Oxyrase remains deoxygenated, even if they are exposed to air when loading syringes, as the enzymatic reaction maintains

low oxygen levels. When loading the syringes for pumping to the microfluidic devices, they can be aerated if loaded too fast, potentially reoxygenating solutions.

2.5.4 Microfluidic Fabrication Enhancements

After off-device verification of the DAF-FM probe, NO standards, and hypoxic systems, it is necessary to validate proper fabrication of microfluidic devices. Essential to this validation is the ability to reproducibly fabricate masters, or molds for the microfluidic devices. This was accomplished first by properly calibrating all equipment available in the lab, in particular the detector that monitors the light output of the UV flood source. Also, determination of the conditions needed to re-use silicon wafers by cleaning proved essential in developing new microfluidic devices, as the cost in producing a new master was significantly reduced. To verify the absence of overexposure, and to verify the dimensions of the channel with equipment available in the lab, cross sections of the channel were prepared and analyzed under the inverted microscope. Channels intentionally overexposed showed clear t-topping, a phenomena resulting from the changes in refractive index as the photoresist cures when overexposed, whereas channels exposed after proper dosing of light appear as the desired rectangles. Furthermore, the aspect ratio of the channels can be easily estimated using this method, offering validation of the dimensions of the channels.

Furthermore, as an attempt to improve the throughput of analyses performed with these devices, an attempt was made to use disposable plastic syringes instead of the glass Hamilton Gastight syringes typically used in past work. This substitution would offer significant time advantages in preparing the samples, because much time is spent the process of cleaning these syringes. To determine the feasibility of the use of the disposable syringes, an experiment was conducted in which a long serpentine channel was filled with buffer, and then fluorescein was pumped into the device, and then observed under the fluorescence microscope. The time taken for the fluorescein to flow from the beginning of

the serpentine channel to the end was then recorded, and compared for multiple syringes with a given set of hoses and fittings. It was found that the Hamilton syringes offered excellent reproducibility in time, and therefore flow rate, but the disposable syringes, while not having a statistically different mean from the Hamilton syringes, had significantly greater variation in flow rate, making them undesirable for use in these devices.

Also, the role of aging and multiple cleanings of the Tygon tubing was investigated, as it was noticed that reproducibility of the performance in microfluidic devices was reduced as more experiments were performed. It was determined that as the Tygon tubing is routinely cleaned as a part of the experiments, it becomes more brittle. This brittle nature resulted in lower reproducibility of flow rates as investigated by this method, and this was resolved by replacing the tubing. It is estimated this tubing should be replaced every 30 cleaning cycles.

After a clear understanding of the pumping systems was achieved, adaptation of the microfluidic device for readout in the plate reader was conducted initially by monitoring of fluorescein transport across the membrane. Fluorescein was chosen because of its excellent stability, and excitation and emission at approximately the same wavelengths as DAF-FM-NO. This was most valuable for determining proper alignment methods, and at the same time, determining crosstalk. Alignment, procedurally discussed above, was achieved by placing a 3 µM standard adjacent to a blank standard in a two dimensional grid on a PDMS well-plate, with wells punched into PDMS to mimic the design of a microfluidic device. Alignment was adjusted until the standards containing fluorescein showed reproducible values, with the wells containing no analyte showed minimum and reproducible values. Furthermore, pumping fluorescein under the membranes in the microfluidic device, of-

fered an approach for validating the pumping, device fabrication, and readout in a manner independent of the more challenging NO measurements.

2.5.5 NO Measurements on Microfluidic Device

After determining feasibility of the plate reader for detection of a fluorescent compound in microfluidic devices, the use of DAF-FM for detection of NO was investigated. Early investigations with the probe and buffer systems showed calcium dependence in signal; as shown in figure 2.9, fluorescence signal of a DAF-FM-NO solution was increased when it was made in buffer containing calcium. As mentioned, this has been reported in the literature when the DAF-FM probe was used intracellularly, but in many of these cases, the absence of calcium in the buffer will greatly inhibit NO producing enzymes, reducing the signal of DAF-FM-NO because there is less NO available to react. While no studies mentioned here or later used varying calcium concentration, this is of particular interest because an absence of calcium in a buffer has been used to inhibit NO production.

Once the behavior of the DAF-FM probe in solution was understood, the microfluidic system was then optimized for NO detection in pore diameter and probe concentration. Both parameters were optimized through the fabrication of a series of devices with polycarbonate membranes varying in pore diameter from 0.1 through 0.6, and then analyzing a series of DEANO standards with 20 µM DAF-FM above the membrane, as summarized in table 2.2. Empirically, the 0.2 µm pore diameter membrane was determined to be the most optimal as it allowed for sufficient sensitivity and good reproducibility. The sensitivity is dependent upon the amount of NO that can cross the membrane, the larger the pores, the more NO will transport across the membrane. The reproducibility however is limited by the amount of inconsistent bulk flow of solution across the membrane, resulting in varying probe and NO concentrations in the different wells, and irreproducible varying signals. A smaller pore size will then result in a higher backpressure towards fluid crossing

the membrane, allowing for better reproducibility. In this case, the optimal pore diameter considering both factors was $0.2~\mu m$.

The probe concentration of 20 μ M was also optimized for sensitivity and reproducibility through the analysis of DEANO standards, with the calibration curve parameters and reproducibility summarized in table 2.2. 20 μ M DAF-FM was selected because it offered the best reproducibility at the high and low concentrations in the relevant dynamic range, in addition to an acceptable detection limit. In choosing an optimal DAF-FM concentration, there are two parameters to consider, first, a sufficiently low concentration, minimizing background, is needed that a sufficiently low detection limit is achieved. However, the probe concentration also must be high enough that the system is not stoichiometrically limiting the upper end of the dynamic range. To determine this, calibration between 1 μ M and 9 μ M NO was performed, and the linearity, detection limit, and reproducibility at the extremes of the dynamic range considered.

After final optimization of the microfluidic system was complete, measurement of NO release from hypoxic RBCs was achieved by pumping hypoxic RBCs, normoxic RBCs, and DEANO calibration standards in the same microfluidic device. After flowing for 30 minutes, the devices were analyzed in the plate reader, and calibrated to DEANO standards on the same device. As shown in figure 2.10, significantly more NO was detected from hypoxic RBCs than from normoxic RBCs. Furthermore, these measured values were significantly greater than those observed when DAF-FM probe is mixed with a RBC sample in a microcentrifuge tube, centrifuged, then the supernatant analyzed, as had been the previous method used in our group. The microfluidic method offers a higher recovery of the NO because after the NO is transported across the polycarbonate membrane, there is

a much lower concentration of proteins and peptides with which it can interact, therefore it is more likely to react with the DAF-FM probe, resulting in higher signals.

Finally, these studies show that for investigation of the ability of RBC-derived NO to cross an endothelial barrier, a polycarbonate track-etched membrane is NO-permeable, and therefore can be used as a support structure to culture a layer of endothelial cells on.

REFERENCES

REFERENCES

- 1. Hediger, S.; Sayah, A.; Horisberger, J. D.; Gijs, M. A. M., *Biosens. Bioelectron.* **2001,** *16* (9-12), 689-694.
- 2. Iannacone Jamie, M.; Jakubowski Jennifer, A.; Bohn Paul, W.; Sweedler Jonathan, V., *Electrophoresis* **2005**, *26* (24), 4684-90.
- 3. Kuo, T.-C.; Cannon, D. M., Jr.; Tulock, J. J.; Shannon, M. A.; Sweedler, J. V.; Bohn, P. W., *Abstracts of Papers, 224th ACS National Meeting, Boston, MA, United States, August 18-22, 2002* **2002**, ANYL-131.
- 4. Tolan, N. V.; Genes, L. I.; Subasinghe, W.; Raththagala, M.; Spence, D. M., *Analytical Chemistry* **2009**, *81* (8), 3102-3108.
- 5. Hulvey, M. K.; Genes, L. I.; Spence, D. M.; Martin, R. S., *Analyst* **2007**, *132* (12), 1246-1253.
- 6. Genes, L., I.; Tolan, N., V.; Hulvey, M., K.; Martin, R. S.; Spence, D., M., *Lab on a Chip* **2007**, *7* (10), 1256-1259.
- 7. Oblak, T. D.; Root, P.; Spence, D. M., Analytical Chemistry 2006, 78 (9), 3193-3197.
- 8. Letourneau, S.; Hernandez, L.; Faris, A. N.; Spence, D. M., *Anal. Bioanal. Chem.*, No pp yet given.
- 9. Ignarro, L. J.; Buga, G. M.; Wood, K. S.; Byrns, R. E.; Chaudhuri, G., *Proc. Natl. Acad. Sci. U. S. A.* **1987**, *84* (24), 9265-9.
- 10. Palmer, R. M.; Ferrige, A. G.; Moncada, S., *Nature* **1987**, *327* (6122), 524-6.
- 11. Hakim, T. S.; Sugimori, K.; Camporesi, E. M.; Anderson, G., *Physiological Measurement* **1996,** *17* (4), 267-277.
- 12. Kelm, M.; Feelisch, M.; Deussen, A.; Schrader, J.; Strauer, B. E., *Journal of Cardiovascular Pharmacology* **1991**, *17*, S95-S99.
- 13. Lee, Y.; Kim, J., Analytical Chemistry **2007**, 79 (20), 7669-7675.
- 14. Villeneuve, N.; Bedioui, F.; Voituriez, K.; Avaro, S.; Vilaine, J. P., *J Pharmacol Toxicol* **1998**, *40* (2), 95-100.
- 15. Hulvey, M. K.; Martin, R. S., Anal. Bioanal. Chem. 2009, 393 (2), 599-605.
- 16. Cha, W.; Tung, Y. C.; Meyerhoff, M. E.; Takayama, S., *Analytical Chemistry* **2010**, *82* (8), 3300-3305.

- 17. Li, C. M.; Zang, J.; Zhan, D.; Chen, W.; Sun, C. Q.; Teo, A. L.; Chua, Y. T.; Lee, V. S.; Moochhala, S. M., *Electroanalysis* **2006**, *18* (7), 713-718.
- 18. Gunasekara, D. B.; Hulvey, M. K.; Jensen, D. T.; Mainz, E. R.; Caruso, G.; Lunte, S. M.; Culbertson, C. T., *Abstracts, 45th Midwest Regional Meeting of the American Chemical Society, Wichita, KS, United States, October 27-30* **2010**, MWRM-405.
- 19. Hulvey, M. K.; Frankenfeld, C. N.; Lunte, S. M., *Analytical Chemistry* **2010,** *82* (5), 1608-1611.
- 20. Palmer, R. M. J.; Ashton, D. S.; Moncada, S., *Nature* **1988**, *333* (6174), 664-666.
- 21. Buchvald, F.; Baraidi, E.; Carraro, S.; Gaston, B.; De Jongste, J.; Pijnenburg, M. W. H.; Silkoff, P. E.; Bisgaard, H., *J Allergy Clin Immun* **2005**, *115* (6), 1130-1136.
- Wang, X.; Bryan, N. S.; MacArthur, P. H.; Rodriguez, J.; Gladwin, M. T.; Feelisch, M., *The Journal of biological chemistry* **2006**, *281* (37), 26994-7002.
- Hirata, Y.; Hayakawa, H.; Kakoki, M.; Tojo, A.; Suzuki, E.; Kimura, K.; Goto, A.; Kikuchi, K.; Nagano, T.; Hirobe, M.; Omata, M., *Hypertension* **1996**, *27* (3 Pt 2), 672-8.
- 24. Braman, R. S.; Hendrix, S. A., *Analytical Chemistry* **1989**, *61* (24), 2715-2718.
- 25. Pelletier, M. M.; Kleinbongard, P.; Ringwood, L.; Hito, R.; Hunter, C. J.; Schechter, A. N.; Gladwin, M. T.; Dejam, A., *Free Radic Biol Med* **2006**, *41* (4), 541-8.
- 26. Kojima, H.; Nakatsubo, N.; Kikuchi, K.; Kawahara, S.; Kirino, Y.; Nagoshi, H.; Hirata, Y.; Nagano, T., *Analytical Chemistry* **1998**, *70* (13), 2446-2453.
- 27. Kojima, H.; Urano, Y.; Kikuchi, K.; Higuchi, T.; Hirata, Y.; Nagano, T., *Angewandte Chemie-International Edition* **1999**, *38* (21), 3209-3212.
- 28. Miranda, K. M.; Espey, M. G.; Wink, D. A., *Nitric Oxide-Biology and Chemistry* **2001**, *5* (1), 62-71.
- 29. Zhang, X.; Kim, W.-S.; Hatcher, N.; Potgieter, K.; Moroz, L. L.; Gillette, R.; Sweedler, J. V., *Journal of Biological Chemistry* **2002**, *277* (50), 48472-48478.
- 30. Ye, X.; Kim, W.-S.; Rubakhin, S. S.; Sweedler, J. V., *Analyst (Cambridge, U. K.)* **2004,** *129* (12), 1200-1205.
- 31. Mainz, E. R.; Gunasekara, D. B.; Caruso, G.; Jensen, D. T.; Hulvey, M. K.; da Silva, J. A. F.; Metto, E. C.; Culbertson, A. H.; Culbertson, C. T.; Lunte, S. M., *Anal Methods-Uk* **2012**, *4* (2), 414-420.
- 32. Halpin, S. T.; Spence, D. M., *Analytical Chemistry* **2010**, 82 (17), 7492-7497.
- 33. Oblak, T. D.; Meyer, J. A.; Spence, D. M., *Analyst* **2009**, *134* (1), 188-193.

34. Ku, C. J.; Oblak, T. D.; Spence, D. M., *Analytical Chemistry* **2008**, *80* (19), 7543-7548.

Chapter 3 - Membrane Based Devices for Monitoring Cell-Cell Communication: Elucidating a Mechanism of Hypoxic Vasodilation

3.1: Introduction

3.1.1 Intracellular NO Measurements Using Microfluidic Devices

NO release from bovine pulmonary artery endothelial cells (bPAECs), has been previously monitored by the Spence group using electrochemistry^{1, 2} or through the intracellular fluorogenic probe DAF-FM-DA.^{3, 4} This intracellular probe contains two acetate groups adjacent to the fluorine atoms on the molecule shown in figure 2.3. This increases the cell membrane permeability of the dye, and once inside the cell the acetate groups are cleaved by intracellular esterase, reducing the permeability of the dye, making it identical to DAF-FM^{5, 6}, which was described in chapter 2. The intracellular nature of the probe increases its utility through detection by fluorescence microscopy,⁷⁻⁹ flow cytometry,¹⁰⁻¹² or more recently, through cellular lysis and electrophoretic separation followed by laser induced fluorescence detection.¹³

While this intracellular fluorogenic probe has the significant advantage of detection capability with common laboratory equipment such as fluorescence microscopes and flow cytometry, until recently, ¹³ the probe could not be used in a quantitative manner. Importantly, the probe is also unable to elucidate the source of NO. For example, endothelial cells contain endothelial nitric oxide synthase ^{14, 15} (eNOS) which can synthesize NO from L-arginine, but it is also possible that NO derived from the RBC (see also chapter 2) could diffuse across the endothelial cell membrane, react with the DAF-FM probe, increasing fluorescence. This can be reliably verified however through the use of L-NAME as a eNOS inhibitor ^{16, 17}. In this construct however, it is not possible to determine the source of the NO, as extracellular NO could diffuse into the cell, then react with the probe.

As discussed in section 1.1, an objective of this work is to determine the source of NO that reaches beyond an endothelial layer, to where the smooth muscle would be *in vivo*.

It is here where NO can participate in vasodilation in the smooth muscle. Therefore, to determine the NO beyond the endothelial layer, the extracellular fluorogenic probe, DAF-FM was used above an endothelial layer cultured on the membrane in the device shown in figure 2.1, and hypoxic RBCs pumped underneath this layer.

3.1.2 A Proposed Role for RBC-derived ATP in Hypoxic Vasodilation

The determination of the origin of the NO participating in vasodilation is important, because as discussed in chapter 1, the source of NO-mediated vasodilation is an actively debated topic in the current literature. It is known from chapter 2 and from others ¹⁸⁻²¹ that hypoxic RBCs release significantly more NO in comparison to normoxic RBCs. Furthermore, it was reported by the Spence group, ²² and others, ^{23, 24} that hypoxic RBCs also release ATP. This ATP is then able to activate eNOS in the endothelium by increasing calcium transport into the cell. ^{25, 26}

Therefore, there are two clear mechanisms by which NO may reach the smooth muscle in hypoxic tissue: firstly, it could be released from the RBC, diffuse through the endothelium, and to the smooth muscle, or ATP released from the RBC could activate eNOS, producing NO in the endothelium, which could then interact with the smooth muscle. While both may contribute, we hypothesize the ATP mediated NO release from the endothelium is more likely because it enables the unstable free radical molecule, NO, to diffuse a shorter distance. There are many recognized scavengers of NO in the bloodstream, such as glutathione, hemoglobin, and similar antioxidant systems can be found within the endothelial cells. ATP does not have this problem, and by stimulating NO production closer

to the smooth muscle, it is able to improve the chances of NO reaching the smooth muscle by reducing this distance.

To test this hypothesis, a microfluidic model of a blood vessel was developed, consisting of a channel mimicking a flowing bloodstream, through which RBCs can be pumped, and also a polycarbonate membrane that can act as a scaffold for cell culture. The microfluidic device is required because of the short half-life of NO,³⁰ as biologically relevant diffusional distances are used within the microfluidic model to reduce the time the bloodstream NO needs to be exposed to blood components.

3.1.3 Need for Confluent Cells

An important consideration in the experimental design of this system is achieving a confluent endothelial layer, which is reproducible from device to device³¹. As the polycarbonate membranes are not transparent, the cells cannot be observed using optical microscopy to determine their confluency, as would occur in a culture flask. While commercially available systems are available (Millicell ERS system by Millipore) to determine the confluency of a cell layer on a larger polycarbonate membrane,³² these measurements have only recently been performed in microfluidic systems.^{3, 33} Other methods to determine cell layer confluence involve determining the permeability of the cell layer to fluorescent molecules.³⁴ To improve the reproducibility of endothelial cell culture, which ultimately translated to improved results shown below, a trans-endothelium electrical resistance system integrated into the membrane based microfluidic device was developed.³

3.1.4 Basis of Trans-endothelium Electrical Resistance (TEER) Measurements

The basic premise for determining cell confluency by resistance measurements is that cell layer confluency is proportional to the impedance of the layer. If it is assumed that the major component of this impedance is resistance, one can then determine the resistance by applying a voltage across the cell layer, measuring the resulting current, and solving for resistance using Ohm's Law. However, to reduce the risk of observing faradic current from electrochemical processes, and because many cell types are known to respond to such a polarization,³⁵ it was desirable to use a potential pulse to determine the impedance. The commercial TEER system described above applies a pulse at approximately 12 Hz, so in the microfluidic system a value close to that of 20 Hz was selected. At this potential, however, the resulting current from the pulses contained a capacitive component, as an exponential decay was present as shown in figure 3.5, resulting in data similar to that seen in prior bipolar pulse techniques implemented in conductivity detectors. ³⁶⁻³⁸

At this point, determination of the RC time constant by fitting an exponential to the current data was considered, however this was computationally intensive for real-time data analysis. Instead, the individual current decays were integrated with respect to time, resulting in a charge value that was proportional to the impedance. These values were then considered proportional to the cell confluency as described in the recent manuscript.³

3.2 Methods

3.2.1 Microfluidic Device Fabrication

Microfluidic devices were fabricated as described in 2.3.1. Briefly, molds for microfluidic devices, or masters, were fabricated on silicon wafers using photolithography with channels 100 μm tall by 200 μm wide. PDMS slabs were cast using soft lithography methods described in 2.3.1, with polycarbonate track etched membranes with pore diameters of 0.2 μm. A change in well diameter to 1/8 inch was necessary to have a smaller volume of solution above the cells, as the larger volumes used in previous work resulted in excessive DAF-FM background signal. To facilitate this change to smaller well volume while maintaining compatibility with the plate reader, an additional guide, prepared by

removing the bottom of a standard well plate, was placed over the microfluidic device before insertion in the plate reader.

3.2.2 Culture of Endothelial Cells onto Microfluidic Device

Endothelial cell culture was accomplished using bovine pulmonary arterial endothelial cells that were cultured in T-25 culture flasks with DMEM containing 5.5 mM glucose, 10% (v/v) fetal bovine serum, and penicillin/streptomyocin. When cells were 80% confluent as verified with optical microscopy, they were either subcultured at a 1:3 ratio into new flasks or prepared for culture on microfluidic devices.

Microfluidic devices were prepared for cell culture by coating each well in the polycarbonate membrane with 12 μ L of 50 μ g/mL fibronectin, and subsequent exposure to UV light to sterilize. Completed devices were stored in a humidified 5% CO₂ incubator until use. Devices were not stored longer than 24 hours before use.

For subculture onto microfluidic devices, cells are detached from the flask with trypsin/EDTA, then washed off with culture media, and centrifuged at 1500 rpm for 5 minutes. The pellet was then resuspended in 400 μ L of culture media. 12 μ L of this solution were then pipetted into each well. After two hours media was changed, and every hour thereafter. The cells were cultured on the device for 12 hours prior to experimentation, with media changes.

Cells were then rinsed with HBSS three times and incubated with 1 mM L-NAME for 30 minutes in order to inhibit eNOS within the cells. The cells are then rinsed three times and prepared for flowing RBCs, by placing 5 µM DAF-FM in HBSS on the cells.

3.2.3 Verification of Use of 1/8" Wells

Previous work described in chapter 2 used wells that were ¼ inch in diameter. While this work presented here required smaller wells to observe NO production from cells, therefore it was necessary to validate that NO release from hypoxic RBCs could still

be observed in the smaller wells. In measurements performed on n=4 devices, NO release from hypoxic RBCs was shown to be statistically equivalent to that in figure 2.10.

3.2.4 Optimization of DAF FM for Extracellular Measurement

The concentration of DAF-FM above the bPAEC layer was optimized by placing 1 μ M ATP in varying concentrations of DAF-FM (from 3 μ M to 20 μ M) on endothelial cells treated with and without L-NAME. Standards from 100 nM DEANO to 2 μ M DEANO were also investigated on these devices. An optimal concentration of 5 μ M DAF-FM was determined as the NO release from the bPAECs was significantly greater than those inhibited with L-NAME and within the linear range of the DEANO standards.

3.2.5 Analysis of NO Release

DEANO standards were prepared in 5 μ M DAF-FM, and placed onto standard wells in the microfluidic device. After flowing RBC samples for 30 minutes at 1 μ L/min at 37 °C, the microfluidic device was transferred to the plate reader, and a black microplate with bottoms drilled out placed over the wells to minimize crosstalk and provide for optimal alignment. Fluorescence analysis was performed with an excitation wavelength of 485 nm and an emission of 515 nm.

3.2.6 Development of Software for Real-time TEER Measurements

The trans endothelial electrical resistance measurement system for use in micro-fluidic cell culture was based on a commercially available system consisting of a current generator that produced a square wave at approximately 12 Hz across a cell layer, and measured the resulting potential drop, which, through Ohm's law, can be converted to a resistance measurement.

To mimic this in a microfluidic system, a 12 Hz potential wave with amplitude of 1 V was applied across the cell layer using an analog output on a National Instruments DAQ board and the resulting current was measured. On an additional channel, the applied wave

was measured to assist in synchronizing timings. Between 20 and 40 periods of the current resulting from the square wave were collected at an acquisition rate of 1000 Hz, and analyzed by the software in real time.

As the current resulting from an resistive and capacitive (RC) circuit decays exponentially upon applying a DC potential, the first approach to converting these current versus time profiles to impedance (while the commercial system measures resistance, this value should be more appropriately described as an impedance, as the commercial (nor our) system make any attempt at separating the resistive and capacitive components) values was made through the use of nonlinear curve fitting with MATLAB scripts integrated with LabView.

Ultimately, improved reproducibility, along with optimal utilization of computing time, was achieved by analyzing the resulting current profiles by integrating them with respect to time. This method was computationally simpler and inherently averages the current data, reducing the signal to noise ratio. These average values, with units of Coulombs, were then proportional to conductance, or inversely proportional to resistance, allowing for their use as a TEER value.

3.2.7 Detection of RBC ATP

In order to verify the function of diamide as a ATP release inhibitor, and to verify previous work showing that hypoxic RBCs release significantly more ATP than normoxic RBCs²², static measurements of ATP release were performed using the luciferin-luciferase assay. For calibration and verification of assay function, ATP standards were prepared in normal PSS. A luciferin-luciferase solution was prepared by dissolving 100 mg of firefly lantern extract in 5 mL of deionized water. Approximately 2 mg of luciferin were then added to this mixture, and then centrifuged to remove insoluble components. Samples were

mixed 1:1 with the luciferin-luciferase solution and analyzed 10 seconds after mixing with a custom luminometer system fabricated in-house.

Briefly, the luminometer contained a Hamamatzu PMT, driven at 800 mV stored in a light-tight box. Current resulting from the PMT was amplified and converted to a potential with an Oriel i-V amplifier. The resulting potential was then recorded and averaged for 10 seconds using LabView software and a NI USB-6009 analog to digital converter.

Diamide inhibition of ATP release from RBCs was achieved by incubating 200 μ M diamide in PSS with a 7% RBC sample for 30 minutes. These samples were then centrifuged, and the supernatant replaced with PSS. As diamide inhibition of ATP release is known to be reversible³⁹, experiments were performed as close as possible to the time (within an hour) of removing the diamide solution.

3.3 Results

3.3.1 Quality of Cell Culture

Endothelial cell quality was measured prior to culture onto a microfluidic device, using optical microscopy to verify their cobblestone appearance, general confluency, and cellular health, observed by a lack of vacuoles, as shown in figure 3.1. After the cells were cultured onto the polycarbonate membrane, the cells cannot be visualized as easily as they can in culture flasks, because the polycarbonate membranes are not transparent. To observe their coverage over the microfluidic well, the cells were labeled with a nuclear dye, Hoechst 33342, which is a fluorescence stain which binds to nuclear material in the cell, and can be observed under a microscope with an excitation maximum of 350 nm and

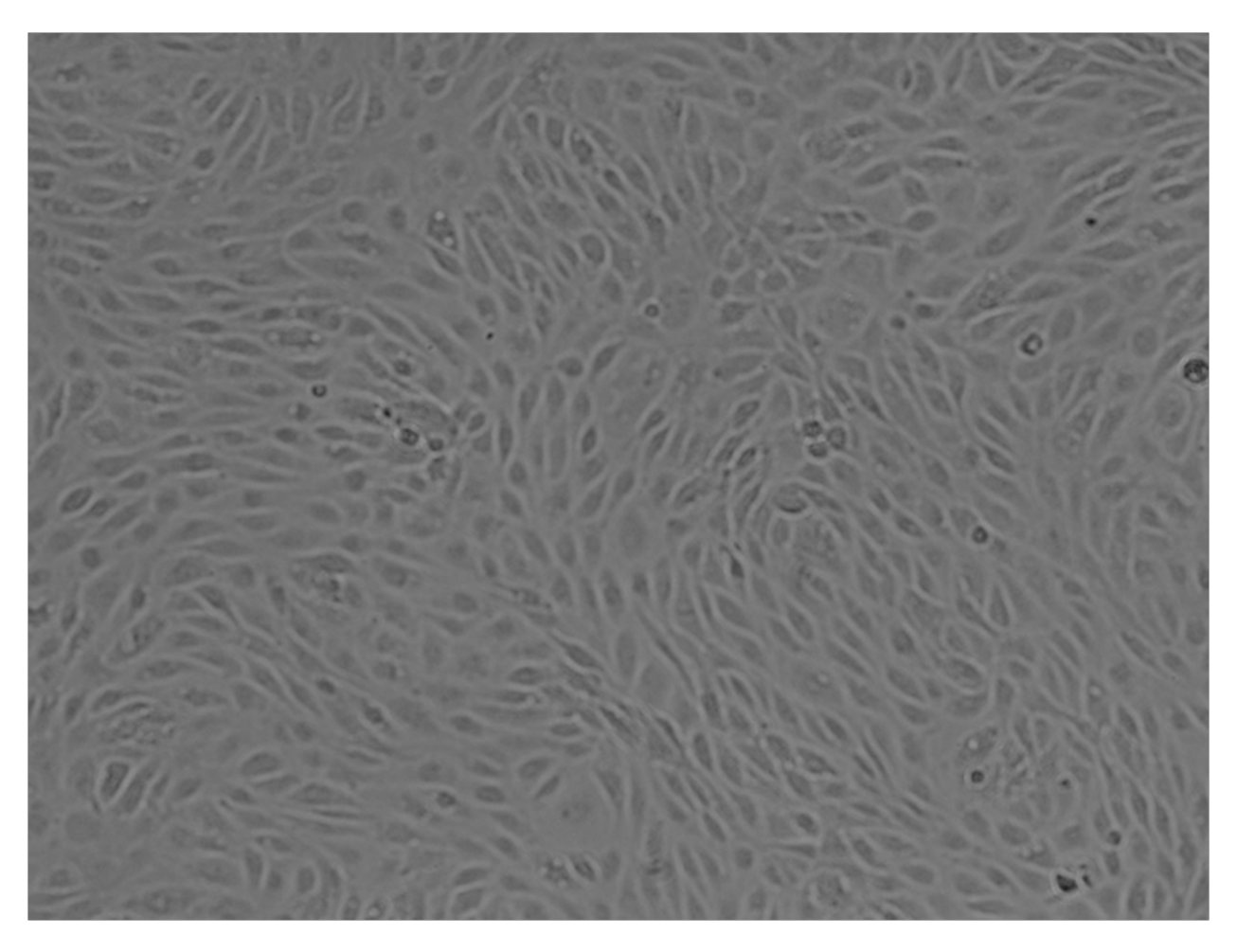


Figure 3.1: bPAECs in Culture Flask: Shown here are endothelial cells that exhibit the cobblestone appearance and high confluency often expected with endothelial cells. Cells were not used in microfluidic analyses unless this appearance was present. Furthermore, the absence of large vacuoles, which store excess waste products in the cell, in these cells suggest healthy cells.

an emission of 460 nm. This dye was chosen because its optical properties do not interfere with those of the DAF-FM probe.

3.3.2 NO Standards in 1/4" Versus 1/8" Wells

To improve the signal intensity of DAF-FM interacting with endothelial NO, the volume of each microfluidic well was reduced by shrinking the well diameter from 0.25 inches as described in chapter 2 to 0.125 inches. As this well size was not effective in determining NO release as described in chapter 2 due to insufficient alignment, a new alignment mechanism was developed where a traditional plate's bottom was removed with a Dremel tool, and placed over the microfluidic device before analysis. This improved this signal to noise sufficiently, and reduced the well-to-well crosstalk to almost nothing. As the volume of the wells, and ultimately the number of DAF-FM molecules were reduced to about 30% of their original value, signals from NO standards were similarly reduced by 30%. Linearity of standards was still observed, and when calibrated to these standards, NO transport as a result of release from hypoxic RBCs was found to be statistically equivalent to that described in chapter 2, for n=4 human RBC samples.

3.3.3 DAF-FM Optimization with Acetylcholine and ATP

Less NO was detected in the wells containing endothelial cells in those observing only RBC NO release Therefore, a new optimization of DAF-FM concentration needed to be performed. For these experiments, it was found as shown in figure 3.2 that to achieve

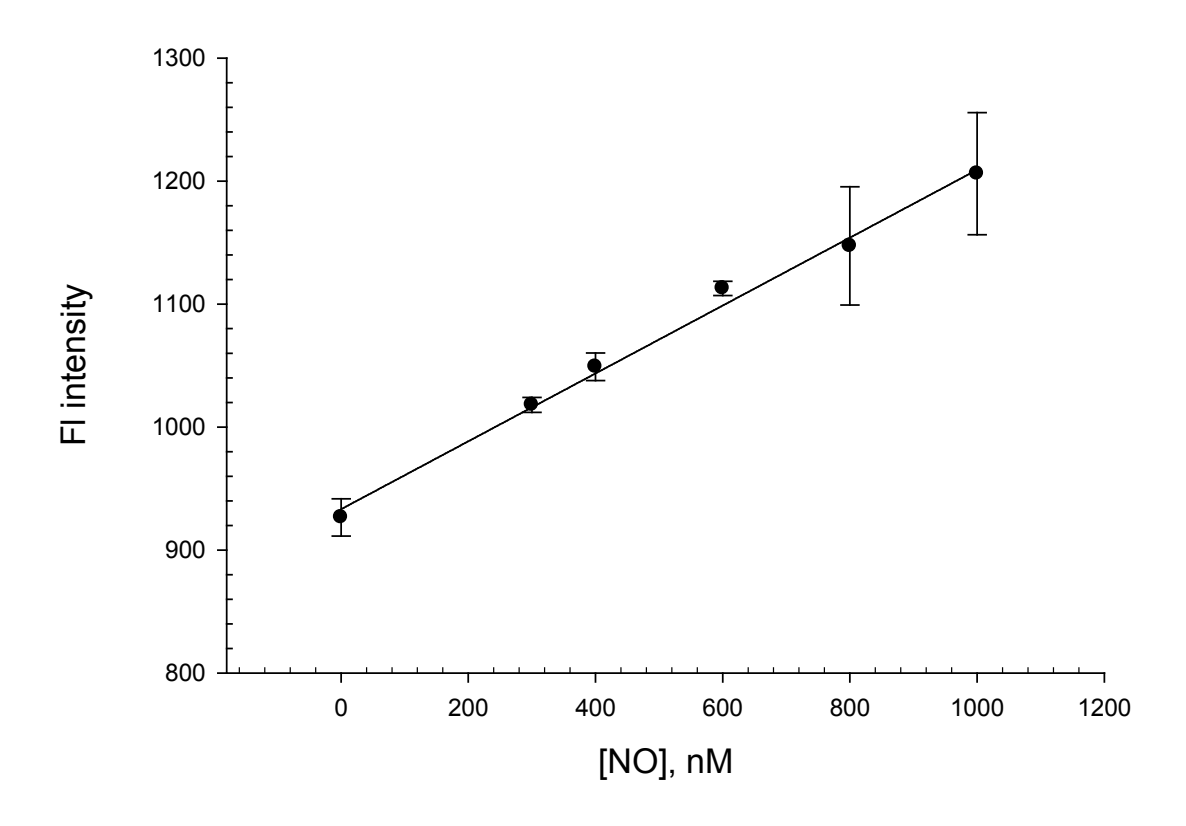


Figure 3.2: Sample calibration for NO release above membrane: Standards for these experiments were mixed with DAF-FM at a final concentration of 5 μ M and incubated at 37 °C. Shown here are n=4 samples in a single microfluidic device with error bars as standard deviations. A detection limit around 200 nM, with standards placed above the membrane, was common for these assays in the plate reader.

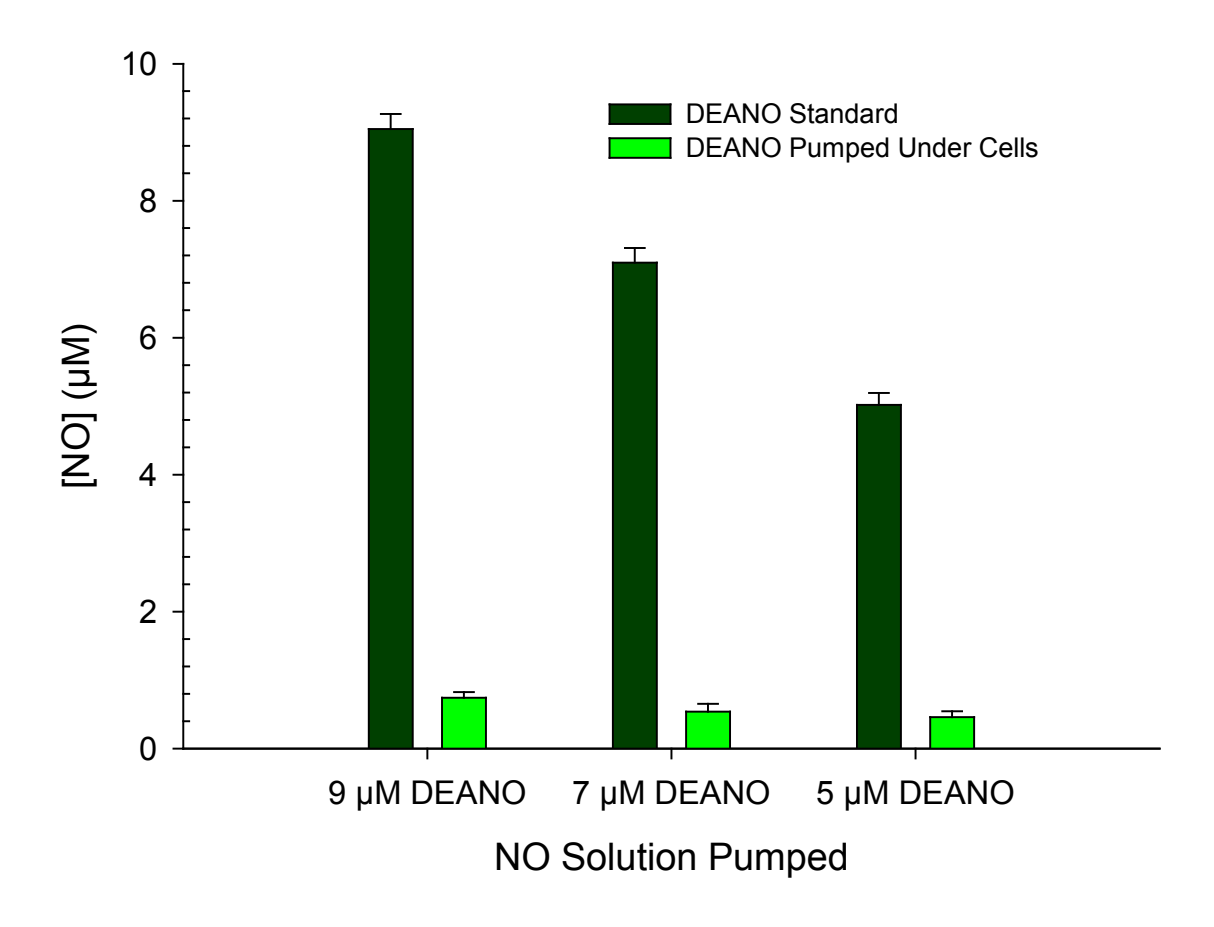


Figure 3.3: Endothelial Cells Decrease NO Transport Across Barrier: Shown here in n=4 devices, the presence of endothelial cells significantly reduces (p < 0.01) the amount of NO standard which is able to cross a polycarbonate membrane.

linear response to DEANO standards between 300 and 1200 nM, a DAF-FM concentration of 5 µM should be used and the microfluidic device operated at 37 °C.

It was determined this was an acceptable linear range for endothelial NO release by incubating endothelial cells with 100 μ M acetylcholine, a known calcium transport inducer, in addition to incubation with ATP.

3.3.4 Endothelial Cells Block NO Transport

After reliable calibration and measurement of endothelial cell derived NO was achieved, it was desirable to see if DEANO derived NO would cross an endothelial layer. A device similar to that described in chapter 2, but with the 0.125 in. diameter wells was used. In one half of the device, DEANO standards were pumped into wells containing just DAF-FM. In the other half of the device, the wells contained a confluent layer of endothelial cells, and the concentration of NO which crossed either the polycarbonate membrane or polycarbonate membrane plus endothelial cells was determined. For n=4 devices, as shown in figure 3.3, it was determined that the presence of a confluent layer of endothelial cells significantly reduced the NO that crossed the barrier, suggesting that RBC released NO may not cross the barrier.

3.3.5 ATP Release from Hypoxic RBCs

To further characterize the role of the RBC in the role of hypoxic vasodilation, it was necessary to verify the release of ATP from hypoxic RBCs and the effectiveness of diamide as an ATP release inhibitor. This was performed in a traditional cuvette using the luciferin-luciferase assay as described above. As shown in figure 3.4, there is a significant increase in ATP release from RBCs under hypoxic condition over RBCs under normoxic

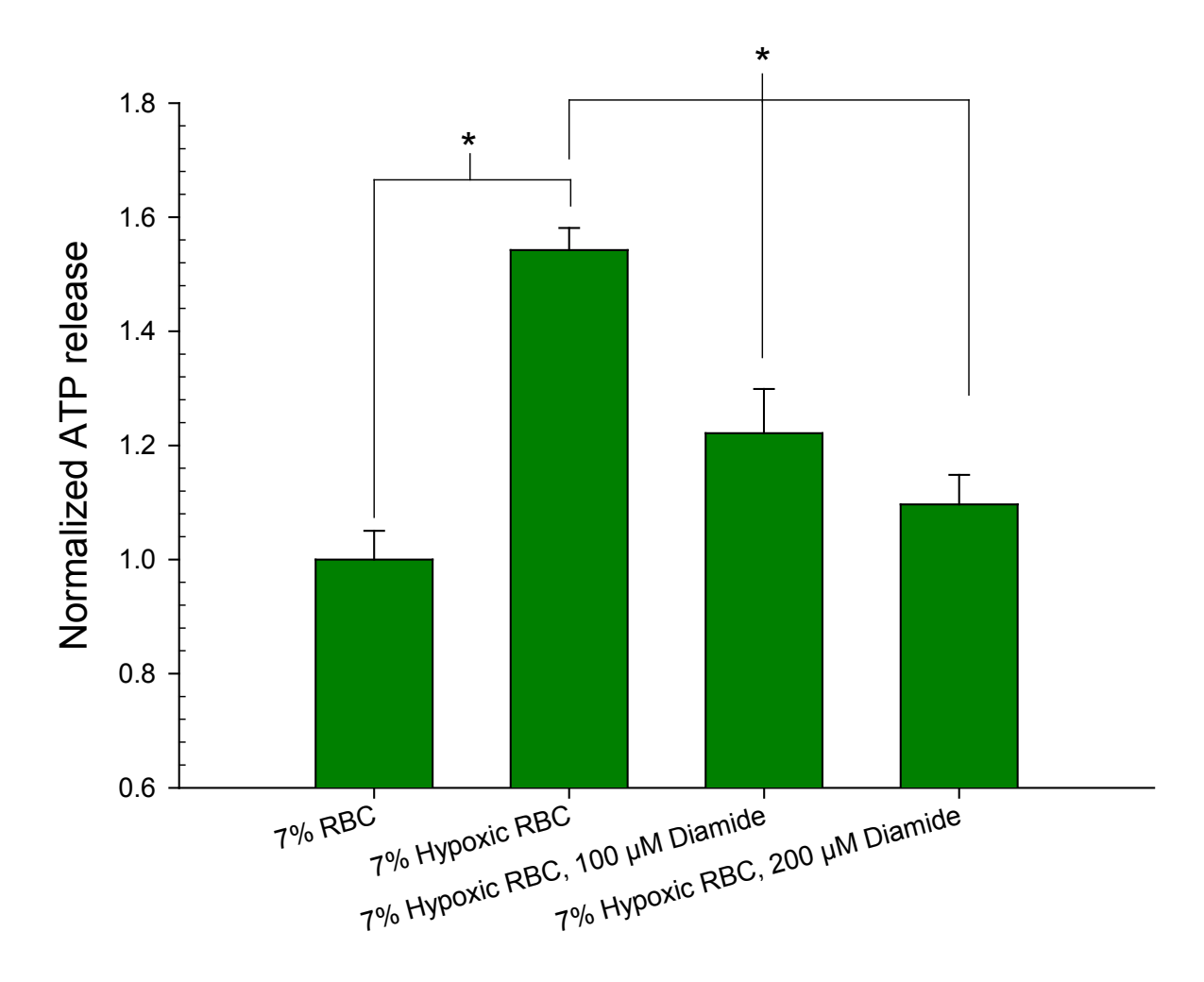


Figure 3.4: ATP Release and Inhibition from Hypoxic RBCs: As shown in figure 3.4, ATP release is significantly greater (n=3 human samples) under hypoxic conditions (*p < 0.03). Furthermore, this ATP release is inhibited, or significantly reduced in the presence of 100 μM or 200 μM diamide (*p < 0.03)

conditions. Furthermore, RBCs incubated with diamide, a known cell membrane stiffener, reduces the increase in hypoxic RBCs to that of normoxic RBCs.

3.3.6 TEER Data Processing

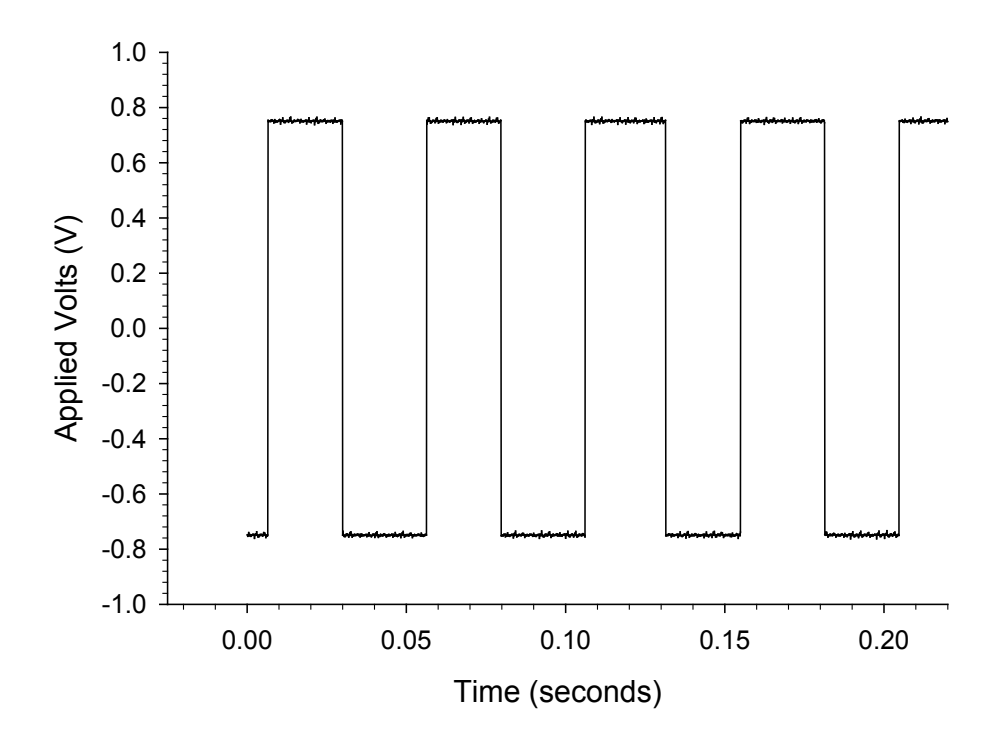
An important component in achieving the reproducibility necessary for this work was culturing the endothelial cells on the microfluidic device long enough to achieve reproducibly confluent layer. The cell culture time was verified using a microfluidic trans-endothelium electrical resistance measurement, developed in collaboration with Paul Vogel, within the Spence group. An example of the data obtained from the TEER system is shown in figure 3.5, where a square wave excitation potential was applied across the cells from a common aluminum electrode under the cell layer, to a copper electrode temporarily placed in the cell media for the duration of the measurement (tens of seconds). From this applied potential square wave, a current is measured which is characteristic of an RC circuit, having an exponential functional form as described in equation 3.1, where I is current, t is time, R is resistance, and C is capacitance

3.1
$$I(t)=I_0 e^{-t/RC}$$

These RC current decays were then integrated with respect to time to achieve a value in coulombs, which is indirectly proportional to resistance as shown in equations 3.2, where Q is charge, and V is voltage.

3.2
$$\int Q \partial t = \partial I / \partial t + c = V/R$$

As charge is inversely proportional to resistance, the charge should reach a minimum value at maximum cell confluency, as opposed to the commercial system which displays a resistance value, and maximum confluency is achieved when resistance is at a maximum.



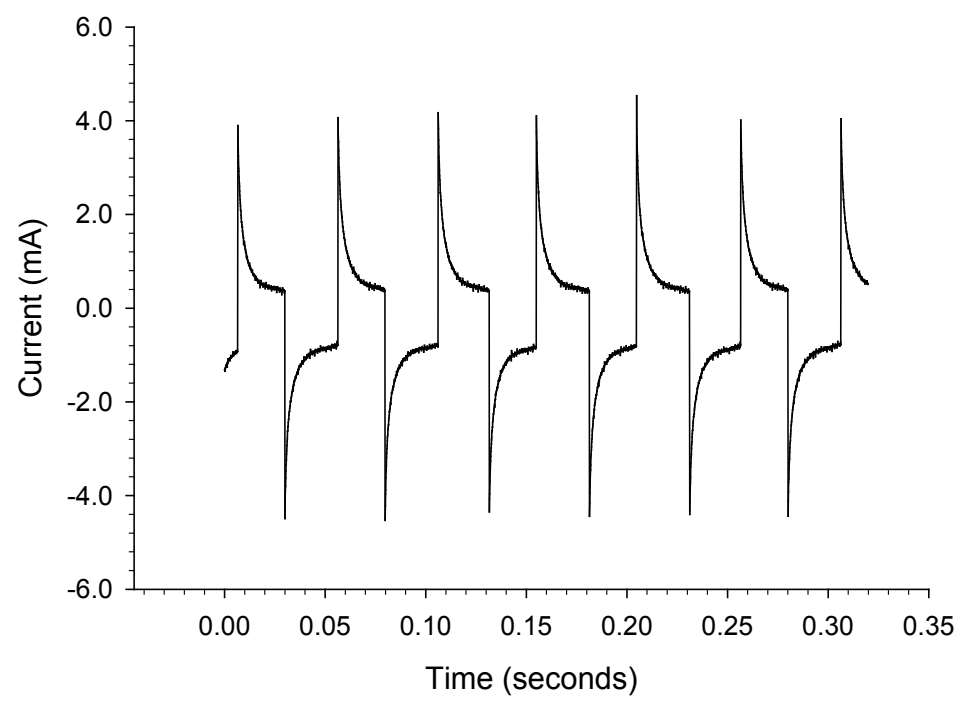


Figure 3.5: TEER system for determining endothelial cell confluency: (Top) is the perturbation used in the system, a square wave at 20 Hz. (Bottom) The resulting current through the electrodes was then measured, and an example output is shown in the bottom. These current versus time curves were then integrated, and the resulting charge values averaged for a set of 40 decays to produce a TEER signal, in units of charge.

Using this system, an optimal culture time of 8 hours was determined for endothelial cells on a microfluidic device.

3.3.7 NO Above Endothelial Layer Measurement

After reproducible confluent layers of endothelial cells could be cultured on the microfluidic device, and the verification shown in figure 3.3 that NO standards did not cross a confluent layer of endothelial cells, it was then desirable to determine the effect of RBC released ATP and NO on the amount of NO that is observed pass an endothelial barrier. Therefore, a set of inhibition studies were performed on both the endothelial cells and RBCs in which diamide was used to inhibit RBC ATP release, and L-NAME to inhibit endothelium NO synthesis. As shown in chapter 2, and figure 3.4, hypoxic RBCs release both NO and ATP. The RBC NO release does not have a known inhibitor, but ATP release, with a well understood pathway, has several. Diamide was chosen in this case as it is known to stiffen RBC membranes, reducing ATP release. While RBC NO release cannot be inhibited, endothelial NO release can be inhibited with L-NAME, an arginine analog which is a competitive inhibitor for eNOS.

As shown in figure 3.6, two sets of experiments were performed for each RBC sample: one on endothelial cells with L-NAME, and one on endothelial cells retaining eNOS function. In the presence of hypoxic RBCs, a significant increase over 7% RBCs was observed in NO production; however no significant difference was observed in endothelial cells treated with L-NAME. Furthermore, RBCs treated with diamide prior to exposure to hypoxic conditions did not result in an NO significant increase over normoxic

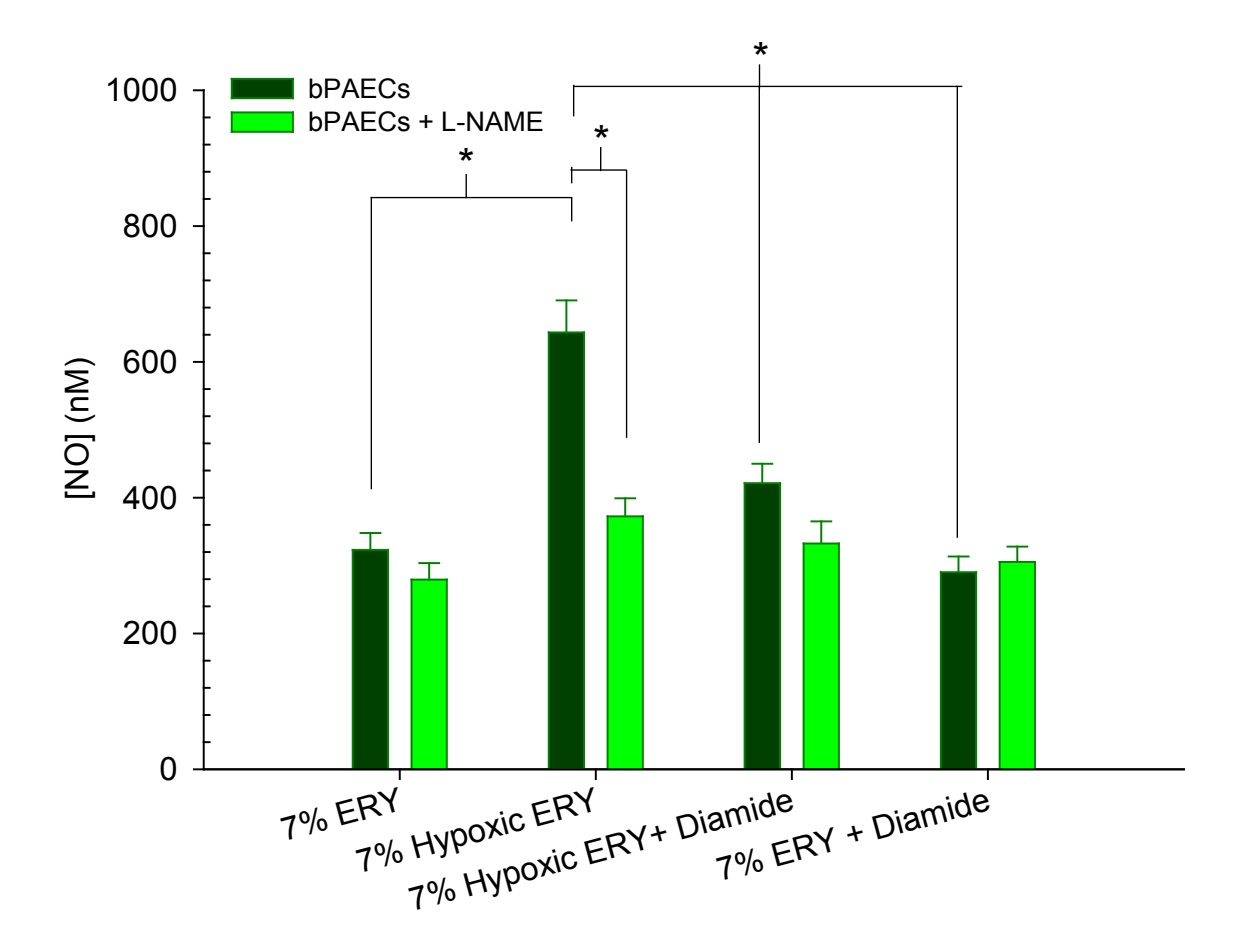


Figure 3.6: NO Past Endothelial Barrier is Endothelial-Derived. Calibrated to NO standards above the membrane, significantly more NO (p < 0.05) is detected in the presence of hypoxic RBCs, but not when endothelial NO is inhibited with L-NAME. Furthermore, incubation of RBCs with diamide prior to inducing hypoxia and flowing under the microfluidic device, no difference is observed, suggesting the NO which is detected requires both eNOS function and ATP release from the RBCs.

RBCs (n=4 devices). These findings suggest that NO which is able to cross an endothelial barrier requires both eNOS function, and ATP release from hypoxic cells.

3.4 Conclusions

3.4.1 Cell Culture and NO detection on Microfluidic Devices

One of the most integral requirements of these experiments was the quality of cells used in culture on the microfluidic device. While little difference was observed in relation to cell division number, health of the cells, as judged by presence of vacuoles, was important, to ensure the presence of healthy cells. Furthermore, minimizing time exposed to trypsin in cell culture was also important to obtaining NO signals simply in the presence of exogenous ATP, as observed in device optimization.

In addition to cell culture, one of the largest challenges in this work was obtaining a signal from the low concentration of NO released from a relatively smaller number of endothelial cells relative to the number of RBCs investigated in chapter 2. Reducing the well diameter, and ultimately the well volume by a factor of approximately 3 allowed the NO released by the endothelial cells to be at a sufficiently high solution concentration to be above the detection limit of the DAF-FM probe in the plate reader. Furthermore, the addition of a well plate, with the bottom removed, as a guide for microfluidic device alignment greatly simplified the process of aligning a microfluidic device in the plate reader.

As in this experiment, NO which reached beyond an endothelial layer was more relevant to predicting vasodilation than that released in a flowing channel, calibration was somewhat simpler, as standards DEANO standards could be pre-mixed with DAF-FM off chip, and then pipetted onto wells contained in the microfluidic device prior to experimentation. As standards did not require flow, they did not need to use the available flow channels, so that more replicates of the different inhibition studies could be performed on each microfluidic device. Also, obtaining linear response of DAF-FM to DEANO standards

required incubation at 37 °C, requiring the microfluidic device to be housed in a humidified oven during experimentation, potentially increasing the response of the endothelial cells over previous work where room temperature was used.

In determining the optimal linear range for endothelial cell investigation a series of stimuli which were easy to reproduce included 1 μ M ATP in HBSS, which is known to activate purinergic receptors on endothelial cells, and 100 μ M acetylcholine, which causes an increase in intracellular calcium in the endothelial cell. Both suggested that a linear range between 300 nM and 1200 nM would be an effective choice for observing endothelial NO release.

Once reproducible endothelial cell culture could be achieved, and in particular the time needed for a layer of cells on a polycarbonate membrane to reach constant confluency was determined, NO standards, in the absence of RBCs, were pumped underneath layers of endothelial cells, and through bare membranes, and the NO which crossed the barriers determined. In the absence of endothelial cells, standard curves similar to those used in chapter 2 were observed, but in the presence of endothelial cells, the NO which crossed the endothelial barrier was significantly reduced, suggesting that RBC derived NO may not cross an endothelial barrier.

3.4.2: Inhibition Studies of ATP Release and eNOS-derived NO

It is not possible under hypoxic conditions to inhibit NO release from RBCs; therefore it was desirable to verify the ability to inhibit ATP released using previously known mechanisms²². Diamide was chosen because it is known to stiffen RBC membranes, reducing ATP release as a result of hypoxia. To validate the function of the inhibitor, RBCs were treated with diamide, then centrifuged, then made hypoxic with the Oxyrase enzyme system. As shown in figure 3.4, a significant increase over normoxic RBC ATP release (p <

0.03, n=3 human samples) was only observed in hypoxic samples without diamide, showing the effectiveness of diamide as an inhibitor.

3.4.3 TEER Measurements on a Microfluidic Device

After reliable quantitative determination of NO and ATP inhibition were achieved, reliable cell culture was needed to improve the reproducibility of these experiments, in particular those used to obtain figure 3.3. The integral component to achieve this reproducibility came from a project with another student in the lab. The goal of this project was to determine when endothelial cells on a microfluidic device were at optimal confluency, with the intention that this system would be used in blood brain barrier permeability studies. In this project, a LabView based system which, as shown in figure 3.5, applied a square wave potential across a cell layer, measured and recorded the resulting current, and in real time was developed. The resulting current was integrated as a function of time to obtain charge passed across the cell barrier in a given pulse. This signal was then inversely proportional to the resistance, or confluency of the layer. Using this technology, we showed that endothelial cells do not reach a constant confluency for at least 8 hours after culture onto a microfluidic device, and considering that previous attempts only used one or two hours of incubation time to achieve confluency, it was suspected that an extended incubation time would allow for a more confluent, and therefore more accurate model to study transport of compounds across an endothelial barrier. After implementation of an extended incubation time, the data obtained in figure 3.3 was much more reproducible.

3.4.4: NO Available to the Smooth Muscle Requires RBC ATP Release and eNOS Function

Once reliable cell culture and manipulation of RBC ATP and NO release were achieved, investigating the cell-to-cell communication between the RBC and endothelial cells was possible, and it was possible to determine the origin of the NO which was able to reach the upper side of the endothelial barrier. To detect this NO, the DAF-FM extracel-

lular probe was utilized to detect NO as opposed to the intracellular diacetate form used previously in our group, because we were interested in determining how much NO would be able to access the smooth muscle. One potential outcome for the NO released from the RBC is that it diffuses across the endothelium membrane, as it is lipophilic, and then consumed intracellularly in the endothelium. If the intracellular probe was used, there would be no way to determine the source of the NO.

Furthermore, from the work in chapter 2, it is known that the microfluidic system utilized to model a blood vessel in vitro does not obstruct transport of NO across the polycarbonate membrane; indeed these devices can be used to determine NO release from the RBCs. Therefore, if RBC released NO is not observed to cross the endothelial barrier, the endothelial cells must be preventing its potential transport to the smooth muscle.

Figure 3.7 shows NO which is above an endothelium, calibrated to standards pipetted onto separate wells on the same microfluidic device. The first set of data in figure 3.7 indicates basal NO release from endothelial cells in when RBCs are pumped underneath with no stimulus for ATP nor NO release, however basal levels of both are likely present. Signals of less than 500 nM are consistent with previous experimental results¹. Values reported in Hulvey et al. are slightly lower than those reported here, however instantaneous electrochemical investigation was used there, in a smaller volume, whereas here we are using a large volume, but integrating (with the DAF-FM probe) the NO over the course of 30 minutes.

The second set of bars in figure 3.7 show a statistically significant increase in NO detected above the endothelial layer when endothelial cells are exposed to hypoxic RBCs. Importantly this increase is not observed when endothelial NO production is inhibited with

L-NAME. Therefore, this suggests the NO observed beyond the endothelium in the presence of hypoxic blood components is endothelial derived.

The third set of bars shows the NO detected above the endothelial barrier when RBC ATP release is inhibited by diamide, as shown in figure 3.4. In this case, the NO detected above the cell layer is significantly reduced from the increase seen for hypoxic RBCs interacting with NO-synthesis active endothelial cells, showing the NO which crosses the endothelial barrier is ATP-mediated. It is worth noting that after incubating RBCs with diamide, the NO release, using the device described in chapter 2, is statistically equivalent (n=3 samples) to those not incubated with diamide, therefore, diamide does not affect RBC NO release.

Considering the data shown here and in chapter 2, we now know that hypoxic RBCs release increased amounts of both ATP and NO. This data shown in figure 3.3 suggest NO which is pumped under an endothelial barrier is prevented from crossing this barrier, and then the data shown in figure 3.7 suggest NO released from hypoxic RBCs does not cross the barrier as well. ATP however, as suggested by diamide inhibition, does play a role in the NO which crosses the endothelium; specifically, when ATP release from hypoxic RBCs is inhibited by diamide, a significant increase in NO above the endothelial barrier is not observed.

Considering these findings, this data suggests that NO increase which is available past an endothelial layer resulting from hypoxic RBCs is observed only with ATP release from the RBCs and when eNOS is not inhibited, showing a major role for RBC ATP release in vasodilation.

REFERENCES

REFERENCES

- 1. Hulvey, M. K.; Martin, R. S., Anal. Bioanal. Chem. 2009, 393 (2), 599-605.
- 2. Hulvey, M. K.; Genes, L. I.; Spence, D. M.; Martin, R. S., *Analyst* **2007**, *132* (12), 1246-1253.
- 3. Vogel, P. A.; Halpin, S. T.; Martin, R. S.; Spence, D. M., *Analytical Chemistry* **2011**, 83 (11), 4296-4301.
- 4. Genes, L. I.; Tolan, N. V.; Hulvey, M. K.; Martin, R. S.; Spence, D. M., *Lab on a Chip* **2007**, *7* (10), 1256-1259.
- 5. Kojima, H.; Urano, Y.; Kikuchi, K.; Higuchi, T.; Hirata, Y.; Nagano, T., *Angewandte Chemie-International Edition* **1999**, *38* (21), 3209-3212.
- 6. Kojima, H.; Nakatsubo, N.; Kikuchi, K.; Kawahara, S.; Kirino, Y.; Nagoshi, H.; Hirata, Y.; Nagano, T., *Analytical Chemistry* **1998**, *70* (13), 2446-2453.
- 7. Kojima, H.; Hirata, M.; Kudo, Y.; Kikuchi, K.; Nagano, T., *J Neurochem* **2001,** 76 (5), 1404-10.
- 8. Hartell, N. A.; Archer, H. E.; Bailey, C. J., *Biochem. Pharmacol.* **2005**, *69* (5), 781-790.
- 9. Lepiller, S.; Laurens, V.; Bouchot, A.; Herbomel, P.; Solary, E.; Chluba, J., *Free Radical Biol. Med.* **2007**, *43* (4), 619-627.
- 10. Paul, D. M.; Vilas, S. P.; Kumar, J. M., *Nitric Oxide* **2011**, *25* (1), 31-40.
- 11. Celotto, A. C.; Restini, C. B.; Capellini, V. K.; Bendhack, L. M.; Evora, P. R., *Eur J Pharmacol* **2011**, *656* (1-3), 88-93.
- 12. Rau, C. S.; Yang, J. C.; Jeng, S. F.; Chen, Y. C.; Lin, C. J.; Wu, C. J.; Lu, T. H.; Hsieh, C. H., *Photochemistry and photobiology* **2011**, *87* (2), 441-6.
- 13. Mainz, E. R.; Gunasekara, D. B.; Caruso, G.; Jensen, D. T.; Hulvey, M. K.; da Silva, J. A. F.; Metto, E. C.; Culbertson, A. H.; Culbertson, C. T.; Lunte, S. M., *Anal Methods-Uk* **2012**, *4* (2), 414-420.
- 14. D'Atri, L. P.; Malaver, E.; Romaniuk, M. A.; Pozner, R. G.; Negrotto, S.; Schattner, M., *Curr. Med. Chem.* **2009**, *16* (4), 417-429.
- 15. Kelm, M.; Feelisch, M.; Deussen, A.; Schrader, J.; Strauer, B. E., *Journal of Cardiovascular Pharmacology* **1991**, *17*, S95-S99.
- 16. Sprague, R. S., Stephenson, Alan H., Dimmitt, Reed A., Weintraub, Neal A.,

- Branch, Carrie A., McMurdo, Lorraine, Lonigro, Andrew J., *American Journal of Physiology-Heart Circ Physiol* **1995**, *269* (38), H1941-H1948.
- 17. Sprague, R. S.; Olearczyk, J. J.; Spence, D. M.; Stephenson, A. H.; Sprung, R. W.; Lonigro, A. J., *Am. J. Physiol.* **2003**, *285* (2, Pt. 2), H693-H700.
- 18. Halpin, S. T.; Spence, D. M., *Analytical Chemistry* **2010**, *82* (17), 7492-7497.
- 19. Crawford, J. H.; Isbell, T. S.; Huang, Z.; Shiva, S.; Chacko, B. K.; Schechter, A. N.; Darley-Usmar, V. M.; Kerby, J. D.; Lang, J. D.; Kraus, D.; Ho, C.; Gladwin, M. T.; Patel, R. P., *Blood* **2006**, *107* (2), 566-574.
- 20. Diesen, D. L.; Hess, D. T.; Stamler, J. S., Circulation Research 2008, 103 (5), 545-553.
- 21. Jia, L.; Bonaventura, C.; Bonaventura, J.; Stamler, J. S., *Nature* **1996**, *380* (6571), 221-226.
- 22. Faris, A.; Spence, D. M., *Analyst (Cambridge, U. K.)* **2008,** *133* (5), 678-682.
- 23. Ellsworth, M. L.; Ellis, C. G.; Goldman, D.; Stephenson, A. H.; Dietrich, H. H.; Sprague, R. S., *Physiology* **2009**, *24* (2), 107-116.
- 24. Ellsworth, M. L., Acta. Physiol. Scand. 2000, 168, 551-559.
- 25. Arnal, J. F.; Dinh-Xuan, A. T.; Pueyo, M.; Darblade, B.; Rami, J., Cellular and molecular life sciences: CMLS 1999, 55 (8-9), 1078-87.
- 26. Marrero, M. B.; Venema, V. J.; Ju, H.; He, H.; Liang, H.; Caldwell, R. B.; Venema, R. C., *The Biochemical journal* **1999**, *343 Pt* 2, 335-40.
- 27. Raththagala, M.; Root, P. D.; Spence, D. M., *Analytical Chemistry* **2006**, *78* (24), 8556-8560.
- 28. Reynolds, J. D.; Ahearn, G. S.; Angelo, M.; Zhang, J.; Cobb, F.; Stamler, J. S., *Proceedings of the National Academy of Sciences of the United States of America* **2007**, *104* (43), 17058-17062.
- 29. Stamler, J. S.; Simon, D. I.; Osborne, J. A.; Mullins, M. E.; Jaraki, O.; Michel, T.; Singel, D. J.; Loscalzo, J., *Proceedings of the National Academy of Sciences of the United States of America* **1992**, *89* (1), 444-448.
- 30. Hakim, T. S.; Sugimori, K.; Camporesi, E. M.; Anderson, G., *Physiological Measurement* **1996**, *17* (4), 267-277.
- 31. Gumbleton, M.; Audus, K. L., *J. of Pharm. Sci.* **2001,** *90* (11), 1681-1698.
- 32. Pasternak, A. S.; Miller, W. M., *Biotechnol Bioeng* **1996**, *50* (5), 568-79.
- 33. Douville, N. J.; Tung, Y.-C.; Li, R.; Wang, J. D.; El-Sayed, M. E. H.; Takayama, S.,

- Anal. Chem. (Washington, DC, U. S.) 82 (6), 2505-2511.
- 34. Young, E. W.; Watson, M. W.; Srigunapalan, S.; Wheeler, A. R.; Simmons, C. A., *Anal Chem* **2010**, *82* (3), 808-16.
- 35. Shamloo, A.; Ma, N.; Poo, M.-m.; Sohn, L. L.; Heilshorn, S. C., *Lab on a Chip* **2008**, *8* (8), 1292-1299.
- 36. Caserta, K. J.; Holler, F. J.; Crouch, S. R.; Enke, C. G., *Analytical Chemistry* **1978**, *50* (11), 1534-1541.
- 37. Johnson, D. E.; Enke, C. G., *Analytical Chemistry* **1970**, *42* (3), 329-&.
- 38. Shadpour, H.; Hupert, M. L.; Patterson, D.; Liu, C.; Galloway, M.; Stryjewski, W.; Goettert, J.; Soper, S. A., *Anal. Chem.* **2007**, *79* (3), 870-878.
- 39. Ghigo, D.; Bosia, A.; Pagani, A.; Pescarmona, G. P.; Pagano, G.; Lenti, G., *Ricerca in Clinica e in Laboratorio* **1983**, *13* (Suppl. 3), 375-81.

Chapter 4: Improved Control of Hypoxic Environments in Microfluidic Models 4.1 Introduction

4.1.1 Methods of Achieving Hypoxia and Applications to Sickle Cell Anemia

Previous investigations in the Spence group have used either purging with nitrogen of the Oxyrase enzyme system² to create an hypoxic environment for red blood cells (RBCs). Careful implementation of nitrogen purging provides an opportunity to achieve specific oxygen concentrations for investigating intermediate levels of hypoxia, but the oxygen concentration in solution must be measured after each purging. That is, the creation of hypoxic conditions using nitrogen purging typically is discrete in nature. The Oxyrase system has the advantage of being simple and stable over a long period (hours), but only allows investigations to be performed under continuously hypoxic conditions, as reoxygenation cannot easily occur, because the enzyme is always present in the system. In this case, the system is rather binary, as the oxygen tensions will either be saturated or near anoxic levels.

Hypoxic conditions are known to influence the RBC and its ability to participate in the regulation of vascular tone through the release of nitric oxide,²⁻⁴ and adenosine triphosphate (ATP).^{1,5-7} Furthermore, the behavior of the RBC, with respect to the release of ATP, can vary with shear stress induced by flow.⁸ Based on the ability of the RBC to respond to hypoxia and flow-induced shear, it would be desirable to investigate the effects of hypoxia on the function of the RBCs in flowing streams.

Besides the RBC's response to hypoxic conditions, there are other motivations for creating a flow-based system with exquisite control of oxygen levels. Specifically, a recent interest of the Spence group is the investigation of the mechanism of hydroxyurea,⁹ the only proven therapy for people with sickle cell disease. Due to the importance of oxygen and the kinetics of hemoglobin-based sickling and polymerization in the RBCs of people

with sickle cell disease, it was anticipated that the development of a system that enabled oxygen control in real time and in a flowing stream would benefit studies involving sickle cell RBCs, such as rates of hemoglobin polymerization.

In order to improve the reproducibility involved in performing experiments at intermediate oxygen concentrations, to improve the rate at which oxygen concentration can be changed, and to precisely know the oxygen concentration of a flowing solution, it is necessary to develop a microfluidic system capable of controlling intermediate oxygen concentrations and accurately determine the concentration of oxygen in a flowing system with high precision.

4.1.2 Classical Electrochemical Detection of Oxygen

While fluorescence based techniques for detecting the oxygen concentration in an aqueous solution do exist¹⁰⁻¹², the integration of electrochemical sensors into microfluidic channels enables a simpler approach to determining the oxygen concentration in flowing solutions. This is because the signal to noise ratio in an electrochemical sensor is reduced as the dimensions are reduced (specifically the electrode area¹³) and because the signal is proportional to concentration, as opposed to optical techniques that can be dependent on the number of moles imaged at a given time, or path length (which can be significantly reduced in microchannel based systems). Furthermore, by merging technologies developed by Martin et al.,¹⁴ electrochemical sensors can be more reliable, reusable, and easier to fabricate than previously reported attempts.¹⁵⁻¹⁷

Amperometric based detection of oxygen has been established for several decades, ^{18, 19} and is commercially available (typically known as the Clark electrode, after its first developer) in physical formats similar to a pH electrode. In principal, an amperometric

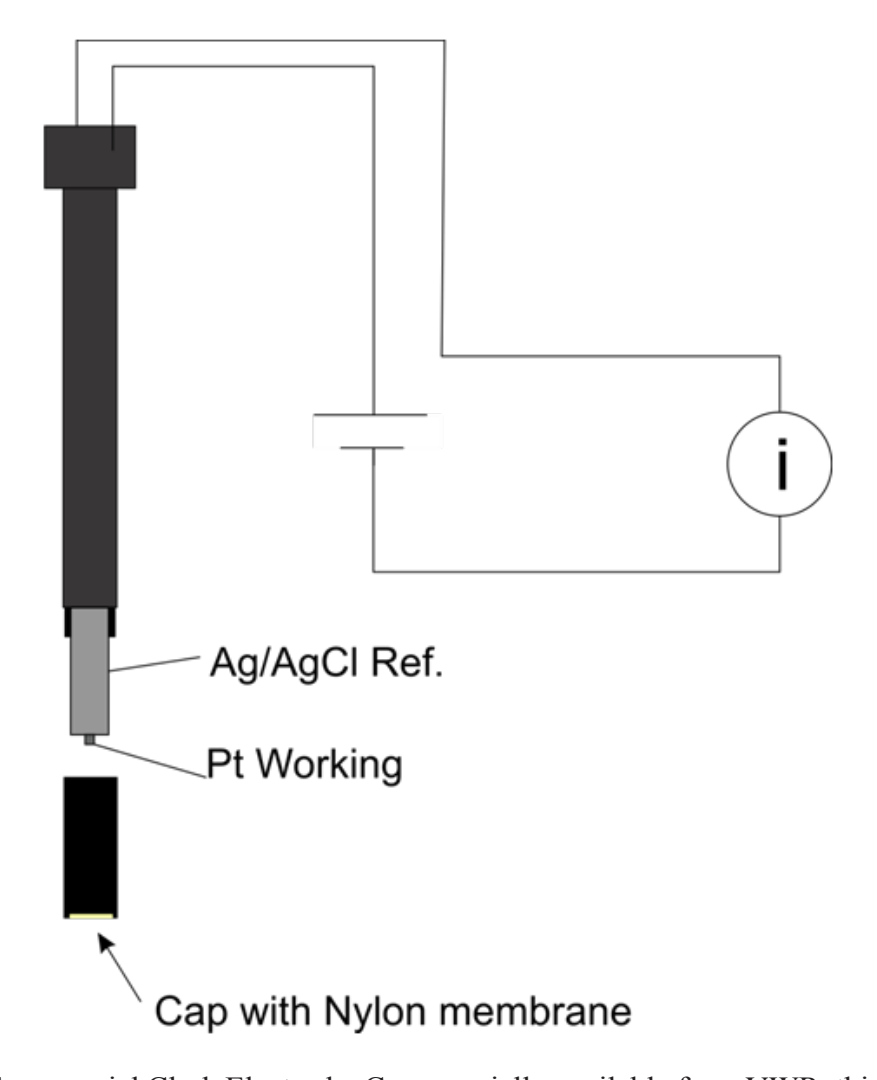


Figure 4.1: A Commercial Clark Electrode: Commercially available from VWR, this electrode has a coaxial electrode system with a silver chloride outer layer with a platinum disk inside. This disk is polished before use (not the reference portion). The cap is filled with the electrolyte solution prior to sealing. The cap contains a nylon membrane which, when screwed tightly to the body, seals over the electrode. The handheld portion of the meter contains a potential source and a means for measuring the current, along with software to perform calibrations.

oxygen sensor functions by reducing oxygen at either a gold or platinum working electrode by reaction 4.1:

4.1
$$O_2 + 4 e^- + 2 H_2O \rightarrow 4 OH^-$$

In practice however, there are several key challenges to long-term operation of an amperometric sensor detecting the reduction of oxygen. First, the reaction listed in 4.1 does not always go to completion, as hydrogen peroxide can be formed as an intermediate by two electron reduction of molecular oxygen. Secondly, the kinetics (and therefore the resulting current in the amperometric measurement) of this reaction are very temperature dependent, presenting a significant challenge during calibration. These problems can (and have) been overcome by using materials compatible with hydrogen peroxide, separating the hydrogen peroxide from cell layers with a physical barrier, by using high pH buffer solutions so the pH change is negligible, or through the use of relative calibration, the most frequent of which involves normalizing the observed current to that of a completely oxygen saturated solution.

While other materials have been investigated,²²⁻²⁴ the large negative potentials (-850 mV vs. a quasi Ag/AgCl reference) used for this reduction reaction, in addition to the pH restrictions mentioned above, restrict the electrode material choice to either gold or platinum. These restrictions are not overly-limiting, however, because the epoxy encasing technique used to form the disk electrodes for a microfluidic device is compatible with these metals.

Due to the high reduction potentials used, and the desire to utilize the sensor with biological samples, a membrane must be placed between the electrochemical sensor and the sample, as shown in figure 4.1. This membrane must be oxygen permeable, ²⁵ but also resistant to fouling by samples presented to the sensor. Furthermore, it should not be permeable to any other species present in the sample that can be reduced at the applied potentials.

In addition, the membrane should allow for selection of an electrolyte solution without concern of its impact on the biological samples and enable the use of a high pH buffer, as the PDMS membrane is not permeable to protons.

Several membrane materials have been utilized since the development of the Clark electrode including nylon, Teflon, Mylar, cellophane, latex and polydimethylsiloxane (PDMS). Of these, nylon is most frequently used in commercial implementations because of its mechanical robustness, high resistance to biofouling, and its high oxygen permeability. PDMS, however, offers higher oxygen permeability, and is easily fabricated into desired shapes and thicknesses. Furthermore, a fairly complete understanding exists of the fouling characteristics of PDMS in the presence of our desired samples (blood components). PDMS is not without limitations; it offer less mechanical stability, which has been a challenge in its use in some laboratory settings such as screens and assays requiring high throughput.

While there are examples in the literature of Clark electrode integration into microfluidic devices, ¹⁵ it is the goal of the work presented as part of this thesis to use a simpler fabrication technique enabling reusable electrodes, which greatly reduce the complexity and cost of using such sensors. Developed by Martin's group, ¹⁴ this technique involves fabricating an epoxy disk that has a gold (working) wire and silver (reference) wire cured into it. These can then be sanded to form disk electrodes flush with a flat surface, ideally suited for sealing a microfluidic channel. A robust sensor fabricated in this manner can then

be easily integrated into a microfluidic system that controls oxygen concentration and/or monitors oxygen concentration in a channel.

4.2 Methods

4.2.1 Verification of Oxyrase Function with Commercial Clark Electrode

Oxyrase enzyme solution was purchased and used as-is from the manufacture, was used as a convenient way to deoxygenate buffer samples in a predictable and reproducible manner without excess foaming of the solution, which frequently occurs when purging with inert gases. It is dissolved at a concentration of 1:10 (from the original, purchased solution) in buffer, and after 30 minutes the buffer is typically hypoxic as shown in figure 4.6.

The rate of deoxygenation was measured with a commercially available Clark electrode from VWR using their pH Symphony system. The commercial electrode consists of a coaxial electrode configuration with a platinum disk at the center, and a Ag/AgCl quasi reference. The electrolyte solution is a KCl solution buffered to neutral pH. The working electrode is polished before each use, and the electrolyte solution changed after polishing. The oxygen permeable membrane is nylon sealed to a threaded cap that can be screwed into place for mechanical stability. It is calibrated to the flux of oxygen across the membrane (a known value in internal lookup tables) in a 100% relative humidity atmosphere. The commercially available sensor is also temperature corrected, however temperature changes were not observed in these experiments. To observe the rate of Oxyrase consumption of oxygen, signal readout was manually recorded from the commercially available sensor.

4.2.2 Deoxygenation with Sodium Sulfite, Argon and Oxyrase

In testing the microfluidic oxygen sensors, solutions were deoxygenated by several means, the most popular being oxygen consumption by reaction with the sulfite ion. The use of Oxyrase to produce deoxygenated solutions was summarized in 4.3.1. All methods

of deoxygenation were confirmed using the commercial Clark electrode prior to use in the microfluidic system.

The simplest method for deoxygenating a solution is similar to that described in chapter 2 for the nitric oxide standards, namely purging with an inert gas. In our lab, nitrogen and argon have been frequently used, and these can show complete deoxygenation of a solution in less than 10 minutes.

Sodium sulfite was used to deoxygenate solutions as the sulfite ion reacts with molecular oxygen according to reaction 4.2:

4.2
$$2SO_3^{-2} + O_2 \rightarrow 2SO_4^{-2}$$

To provide validation of the microfluidic based sensor against the commercial sensor, various concentrations of sodium sulfite were prepared and the signals from the commercial sensor compared to those of the microfluidic sensor.

4.2.3 Fabrication of Epoxy Enclosed Disk Electrodes¹⁴

As summarized in figure 4.2, Armstrong C-7 epoxy and curing agent were used as received from Ellsworth Adhesives. A PDMS mold was prepared by mixing 10:1 PDMS to curing agent then curing the PDMS on a silicon wafer. A retaining ring for the epoxy was prepared from the same 10:1 PDMS by pouring it between a glass ring fabricated in the MSU glass shop and a 4 inch petri dish lid. The retaining ring is sealed to the flat piece of PDMS, forming the mold.

The bulk epoxy and curing agents are mixed 100:6 in a polypropylene centrifuge tube and centrifuged at 500 g for 3 minutes to remove bubbles. Vacuum cannot be used to degas the epoxy, such as with PDMS, because the epoxy curing agent is volatile. The degassed mixture is then poured in the mold and heated for 5 minutes in a convection oven at 75 °C to decrease the viscosity of the mixture. Polished gold wires (200 µm diameter) and a polished silver wire (2 mm diameter) are placed in the epoxy and allowed to cure at room

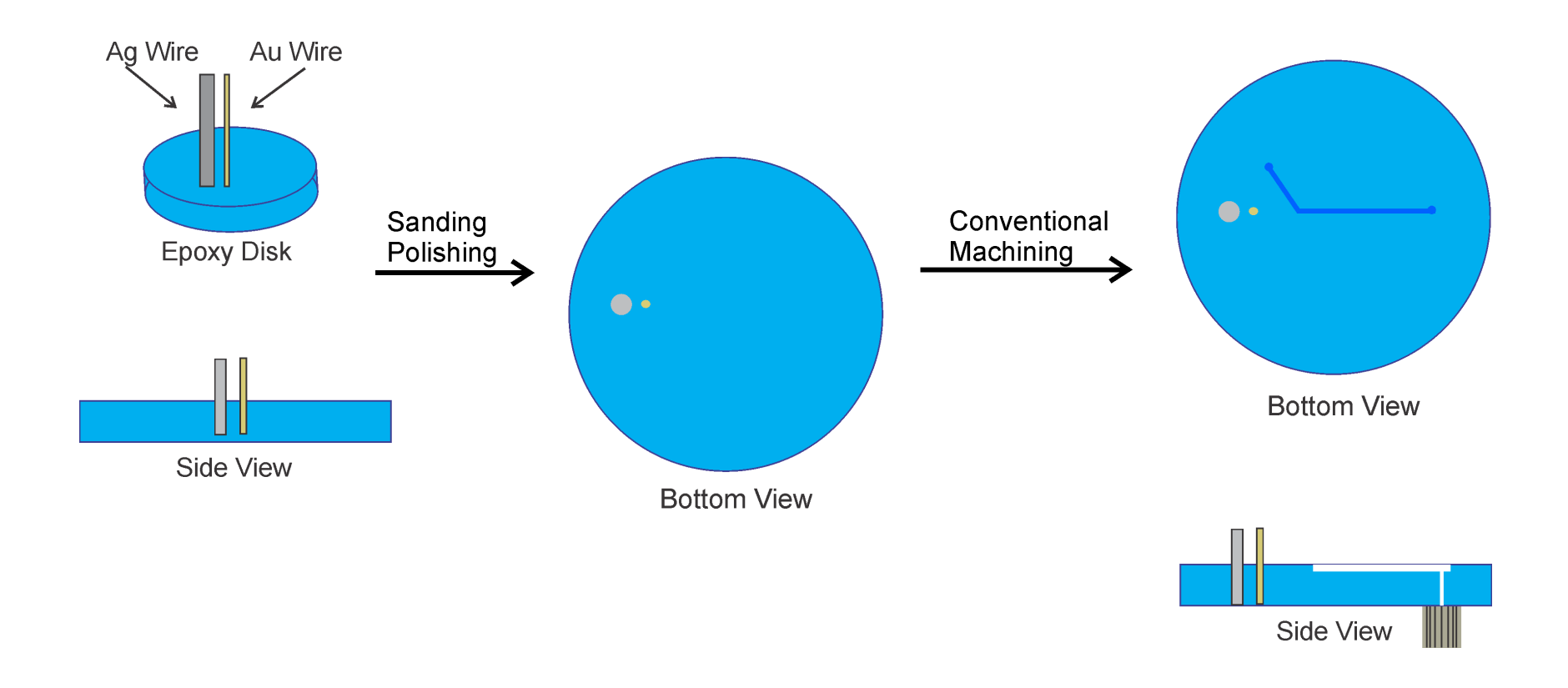


Figure 4.2: Fabrication of epoxy disk encapsulating disk electrodes: In fabricating the epoxy disk containing the electrodes, wires are placed into uncured epoxy, and the epoxy is cured. The resulting disk is then sanded until exposed wires are evident. Lastly, a channel is cut into the epoxy disk using a rotary tool, and a 1/16 inch fitting secured to the opposite side with JB Weld, producing the final electrode disk.

temperature overnight, which will result in hardening. The epoxy is then cured in the oven at 75 °C for 12 hours to finalize curing. The initial curing process is slow (i.e., performed at a lower temperature) to allow escaping of formed bubbles. The final high temperature curing is necessary to ensure complete curing.

After curing, the epoxy disk is removed from the mold, and sanded in progression from 80 grit sandpaper through 500 grit sandpaper until disk electrodes are visible, as verified with a conductivity meter (very thin nonconductive layers of epoxy are not easily visualized). If bubbles form near the electrodes, they can then be filled with epoxy and the sanding process repeated. After completion of the sanding process, the electrodes are polished with a suspension of 0.5 micron alumina in water on a felt polishing pad.

To verify solutions were not leaking along the side of the electrodes, a 200 μm wide by 100 μm tall channel in PDMS was sealed to the electrodes, and 20 ppm fluorescein in phosphate buffered saline was pumped over the electrode for one hour. Fluorescence micrographs were then taken to verify the absence of permeation along the length of the electrode.

In some studies, a channel was fabricated in the epoxy by milling with a 1/32 inch engraving bit and a rotary tool. The depth of the channel was controlled by placing the epoxy disk on a lab jack, and elevating it slowly.

4.2.4 Flow Injection System for Oxygen Detection

Summarized in figure 4.3, a flow injection system was assembled using a 6 port valve (VICI Inc., Houston, TX) and quartz capillary tubing (Polymicro, Phoenix, AZ). Early investigations suggested the Tygon tubing typically used in the lab was somewhat oxygen permeable, thus suggesting the use of the quartz tubing. Syringe pumps (Harvard Apparatus) along with 500 μ L gastight syringes (Hamilton Inc.), were used to propel solutions at flow rates ranging from 0.5 μ L/min to 10 μ L/min. These syringes were luer-termi-

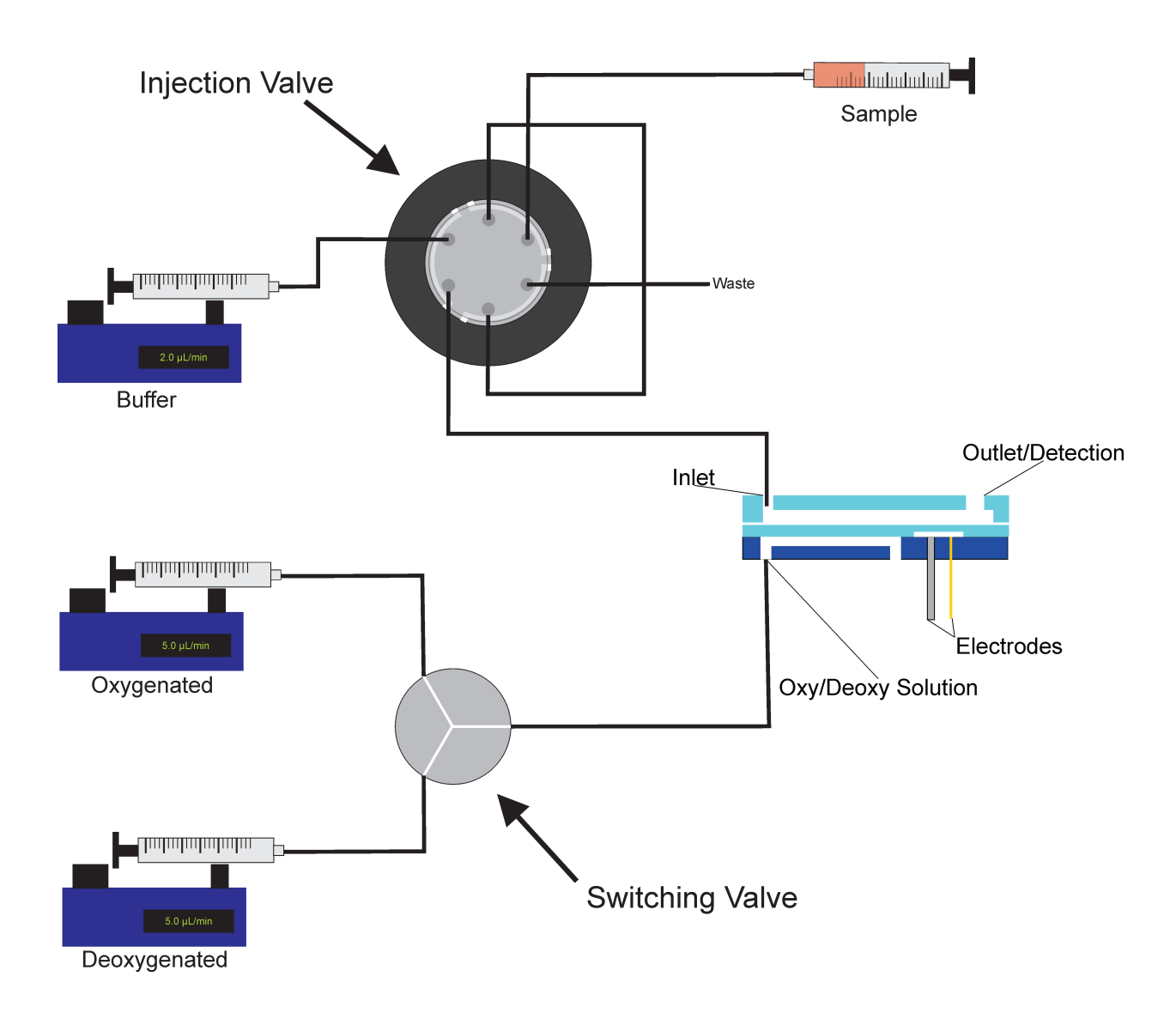


Figure 4.3: Flow injection system used for oxygen detection. Figure location: Shown above is the flow injection system used to inject samples of oxygenated or deoxygenated buffer onto the microfluidic device. Shown in the bottom is the method for changing the solution in the oxygenation/deoxygenation region from oxygenated to deoxygenated buffer. A switching valve is used between two pumps, and all connections made by quartz capillary tubing, allowing for minimal off-chip dead volumes in changing the solutions

nated, and $100~\mu m$ ID capillary tubing was attached to the male luer terminaton through an adapter that enables conversion to the standard 10-32 fitting, which was subsequently adapted to the outer diameter of the capillary tubing with a polymer sleeve.

The length of capillary tubing between the syringe pump and valve was approximately 30 cm in length, mostly for convenience. The injection loop consisted of varying pieces of capillary tubing, usually 250 μ m ID having lengths ranging from 10-30 cm. The valve was connected to capillary tubing 100 μ m in ID, and approximately 15 cm long. The device-to-capillary connection was made by removing the polyimide coating from 7 mm of the end of the capillary through flame exposure, then securing a stainless steel tube over this with JB Weld, producing a reliable, low volume termination compatible with the inlet design mentioned in Chapter 2.

4.2.5 Validation of Flow Injection System with Fluorescence Microscopy

In order to verify the functionality of the flow injection system independently from the electrochemistry, in addition to characterizing the time between injection and detection, custom software was developed in order to employ our existing Olympus MVX10 with mercury arc lamp excitation, fluorescence filter assemblies and Hamamatsu ORCA-ER camera in a same matter as a laser induced fluorescence system.

The flow injection system described in 4.3.5 was used to inject a sample of 10 ppm fluorescein into a 200 μ m wide channel sealed onto a polystyrene Petri dish at 3 μ L/min. The microscope was configured to use a FITC filter cube assembly, which has an excitation bandpass filter allowing 458 nm through 500 nm light to pass, a dichroic mirror with a cutoff at 510 nm, and a bandpass emission filter allowing 510 nm through 560 nm light

to pass, and the optics arranged to have an area of channel approximately 1 mm long fill 200x200 pixels on the camera.

Software to provide fluorescence as a function of time (a feature not available on the software which came with the instrument) was written using LabView 2010 (National Instruments) and Hamamatsu's freely available LabView driver version 2.0.1. Also required on the computer is a 1394 (FireWire) interface and the latest DCAM drivers. It is worth noting that the latest DCAM drivers are incompatible with the Olympus software, yet required for the Hamamatsu LabView drivers.

The software is configured to sum the signal values of each pixel of a defined image area, and plot this as a function of time. Due to restrictions with the camera's rate at which it can capture an image, data collection rates were limited to approximately 15 Hz. Camera parameters such as exposure time (which also fundamentally limits data collection rate) and pixel binning configurations are available as well.

4.2.6 PDMS Membrane Fabrication

Membrane fabrication (shown in figure 4.4) begins with a clean silicon wafer. As summarized in Chapter 2, a layer of featureless SU-8 is cured onto the wafer through lithography because PDMS is less adherent to SU-8 photoresist than bare silicon. Next, a square shaped feature, allowing space for the electrolyte solution after device fabrication, is prepared by placing an additional layer of SU-8, approximately 40 μm thick, using the thinned photoresist techniques described in Chapter 2. This is followed by development, producing the master used for membrane fabrication.

PDMS of lower viscosity is prepared by mixing 5 g of 10:1 PDMS with 1 g of toluene. This mixture is then poured onto the master and spin-coated at 500 rpm for 15 seconds, then 1000 rpm at 30 seconds. It is then cured for 30 minutes at 75 °C. To facilitate

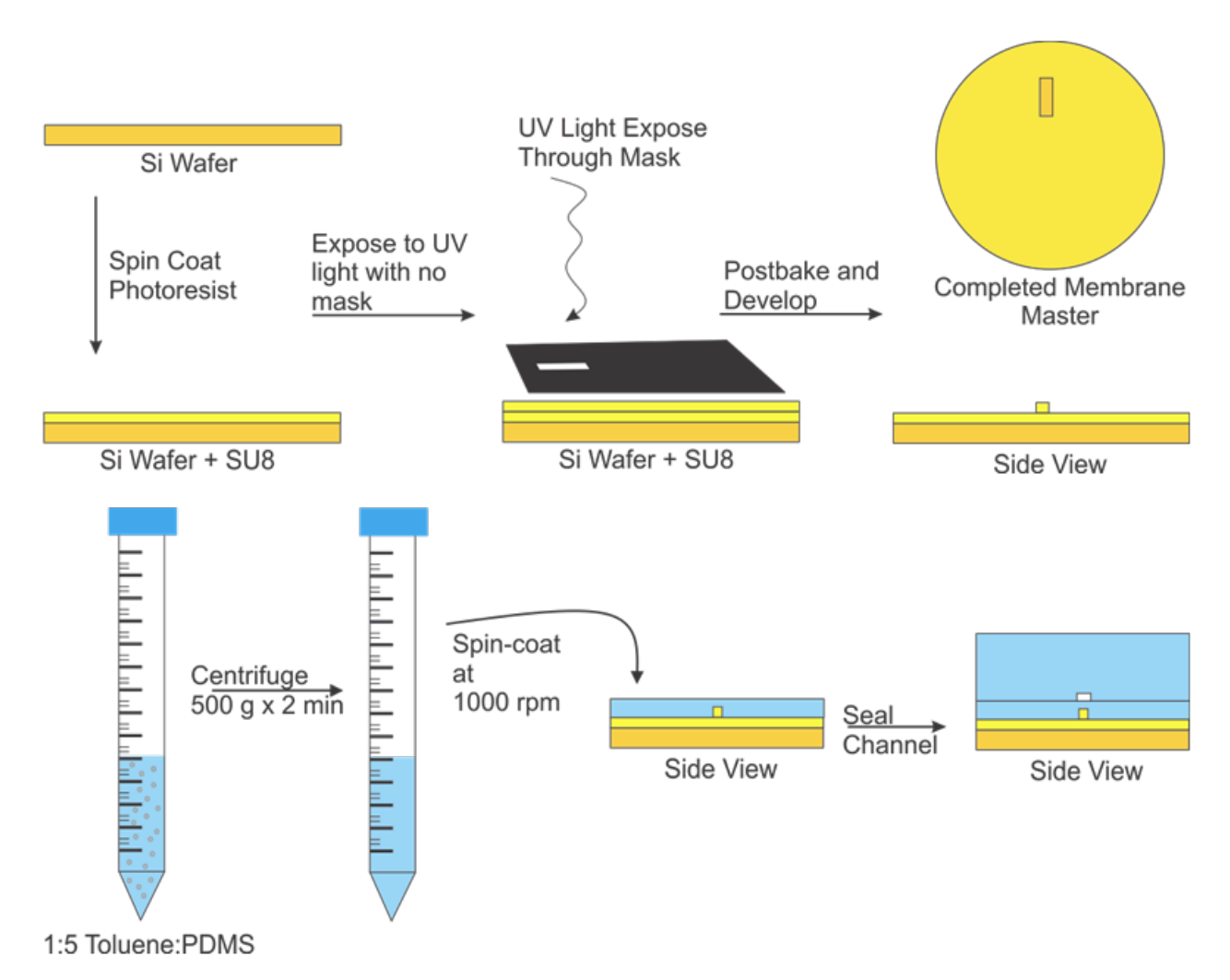


Figure 4.4: Fabrication of PDMS membranes: As shown above, a master is prepared with two layers of SU-8, the top layer containing a square feature which will hold the electrolyte solution above the working electrodes. Below is shown the process of casting a PDMS membrane and subsequent sealing of the channel above the membrane.

removal of the thin membrane, a bead of 10:1 PDMS is poured around the outside of the membrane.

A channel with features punched (inlets and outlets), along with the membrane still on the master, are cleaned with isopropanol, dried, then exposed to air plasma for 2 minutes. The channel and membrane are irreversibly cured together, followed by removal as a single unit. This completed device is then placed over the electrolyte solution.

4.2.7 Operation of Electrochemical Oxygen Detection Device

The epoxy disk containing electrodes is polished, and a AgCl layer is formed on the silver disk by electrolysis from a 3 M KCl solution using a 9 V battery as a potential source. Next, 3 µL of electrolyte solution (100 mM KCl, 25 mM TRIS at pH 10) are pipetted onto the electrodes, and the completed membrane-channel assembly is placed over the electrolyte solution. The flow injection system described in 4.3.4 is connected to the inlet, and the outlet is plumbed to waste off-chip. The outlet plumbing is in contrast to many devices used in the group but was performed in this application because collection of waste over the electrodes can result in changes in baseline signals.

Cyclic voltammetry, operated between 0 V and 1.0 V at 0.1 V/sec, with a quasi-reference system was used to determine that 850 mV versus the Ag/AgCl quasi-reference electrode was the potential to be used for amperometric detection of oxygen.

4.2.8 Observation of Linear Response of Microfluidic Device to Oxygen

While it is desirable to verify linear response of the microfluidic sensor to oxygen, it is difficult to produce reliable oxygen standards for measurement in the laboratory. Therefore, to verify linear response, solutions of varying oxygen concentration were made by measuring precise volumes of 100 mM sodium sulfite into oxygenated solutions, then measuring these solutions with the flow injection system and comparing these signals to those

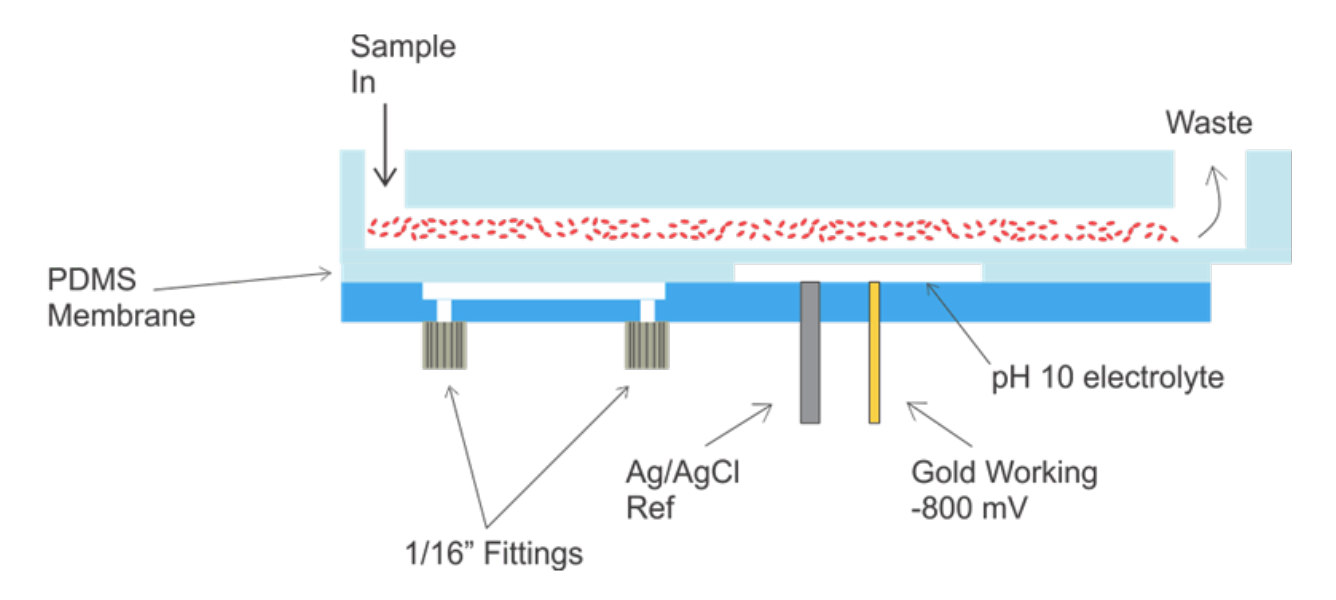


Figure 4.5: Final Device for Measuring and Controlling Oxygen Concentration: Shown in the left portion of the device is a region where a flowing sample can equilibrate oxygen concentration with a larger lower channel. The resulting change will then be measured in the right portion of the device at the Clark electrode fabricated within the epoxy. The waste would then be available for integration into other devices.

obtained using a commercially available oxygen electrode. This allows for verification of the standard concentration immediately before measuring on the microfluidic system.

4.2.9 Assembly of Device to Control Oxygen in Channel

The membrane and analytical channel assembly, which are irreversibly sealed together as described in section 4.3.5, are reversibly sealed to the electrode disk after addition of electrolyte solution. The bottom channel, in the epoxy disk, is much larger than the analytical channel, and contains an oxygenated or deoxygenated solution that is controlled by a switching valve as shown in figure 4.3. The top channel contains oxygenated buffer whose oxygen concentration can be controlled by adjusting the flow rate of the solution and the channel width. Controlling the oxygen level in this channel will enable control of the rate mass transport of oxygen across the membrane. The electrochemical sensor after the region where the two channels interact is then used to determine the change in oxygen tension. A diagram showing the complete device is summarized in figure 4.5.

4.3 Results

4.3.1 Deoxygenation Methods with Commercial Electrode

To briefly describe current efforts at making hypoxic solutions in the Spence group, and to verify the function of both our Oxyrase enzyme system and our commercially available Clark electrode, oxygen concentration in a Hanks' Balanced Salt Solution was monitored as a function of time after addition to Oxyrase. As summarized in figure 4.6, both the Oxyrase enzyme system and purging with a noble gas achieve deoxygenated solutions within 800 seconds. However Oxyrase deoxygenates solutions linearly, whereas the decrease in oxygen tension when purging with noble gases is exponential. Importantly, for many experiments requiring stability in oxygen concentration, Oxyrase maintains a deoxygenated solution for up to two hours. In comparison, samples purged with noble gases can re-oxygenate by exposure to atmospheric oxygen. The deoxygenation of an HBSS solution

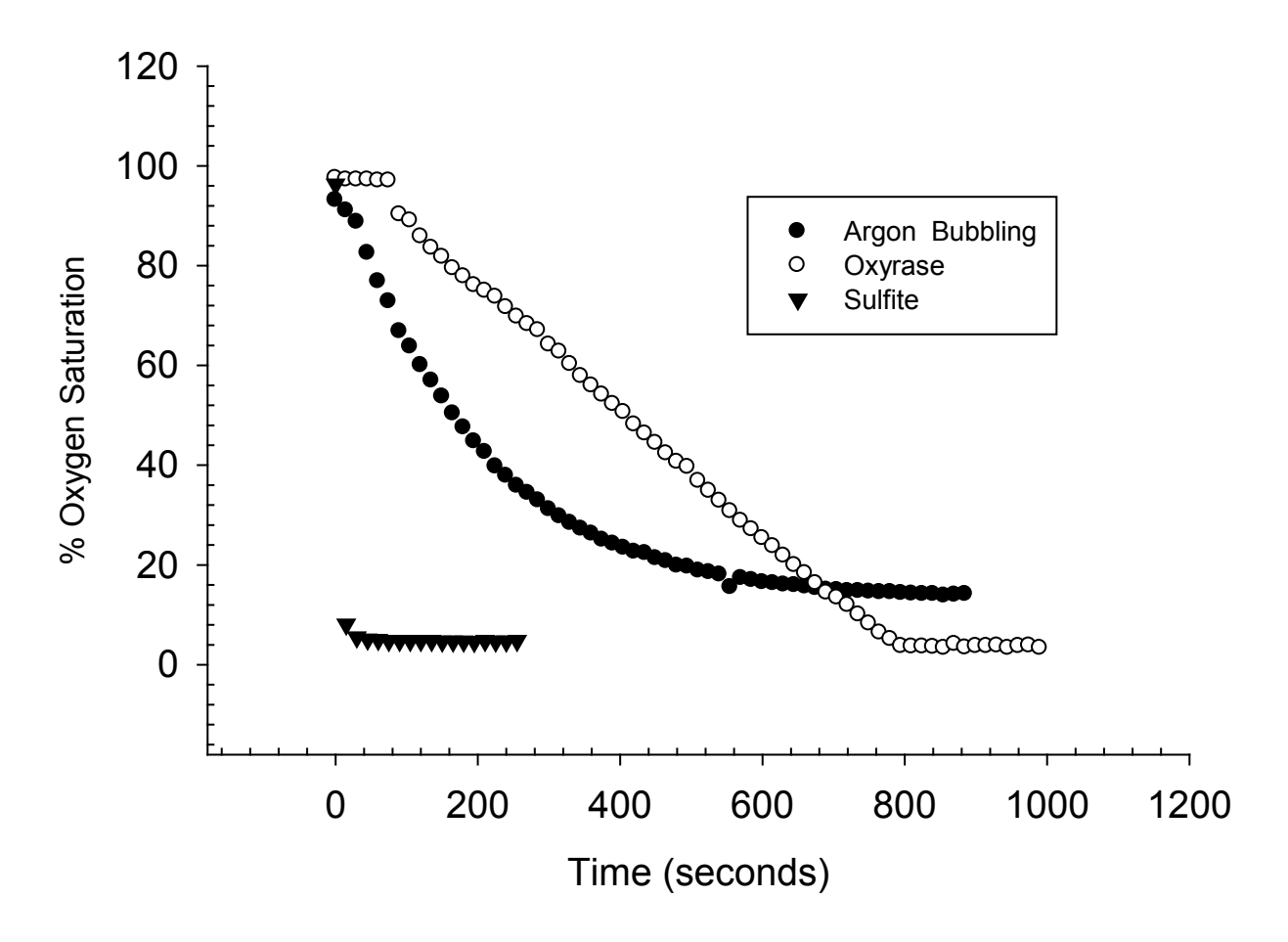


Figure 4.6: Deoxygenation rates of methods used in hypoxic investigations: Three methods of deoxygenation were investigated; first addition of sodium sulfite to solution caused a rapid and sustained deoxygenation. Argon purging resulted in deoxygenation, but this was susceptible to reoxygenation. All methods resulted in deoxygenation in 800 seconds.

with sodium sulfite, exemplifying the rapid reduction in oxygen concentration that occurs with this method of deoxygenation, is also shown in figure 4.6.

4.3.2 Validation of Flow Injection System

To periodically validate the syringe pumping systems and flow injection systems, fluorescein injections were made into a channel similar to that used for electrochemical investigations. These precision of the obtained signals confirmed that the system was a reliable method to verify the function of the flow injection system, and the flow injection system was sufficient for use in characterizing the electrochemical systems.

4.3.3 Validation of Microfluidic Electrochemical System

Once the flow system was determined to be robust, validation of the microfluidic electrochemical system was required. This was performed in two steps; first verifying that the electrode-epoxy-channel interface does not leak, and is stable over several hours, and secondly, by performing electrochemical measurements on a reliable system such as the redox chemistry of the ferricyanide ion.

To verify no leaking in the channel or electrode, a PDMS channel was prepared and sealed over the electrodes, and a 10 ppm fluorescein solution was pumped through the channel for 2 hours. As shown in figure 4.8, no leaking is observed from the channel or around the electrode throughout the course of the experiment.

After verifying the stability of the fluidic portion of the devices, it was desirable to verify the electrochemical reliability with a stable system. First, to compare the Ag/AgCl quasi-reference electrode to a standard Ag/AgCl reference, cyclic voltammetry (CV) was performed to analyze the redox properties of the ferricyanide ion. An example voltammogram investigating this system is shown in figure 4.9.

Once the potentials that should be used to operate in a mass transport limited regime were determined, flow injection was used to verify the amperometric long-term

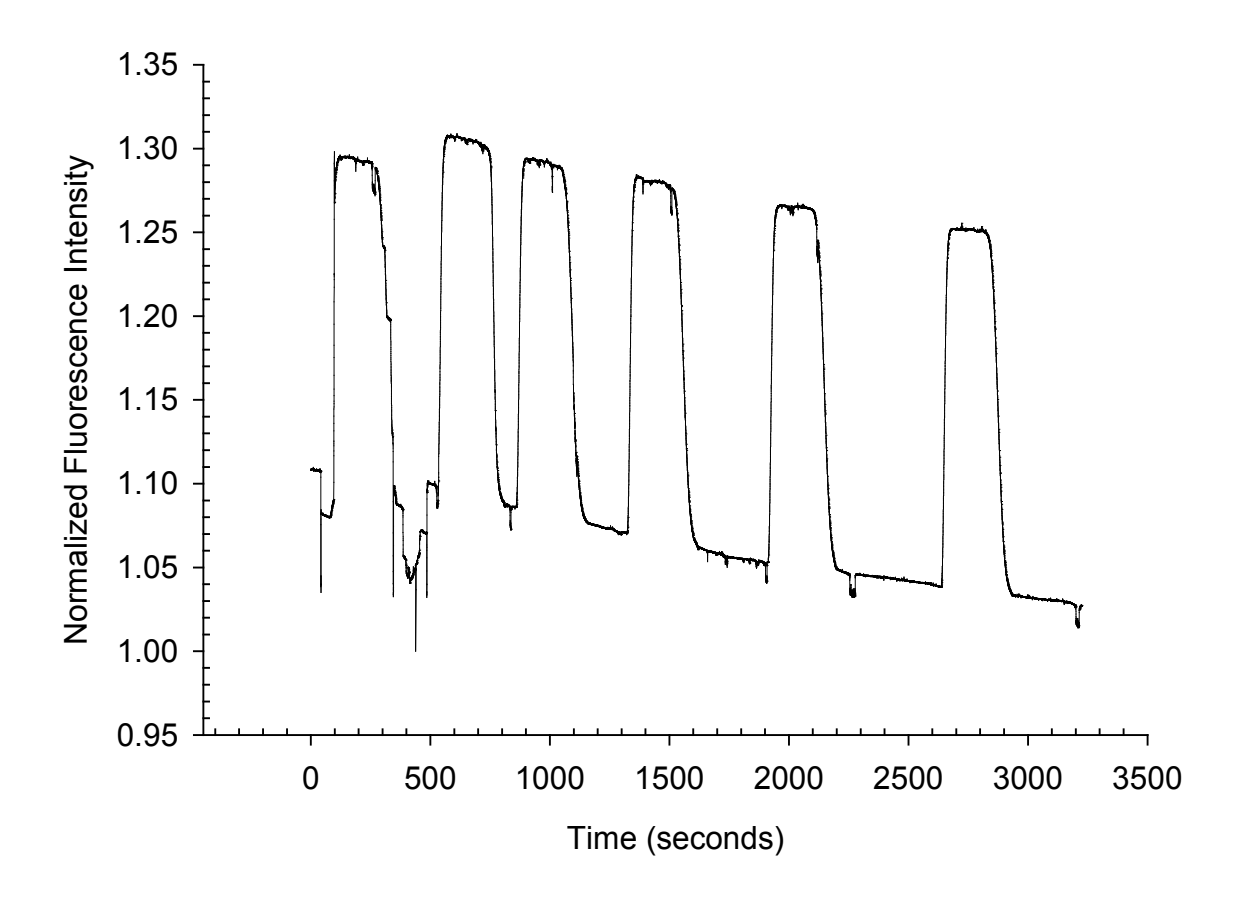


Figure 4.7: Validation of Injection System with Fluorescence as a Function of Time: Shown here is fluorescence as a function of time data validating the use of a large injection loop. Such an experiment was periodically necessary to verify a lack of clogging in the flow injection system, and also to determine the time from injection to detection independent of the membrane limited mass transport in the electrochemical system.

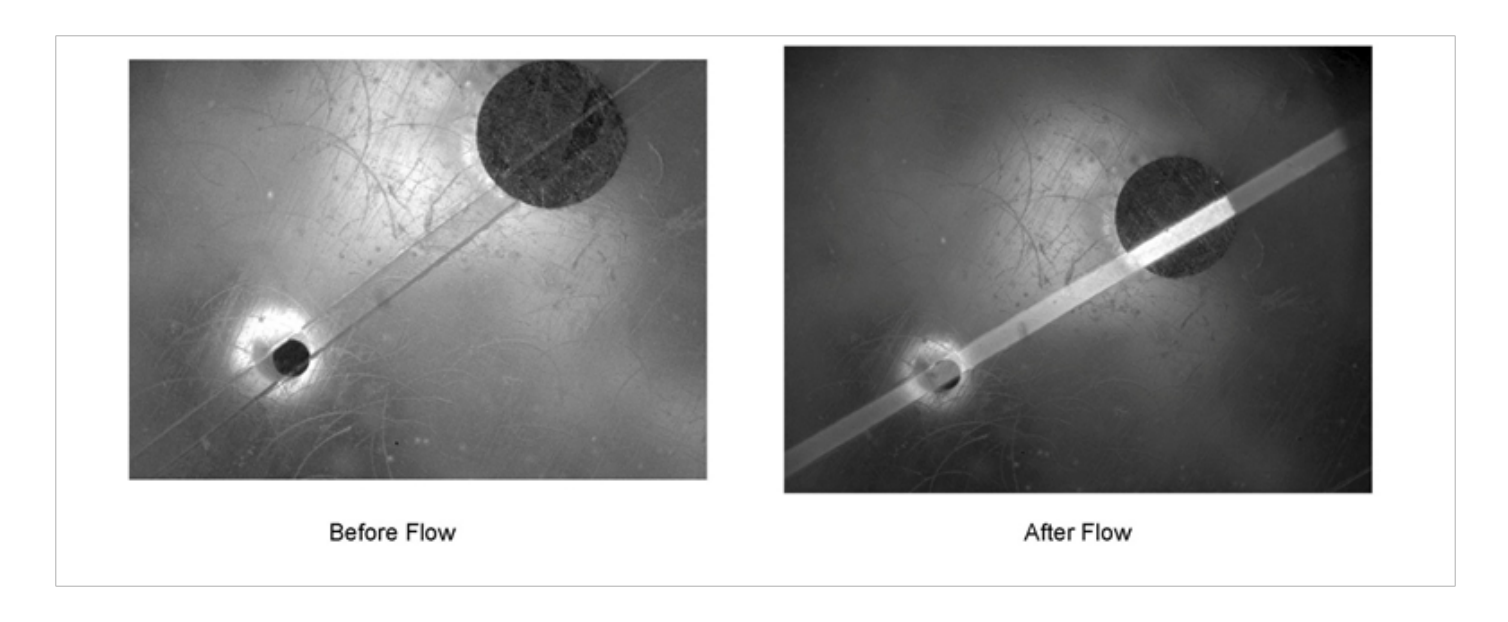


Figure 4.8: Validation of Seal Between Epoxy and PDMS: To verify no solution leaking from the channel, or along the length of the electrode into the epoxy, a picture was taken before and after flowing fluorescein over the electrodes in two hours. In the first picture, we see some autofluorescence around the working electrode that is present in the final image as well.

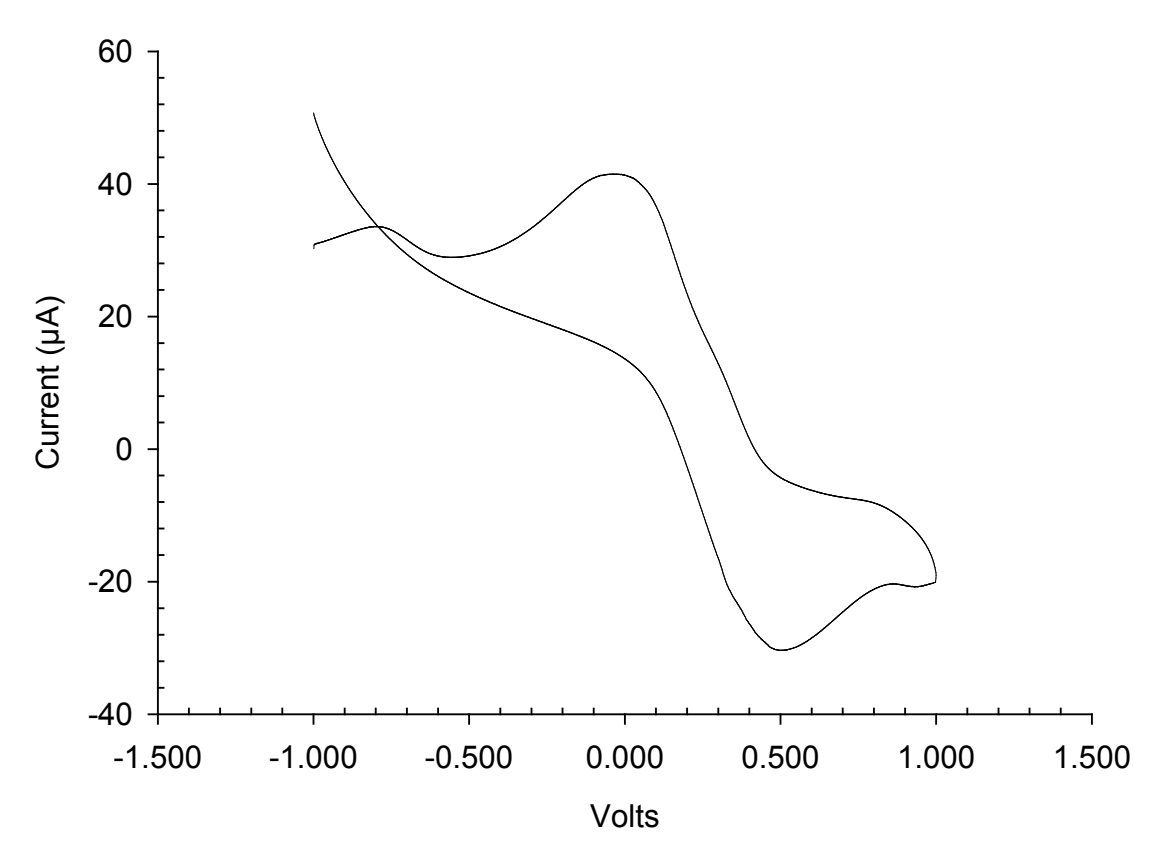


Figure 4.9: Cyclic Voltammetry of Potassium Ferricyanide on Microfluidic Device: Shown here is a voltammogram of 5 mM ferricyanide for the particular Ag/AgCl quasi reference electrode, indicating the potential of the quasi-reference relative to a standard redox system.

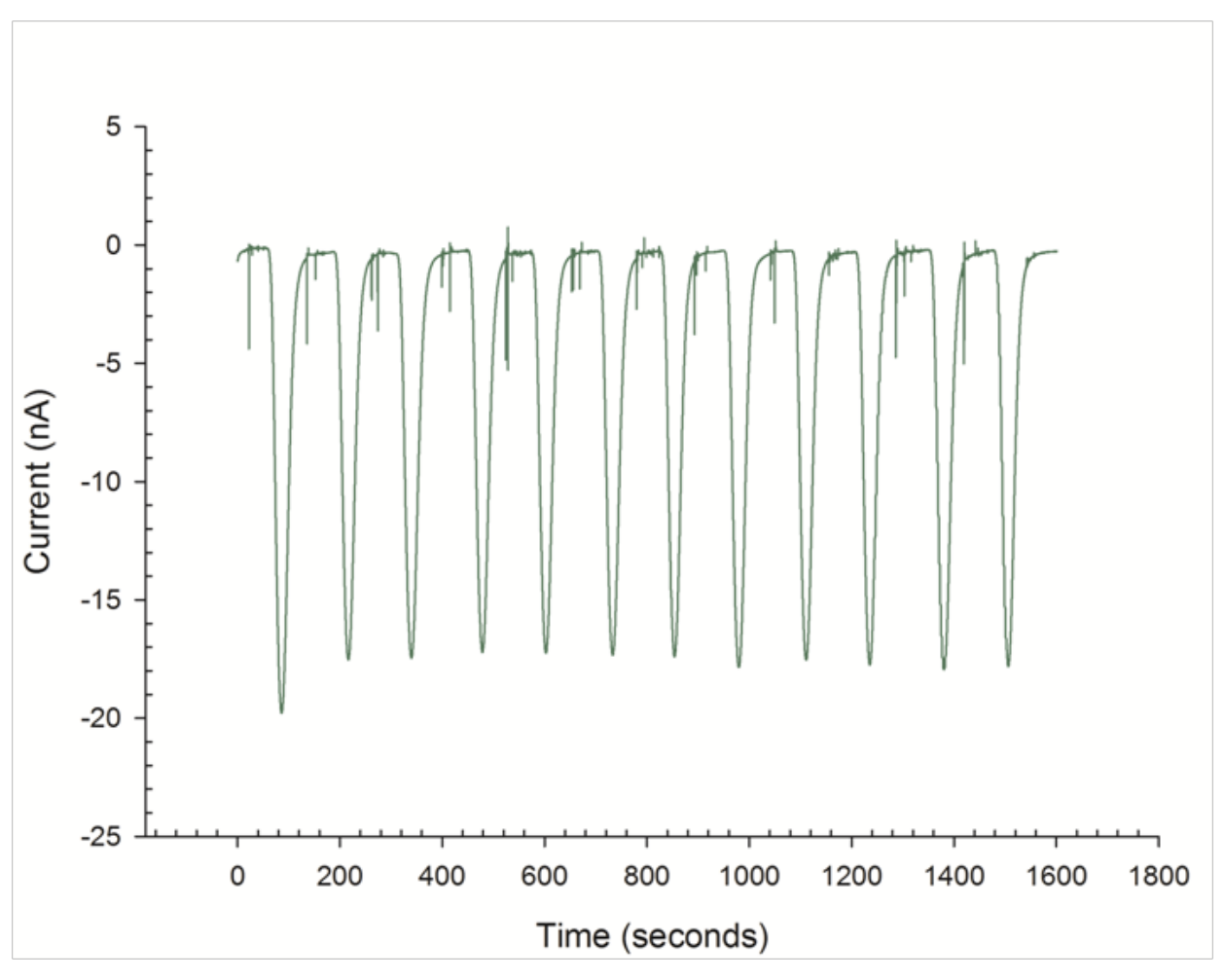


Figure 4.10: Reliability of electrode system verified with ferricyanide injections: As shown in this example, current resulting from injections of 1 mM potassium ferricyanide show peak area reproducibility of less than 5% RSD over the course of three hours (x-axis shortened here so peak detail can be seen). This shows the reliability in both the flow injection system and electrochemical systems for a reliable redox system.

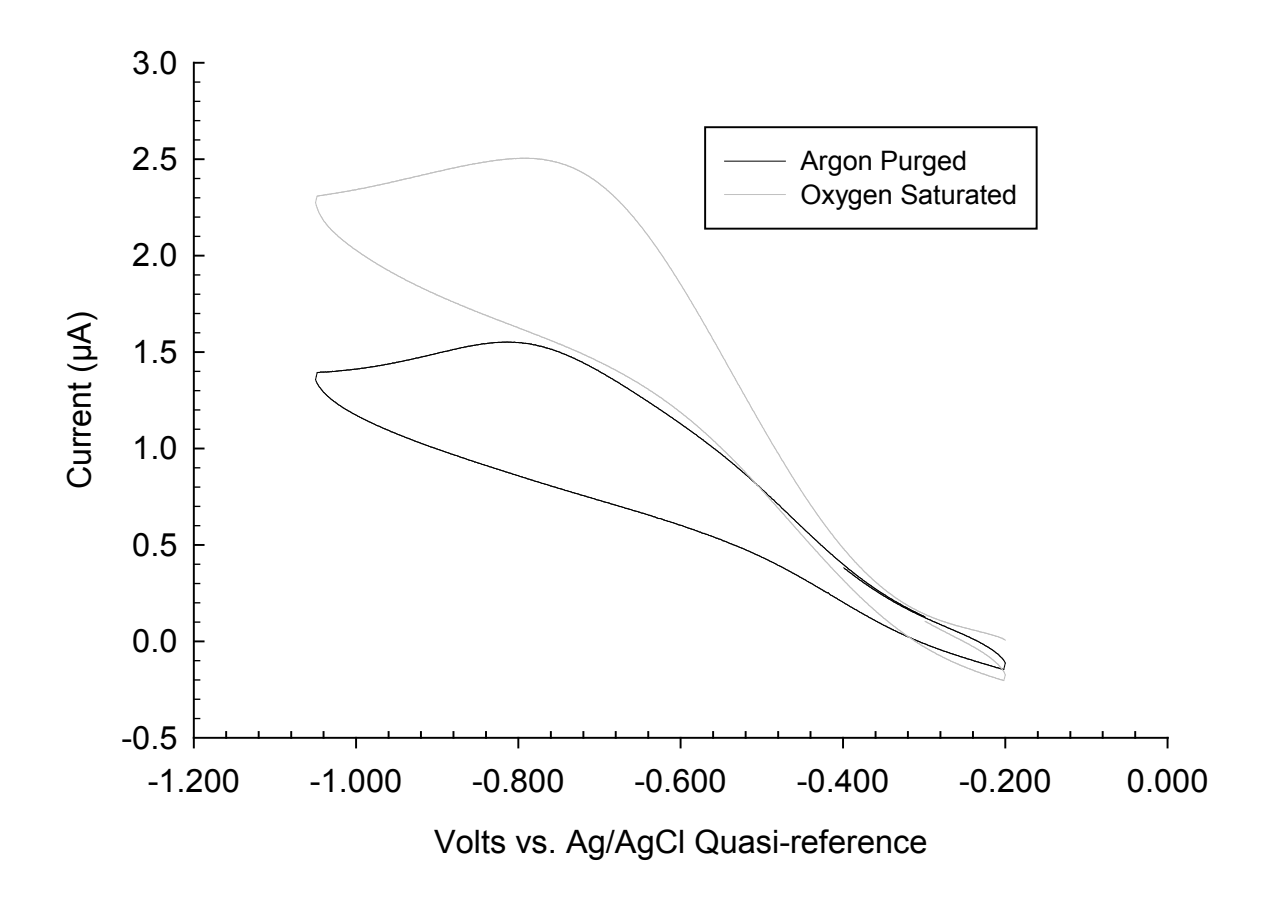


Figure 4.11: Cyclic Voltammetry of an Oxygenated and Deoxygenated Solution: Shown here in grey is the cyclic voltammogram of an oxygen-saturated solution at the gold working electrode, and that of a purged solution in black. Note that a diffusion limited region for oxygen appears beyond about -775 mV, suggesting its use as an amperometric potential for the investigation of oxygen concentration.

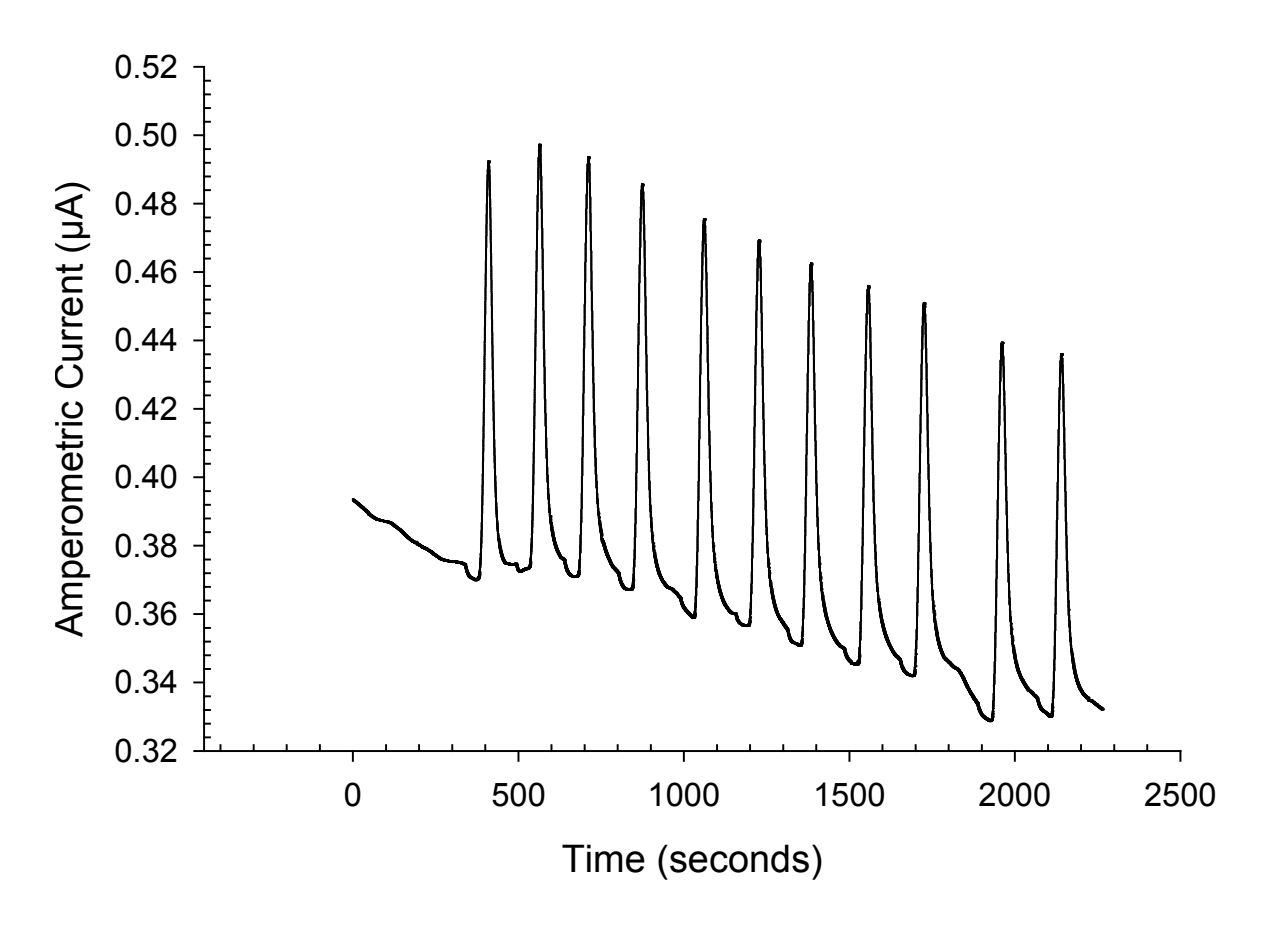


Figure 4.12: Repeated injections of oxygen rich solutions into oxygen poor buffer: Shown here is a series of injections of oxygen rich solution into a deoxygenated solution. Peak area RSD was less than 7% RSD over the course of two hours.

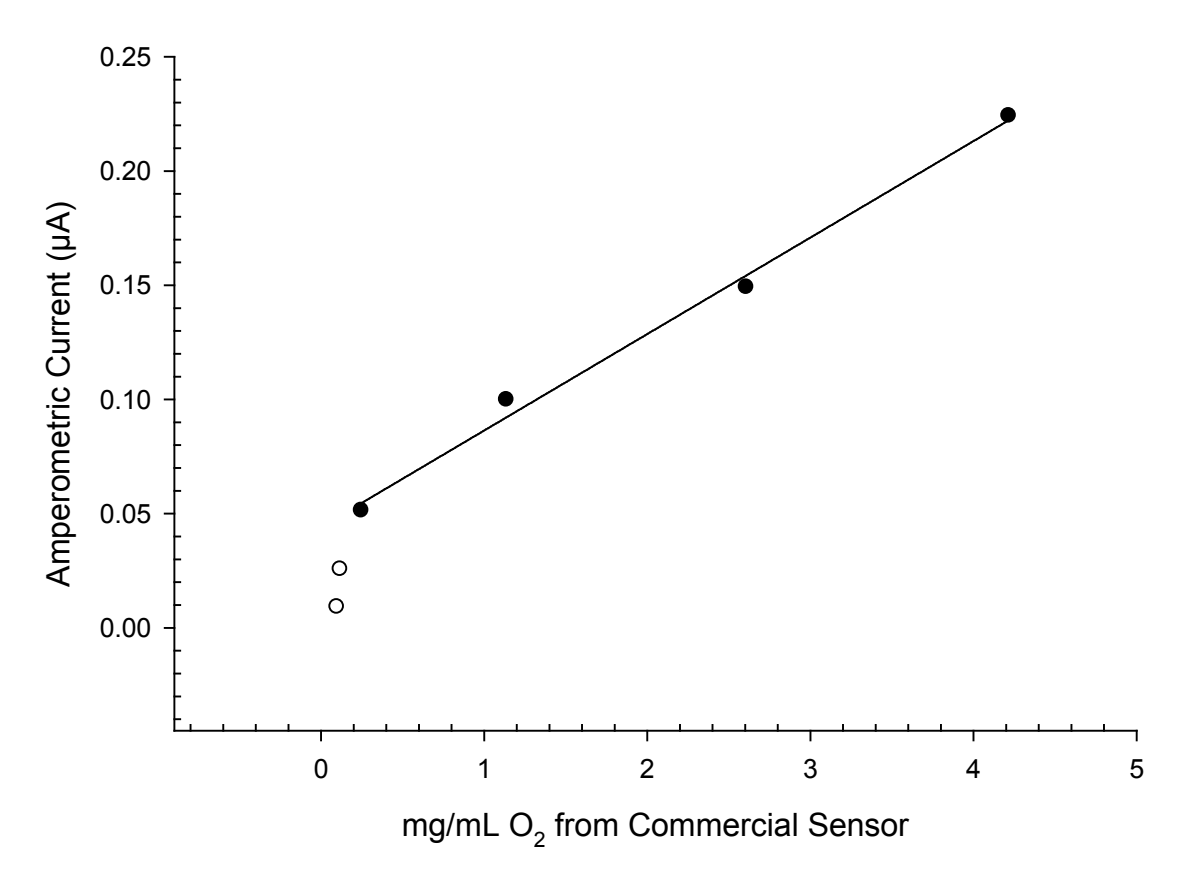
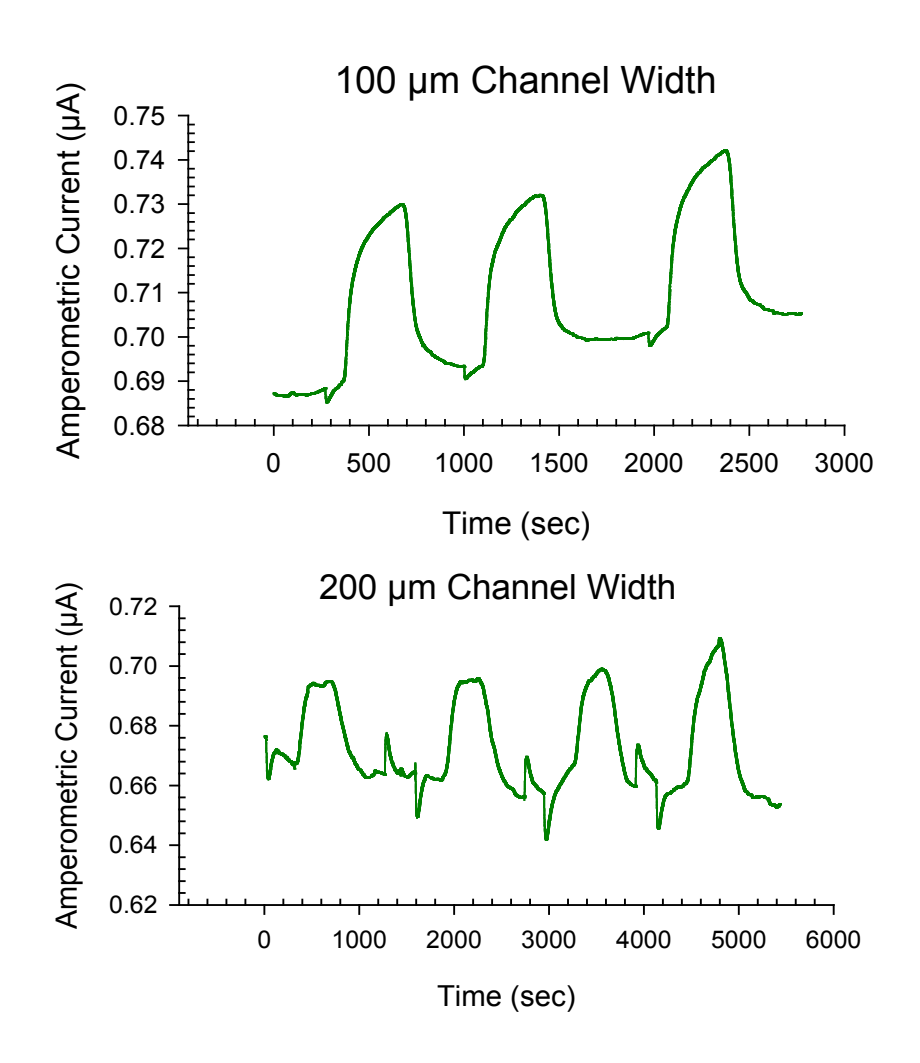


Figure 4.13: Linear Response of Microfluidic Sensor to Oxygen: source: Shown here is the response in peak current of the microfluidic oxygen system as a function of the response of the commercially available sensor for a series of sodium sulfite solutions. Similar linearity was observed for n = 4 devices. (R2 = 0.97 + -0.02). Note that at low oxygen concentrations, linearity is lost, as the commercial sensor is not sensitive to these low concentrations.



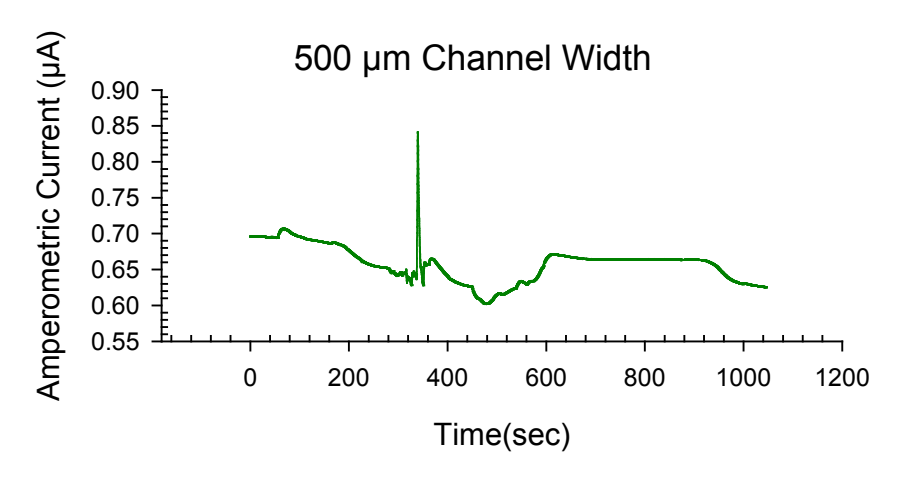


Figure 4.14: Increase in Channel Width Reduces Peak Area Reproducibility: In an attempt to increase the mass transport of oxygen across the PDMS membrane, channel width was increased while channel height reduced to keep a constant volume. Peak area became less reproducible as width increased, as a result of the decreased mechanical stability of the wider channel.

performance of the electrochemical system. As shown in figure 4.10, peak area reproducibility for ferricyanide injections is better than 5% RSD over the course of several hours, suggesting the potential of our quasi-reference electrode is stable over the course of such an experiment.

4.3.4 Reproducibility/function of Oxygen Sensor

Shown in figure 4.11 is a voltammogram of an oxygenated and deoxygenated solution obtained using the gold working electrode in the epoxy disk. While a clear diffusion controlled region cannot be observed because of reaction with water, a potential of -850 mV versus Ag/AgCl reference results in a fairly constant amperometric current that is stable over time. The data shown in figure 4.12 demonstrates this stable current, where injections of oxygen rich solution into oxygen poor buffer is monitored amperometrically. Peak areas in these measurements are better than 7% RSD and are reproducible over two hours, though a changing baseline is present.

4.3.5 Linear Response of Oxygen Sensor to Commercial Sensor

Following the procedure described in 4.3.7, the linear response of the microfluidic sensor was compared to that of the commercial sensor for sodium sulfite solutions of varying concentrations, resulting in the calibration presented in figure 4.13.

4.3.6 Device Design for Oxygen Control

Flow rates in the analytical (top) channel were varied between 0.5 and 5 μ L/min while oxygenated and deoxygenated solutions were switched in the lower channel. However even at the slowest flow rate through a 100 μ m wide channel, the signal observed at the oxygen electrode never changed more than 3-4%, suggesting insufficient mass transport in the oxygen exchange region of the device.

To increase mass transport, the channel width was increased while the height was decreased to maintain a constant volume, but larger interaction surface area. As summa-

rized in figure 4.14, peak reproducibility in the injection of oxygenated buffer into deoxygenated solution resulted in significantly reduced peak area reproducibility as channel width increased.

4.4 Conclusions

4.4.1: Selection of a deoxygenating system

In the investigation of changes in cellular systems under hypoxic conditions, one of the first decisions that needs to be made is how to achieve hypoxic conditions. While many different engineering arrangements exist for establishing oxygen control exist, including deoxygenated chambers, purging with noble gas or chemical means, they each have their advantages and disadvantages. In our laboratory, we actively use three methods: purging with argon or nitrogen, the Oxyrase enzyme system, or oxygen consumption through sodium sulfite.

While purging with a noble gas has the advantage of being readily available, it is somewhat more challenging for biological samples because the high protein content in buffers and samples results in a large amount of foaming in the sample. Furthermore, the handling of human materials, such as human red blood cells, presents a safety challenge as the experimenter does not want to accidentally aerosolize these materials potentially causing a bloodborne pathogen hazard.

Due to these restrictions, the Spence group began using the Oxyrase enzyme system to achieve deoxygenation. While little is revealed about the mechanism of the Oxyrase system by its manufactures, experimentally a rate of deoxygenation similar to that seen with gas purging is observed, as shown in figure 4.6, with both achieving deoxygenation in about 800 seconds.

Oxyrase has the additional advantage that the enzyme remains in the sample as an experiment progresses, meaning exposure to atmospheric oxygen does not result in a need

for re-oxygenation of the sample, as would happen with simple gas purging. This can also be limiting in the instance of trying to monitor hemoglobin polymerization in sickle cell anemia, as one cannot easily re-oxygenate a sample.

A third method investigated for deoxygenating samples investigated here is the use of oxygen-scavenging sodium sulfite. Here, the sulfite will simply react stoichiometrically with oxygen in solution because it is not an enzymatic system so standardization can be prepared as described in figure 4.13. Furthermore, as shown in figure 4.6, deoxygenation occurs rapidly, at a rate that is faster than the commercial Clark electrode can measure.

However, to achieve long-term deoxygenation that is not susceptible to re-oxygenation, excess sodium sulfite is required. Therefore, concentrations between 25-100 mM are often used to ensure that the de-oxgygenation properties are not exhausted. Concentrations this large may likely have an impact upon cellular behavior, which Oxyrase has been shown not to affect in numerous cell systems. Therefore, for cellular systems, Oxyrase may be preferred to sulfite oxygen scavenging, but for the investigation of new oxygen sensing systems as described here, sulfite's low cost, rapid deoxygenation, and ease of use in addition to a lack of protein which can foul electrodes (early investigations used no membrane when detecting oxygen) make it an ideal method of deoxygenation.

Once reliable deoxygenated solutions were prepared, it became necessary to develop an oxygen sensing system compatible with the micro scale and flowing systems. While this has been achieved with more complex fabrication techniques involving chemical vapor deposition steps, 15 these more complicated and more expensive fabrication methods produced electrode systems that are more fragile and limited in reusability, because the working electrode layers (gold in most cases), were too thin to be polished reliably. The technology developed in Martin's lab 14 where a working electrode is sealed in an epoxy disk, and polished to form a disk electrode however offers an exceptionally robust platform

for the integration of electrodes into microfluidic systems, as they are can be polished just like commercially available macro scale electrodes. Furthermore, the epoxy material is amenable to traditional machining techniques, allowing channels and fittings to be incorporated into it.

4.4.2: Flow Injection Systems for Microfluidic Sample Introduction

As a large number of factors can cause baseline drift in electrochemical sensors for oxygen, it was determined a flow injection system would be most useful in characterizing the electrodes and their feasibility for oxygen detection. It was also desirable to determine the response time of the oxygen sensor to oxygen injection, as there is an additional mass transport limiting feature of the PDMS membrane, in other words, we wanted to know if the PDMS membrane posed a large barrier to oxygen sensitivity. Therefore, an analytical technique which could characterize the flow injection system parameters such as time from injection to signal rise orthogonally from electrochemistry was desired. Fluorescence monitoring of fluorescein injections was chosen for this because of the reliability of fluorescein fluorescence.

Furthermore, large injection loops (8 μ L) relative to the flow rates used were used in these studies because initially it was thought that one could monitor the rate of mass transport of oxygen across the PDMS membrane by monitoring the slope at the height of such a peak. The use of fluorescence monitoring of these large peaks allowed me to verify that the slope at the top would approach zero. Unfortunately, in the electrochemical sensing of oxygen, while the slope did decrease at lower flow rate (longer time for oxygen to equilibrate across the membrane), it did not do so reproducibly, so this was not used as a method to predict mass transport.

Nonetheless, the fluorescence system offered an orthogonal way to verify our flow and chip systems did not have excess dead volume in any of the interconnects, therefore if

no peaks were observed in an electrochemical experiment, it must be due to a failure in that particular experiment or system.

Once the flow systems were configured and determined to be reliable, validation of the electrochemical sensor could proceed. After fabrication, it is valuable to verify that there is no leak between the electrode wire and the epoxy, because if solution can leak slowly into this interface over the course of an experiment, the electrode area, and therefore the background current will increase. In these cases, the signal does not increase with the background however because the diffusion distances become too long, and you just observe a reduction in signal to noise.

Propelling a fluorescent solution over the electrodes for an extended period of time is a reliable means of verifying the absence of leaking because if a leak were present, it would collect around the electrode wire, and a bright ring would be observed in the micrograph. As it is not present, and no increase in current is observed in the electrochemical investigations, it can be concluded that there is no leaking around the electrode.

4.4.3: Electrochemistry in the Microfluidic Device

Next, to verify the function of the two electrode cell and its long term reliability, the redox chemistry of the ferricyanide ion was exploited, as ferricyanide is a very stable and robust molecule. Figures 4.9 and 4.10 show the behavior is as expected, and in several experiments run for several hours, the performance indicated in 4.10 is continually observed, suggesting the electrochemical system would be reliable for several hours. Furthermore, we expect this reliability to be maintained in the investigation of oxygen redox chemistry, as a membrane separates the samples from the electrode, preventing fouling.

It was still necessary to validate the long-term (several hours desired for an experiment) reliability of the sensor with oxygen because of several challenges associated with oxygen detection. Firstly, reaction 4.1 does not always proceed to completion; sometimes

hydrogen peroxide is formed as a final product, and in the small volume above the electrodes, can form in high concentration, causing electrode fouling. Also, since PDMS is oxygen permeable, and comprises most of the fluidic system, the effect of oxygen dissolved in the PDMS or transporting across the PDMS was unknown. Also, previous reports suggest that many factors such as temperature or pH can have an impact on the baseline, and the effects of these in our sensor were not known.

To resolve these concerns, experiments such as those shown in figure 4.12 were conducted. After verifying the potential to use for amperometric investigation through cyclic voltammetry, oxygen rich solutions were injected into sulfite deoxygenated buffer. As seen in figure 4.12, the peak areas are reproducible, but the baseline decreases steadily throughout the experiment. It is thought that this is the result of oxygen absorbed into PDMS which slowly decreases in concentration as it is dissolved into the oxygen poor buffer in the channel.

In addition to verifying the longevity and reproducibility of the oxygen sensor, it is also desirable to verify the sensor response is linear with respect to oxygen concentration. Unfortunately, it is challenging to develop reliable and reproducible oxygen standards, so instead, solutions of varying sulfite concentration were measured both with the commercial oxygen sensor, and the microfluidic sensor. For a given solution, the signal from the microfluidic sensor plotted as a function of the signal on the commercial sensor, as shown in figure 4.13. The dark shaded points in the figure were used in determining the line of best fit as summarized in the caption; however in the low concentration region there were several points which fall of the line. It was determined these points do not fit the linear model because the commercially available sensor seems to reach a detection minimum, as it displays the same value, while the signal from the microfluidic sensor continues to

decrease with decreasing sulfite concentration, suggesting the microfluidic sensor has a lower detection limit.

4.4.4 Control of Oxygen Concentration within the Channel

After validation of the longevity of the oxygen sensor, investigations of the use of a channel underneath the analytical channel, using a device as shown in figure 4.5 were initiated. As described above, with a PDMS membrane prepared by spin-coating the 10:1 PDMS without any thinning, little mass transport of oxygen was observed in the oxygen-ation/deoxygenation zone of the device. To increase the mass transport, the membrane fabrication procedure mentioned above to produce a thinner membrane. This time, oxygen transport could be observed, but only with a signal change of a few percent.

In order to further increase the mass transport, as membrane thickness had been reduced as much as possible without frequent tearing, the interfacial area was increased by widening the channel, while also reducing the height, maintaining a constant volume in the channel. Unfortunately, it was not possible to determine if this improved the oxygen transfer rate as the mechanical stability of the channel was significantly reduced. Figure 4.14 shows the resulting current as a function of time plots for oxygen injections into deoxygenated solution into channels of varying width. As channel width increased, the reproducibility of the peak areas decreased significantly, and this occurred because the membrane, which is the fourth wall of the flow channel, was expanding and contracting in the region above the channel cut into the epoxy disk, causing the flow rate to fluctuate, resulting in varying current. This was verified by placing the PDMS devices with wider channels over a portion of the epoxy disk which had no features cut into it, and reproducibility was mostly restored. There was still a decrease in reproducibility as some expansion

and contraction likely occurred over the electrode, but the reproducibility was improved over what is shown in figure 4.14

As previous investigations of RBC biology under hypoxic conditions in our group have been limited to investigating only hypoxic or normoxic conditions, the development of a sensor to determine the oxygen concentration in a flowing solution is a necessary component for developing the capability to modulate the oxygen concentration in the flowing solution.

Future work in this area should verify whether the decreasing baseline seen in figure 4.12 is the result of oxygen absorbed into PDMS, because if it is, then other materials for the channel may need to be considered, such as polystyrene as described in chapter 5. It is possible that oxygen transport is occurring across the membrane sufficient to change the oxygen concentration of the solution, but that oxygen immediately equilibrates with the PDMS channel, preventing its detection at the sensor, and preventing it from having an impact on the cellular behavior.

REFERENCES

REFERENCES

- 1. Faris, A.; Spence, D. M., *Analyst (Cambridge, U. K.)* **2008**, *133* (5), 678-682.
- 2. Halpin, S. T.; Spence, D. M., *Analytical Chemistry* **2010,** 82 (17), 7492-7497.
- 3. Crawford, J. H.; Isbell, T. S.; Huang, Z.; Shiva, S.; Chacko, B. K.; Schechter, A. N.; Darley-Usmar, V. M.; Kerby, J. D.; Lang, J. D.; Kraus, D.; Ho, C.; Gladwin, M. T.; Patel, R. P., *Blood* **2006**, *107* (2), 566-574.
- 4. Diesen, D. L.; Hess, D. T.; Stamler, J. S., Circulation Research **2008**, 103 (5), 545-553.
- 5. Ellsworth, M. L.; Ellis, C. G.; Goldman, D.; Stephenson, A. H.; Dietrich, H. H.; Sprague, R. S., *Physiology* **2009**, *24* (2), 107-116.
- 6. Cao, Z. L.; Bell, J. B.; Mohanty, J. G.; Nagababu, E.; Rifkind, J. M., *American Journal of Physiology-Heart and Circulatory Physiology* **2009**, *297* (4), H1494-H1503.
- 7. Bergfeld, G. R.; Forrester, T., Cardiovascular Research 1992, 26 (1), 40-7.
- 8. Edwards, J., Sprung, Robert, Sprague, Randy, Spence Dana M., *Analyst* **2001**, *126*, 1257-1260.
- 9. Raththagala, M.; Karunarathne, W.; Kryziniak, M.; McCracken, J.; Spence, D. M., *European Journal of Pharmacology* **2010**, *645* (1-3), 32-38.
- 10. Lam, R. H. W.; Kim, M. C.; Thorsen, T., *Analytical Chemistry* **2009**, *81* (14), 5918-5924.
- 11. Luo, W.; Abbas, M. E.; Zhu, L. H.; Zhou, W. Y.; Li, K. J.; Tang, H. Q.; Liu, S. S.; Li, W. Y., *Analytica Chimica Acta* **2009**, *640* (1-2), 63-67.
- 12. Mehta, G.; Mehta, K.; Sud, D.; Song, J. W.; Bersano-Begey, T.; Futai, N.; Heo, Y. S.; Mycek, M. A.; Linderman, J. J.; Takayama, S., *Biomedical Microdevices* **2007**, *9* (2), 123-134.
- 13. Bard, A. J.; Faulkner, L. R., *Electrochemical methods : fundamentals and applications.* 2nd ed.; Wiley: New York, 2001; p xxi, 833 p.
- 14. Selimovic, A.; Johnson, A. S.; Kiss, I. Z.; Martin, R. S., *Electrophoresis* **2011**, *32* (8), 822-831.
- 15. Wu, C. C.; Luk, H. N.; Lin, Y. T. T.; Yuan, C. Y., *Talanta* **2010**, *81* (1-2), 228-234.
- 16. Amatore, C.; Arbault, S.; Chen, Y.; Crozatier, C.; Tapsoba, I., Lab on a Chip 2007,

- 7 (2), 233-238.
- 17. Jobst, G.; Urban, G.; Jachimowicz, A.; Kohl, F.; Tilado, O.; Lettenbichler, I.; Nauer, G., *Biosensors & Bioelectronics* **1993**, *8* (3-4), 123-128.
- 18. Mcarthur, K. T.; Clark, L. C.; Lyons, C.; Edwards, S., Surgery **1962**, *51* (1), 121-126.
- 19. Clark, L. C.; Wolf, R.; Granger, D.; Taylor, Z., *Journal of Applied Physiology* **1953**, 6 (3), 189-193.
- 20. Hitchman, M. L., *Measurement of dissolved oxygen*. Wiley: New York, 1978; p xvi, 255 p.
- 21. Berkenbosch, A.; Riedstra, J. W., *Acta physiologica et pharmacologica Neerlandica* **1963**, *12*, 144-56.
- 22. Zheng, R. J.; Fang, Y. M.; Qin, S. F.; Song, J.; Wu, A. H.; Sun, J. J., Sensors and Actuators B-Chemical 2011, 157 (2), 488-493.
- 23. Haghighi, B.; Bozorgzadeh, S., Analytica Chimica Acta 2011, 697 (1-2), 90-97.
- 24. Morita, K.; Shimizu, Y., *Analytical Chemistry* **1989**, *61* (2), 159-162.
- 25. Yasuda, H.; Stone, W., *J Polym Sci A1* **1966,** *4* (5pa1), 1314-&.

Chapter 5: Conclusions/Future Directions

5.1 Conclusions on Nitric Oxide (NO) Detection from the Red Blood Cell (RBC)

While the DAF-FM fluorogenic probe for nitric oxide (NO) has been used often in the literature for intracellular measurements of NO production in a variety of cell types¹⁻⁴, its use has been limited to qualitative studies typically involving fluorescence microscopy or flow cytometry for readout. While these studies offer insight into NO bioavailability within cells, the source of this NO is not always clear. Previous work utilizing the intracellular DAF-FM-DA probes for NO detection in endothelial cells⁴⁻⁷ concludes that in increase in intracellular DAF-FM-NO fluorescence is the result of intracellular NO production. While inhibition studies suggest the intracellular production by endothelial nitric oxide synthase (eNOS) plays a significant role in those studies, it is also possible that NO from outside the endothelial cell diffuses into the cell, and then reacts with the DAF-FM probe. Furthermore, while though efforts are underway³ by other researchers to quantify NO with these intracellular probes, these efforts have not been attempted until recently.

Here, a device has been developed that can distinguish between NO released from various cells in a complicated matrix in a flowing stream, allow that NO to react with the DAF-FM probe in a controlled environment, and simultaneous perform calibration. Lastly, readout does not require specialized microscopes or imaging software; rather, readout is obtained by placing the microfluidic device into a microplate reader capable of epifluorescence detection. While NO was the analyte of interest in this case, previous work in our group⁸ suggests any fluorogenic probe system could be used in such a geometry. Simplifying the detection scheme for our microfluidic system removes one of the significant

barriers to the implementation of microfluidic technologies outside of academics; the need to develop custom detection hardware for each analysis.

5.2 Conclusions on ATP-NO Investigations

After developing a microfluidic device capable of detecting NO using a fluorogenic probe with a separation step, thereby reducing the effect of the RBC matrix during NO detection, a long-debated mechanism in the literature could be investigated in a controlled manner.^{5, 9-11} Specifically, under hypoxic conditions, it had not been previously known whether RBC derived NO, or ATP-mediated NO production from the endothelium results in smooth muscle dilation. It is well-established that NO has a short half life *in vivo*, particularly around hemoglobin and thiol-containing molecules such as glutathione and albumin.^{12, 13} The work presented within this dissertation suggests this more stable molecule responsible for the signaling may be ATP released from the RBC, as under hypoxic conditions, a NO increase above endothelial cells is only observed when the ATP release pathways and eNOS NO synthesis are not inhibited. It is worth noting that other researchers suggest nitrite is this more stable molecule as there have been reports of administration of nitrite *in vivo* resulting in vasodilation¹⁴. However, it is known that nitrite can cause ATP release from RBCs, ^{15, 16} thereby potentially affecting vascular tone in this same manner.

As the microfluidic device developed in this thesis enables the culture of an endothelium barrier within appropriate diffusional distances from the point of NO release (the hypoxic RBCs), an attempt was made to elucidate the role of hypoxia-induced NO and ATP release. While many of the inhibition pathways of ATP^{17, 18} release from the RBC have been investigated by the Spence group, studies investigating the downstream effects on the endothelium with an RBC/NO release stimulant such as hypoxia. Through these studies, it was determined that hypoxia stimulated RBC ATP release plays a dominant role in the amount of NO that is available for vasodilation, as determined by the amount of NO

that can cross an endothelium barrier. These results suggest that the dominant mechanism responsible for vasodilation under hypoxic conditions requires both the function of ATP release and eNOS stimulation in the endothelium.

A future direction of this research then would investigate the fate of the NO that is released from the RBC under hypoxic conditions. That is, if RBC-derived NO does not play a role in smooth muscle relaxation, then why would the RBC release such high concentrations (~ single digit micromolar) of NO in response to hypoxia. One possibility currently being investigated in the Spence lab is the prevention of ATP-mediated platelet aggregation, which has been shown to exist in our group ^{19, 20}. As it has been shown that NO can reduce platelet aggregation ²¹, perhaps the NO release under hypoxic conditions is to prevent platelet aggregation, which would be undesirable when more blood flow is needed.

5.3 Conclusions on Electrochemical Detection of Oxygen

A shortcoming of the investigations involving the origin of NO that participates in vessel dilation (described above) is the minimal range of oxygen concentrations that were investigated. In fact, the concentrations investigated were rather binary; specifically, the studies were either performed in a normoxic or near anoxic environment. In vivo, oxygen tensions vary much more between normoxic and anoxic. While investigations of RBC exposure to hypoxia have been performed before in the Spence group 17, the RBC-containing solutions were sparged for varying lengths of time, resulting in different levels of hypoxia in the cells, and ultimately a concentration-dependent ATP release. While effective for this experiment, this technique has several limitations: firstly, this was applied to rabbit RBCs, and implementing such a technique in human RBCs increases the risk of aerosolizing a

sample that may contain bloodborne pathogens, though this could be mitigated with proper engineering controls.

More significantly however, as described above, measurement of the ATP release occurred very rapidly after deoxygenation. Using our microfluidic system to attempt to investigate the effects of the resulting ATP release on endothelial cells, these samples, which were deoxygenated for specific times, would need to be loaded into syringes, and pumped for 30 minutes. With these multiple sample handling steps, it is plausible the samples would be re-oxygenated in an irreproducible manner, preventing the investigation of an oxygen concentration dependent response. Therefore, if the deoxygenation could occur on a microfluidic device immediately before interaction with the endothelial cells, more specific control of the experiment could be maintained.

Furthermore, commercially available Clark electrodes for amperometric determination of oxygen do not perform well in less than 5 mL of solution, requiring far larger sample sizes than what was typically handled or available in a typical experiment described in this dissertation. Therefore, to improve reproducibility and to accurately know the oxygen concentration in solution, it was desired to integrate the process of measuring oxygen in a small sample in addition to maintaining the ability to control the oxygen concentration within that solution.

As shown in chapter 4, detection of oxygen using an epoxy-immobilized Clark electrode has been developed. Reproducible oxygen signals can be obtained for repeated injections, and a linear response from the microfluidic sensor was observed relative to the signal of a commercially available sensor. With these capabilities, relative (concentration relative to a saturated solution) oxygen concentrations determination can be readily obtained. To achieve the most reliable detection, however, the channel should not be constructed from PDMS, which is oxygen permeable; instead, polystyrene (or other oxygen

impermeable materials) should be used, so the channel will have no impact on the oxygen concentration in the flow channel.

In addition to detection, it is desirable to be able to modulate the concentration of oxygen within a flowing channel of a microfluidic device. The approach using oxygenated or deoxygenated solutions as a bulk source or sink for oxygen was chosen because flow of solutions can be readily controlled, and the diffusion constant of oxygen across PDMS, the chosen membrane material, increases when solution is on both sides of the membrane²², Unfortunately, as shown in the end of chapter 4, there are engineering challenges that result from using thin PDMS membranes over a large surface area, potentially limiting the application of this technique.

Therefore, it might be easier to contain an oxygen exchange portion of the device within an airtight box, and switching the atmosphere in the box between oxygen rich and oxygen poor. There currently exists a large infrastructure of mass flow controllers, or even bubble flow meters, to control the flow rates of each gas into the box, thereby achieving reproducible oxygen concentration. Such an implementation would take advantage of the oxygen permeability of PDMS, and not likely require fabrication in another material.

5.4 Future Directions for Microfluidic Models

Many of the proposed future directions for microfluidic work involving multiple cell systems, such as those proposed in this dissertation, involve the integration of more cell types onto the device (such as "organ on a chip²⁴, ²⁵" or in the Spence group, more blood components such as platelets, red blood cells and endothelial cells), or the integration of multi-modal detection techniques, such as electrochemistry and chemiluminescence, onto the device. Both of these approaches are frequently halted by the reliability of the individual components of each part of the device. For example, in integrating multiple cell types, there is often a challenge in obtaining cultured cells and primary cells at the same

time. As more cultured types are added, timing needs to be more carefully controlled, and perhaps cell cultures maintained for longer times on the device. Similarly, in the integration of additional detection modes, a single failure in one component of the device can result in the failure of the entire experiment. As more components are integrated, this becomes more probable. To improve the reproducibility of integrating multiple cell types onto the device, particularly in cell culture, systems such as our TEER measurement platform²⁶ could be utilized, or more careful characterization of the cells prior to analysis with staining techniques could be performed before analysis.

As device developers, we can improve the reliability of our device in two ways. First, while PDMS is valuable as a prototyping material, it is in general a poor selection for devices due to its hydrophobicity and flexibility. The hydrophobicity causes challenges with pumping, as aqueous solutions must be pushed against this surface tension causing increased backpressure. Furthermore, as shown below, hydrophobic compounds can partition into the PDMS, and the flexibility of PDMS can cause the layers of the device to delaminate, or channels to deform, as shown in chapter 4, all of which reduce the reliability and utility of the device.

To overcome these limitations, the devices could be fabricated in a wide variety of materials including PMMA²⁷, polycarbonate²⁸, silicon²⁹ or glass³⁰, or polystyrene³¹. Polystyrene, in particular, has the advantage of having a low glass transition temperature, meaning it can be molded at lower temperatures, and is the material from which traditional cell culture products are formed, making ideal for integration of cells onto microfluidic devices. Furthermore, polystyrene is a rigid polymer that is not prone to delamination once

sealed, and is somewhat compatible with oxygen plasma sealing to PDMS, enabling easier integration into other microfluidic-based studies.

5.4.1 Improving Reliability: Polystyrene Devices

In order to use the advantages of polystyrene as mentioned above, yet retain the major advantage of PDMS, rapid prototyping³², it was determined that the same lithographic process that is used to produce PDMS devices can produce PDMS molds from which polystyrene devices could be cast. This would offer the same lithographic control available with soft lithography, but allow us to fabricate polystyrene instead.

5.4.1.1 Motivation

There are several reasons to move to fabricating microfluidic devices out of polystyrene. Firstly, these devices are more rigid and require less careful handling, meaning they are easier to use in an academic setting, and potentially compatible with robotic handling equipment in a more high throughput scenario. Secondly, polystyrene is less likely to absorb hydrophobic compounds like PDMS, as shown in section 5.4.2. This means a wider range of potential pharmaceutical agents can be incorporated into the microfluidic models developed on microfluidic platforms. Thirdly, polystyrene is the most used material in cell culture analyses, with numerous protocols determined for both primary and perpetual cell culture systems. These procedures could then be more easily ported to the microfluidic models. Lastly, commercial infrastructure to mass produce polystyrene devices already exists, through hot embossing³³ or injection molding³⁴ techniques. As a result, less time can be spent on device fabrication, and more on device utilization.

5.4.1.2 Methods of Polystyrene Fabrication

Fabrication of polystyrene devices starts with the same soft lithography as is mentioned in chapter 2, except features will be printed as dark lines on a light background. As shown in figure 5.1, a PDMS replicate of these masters will then have raised features,

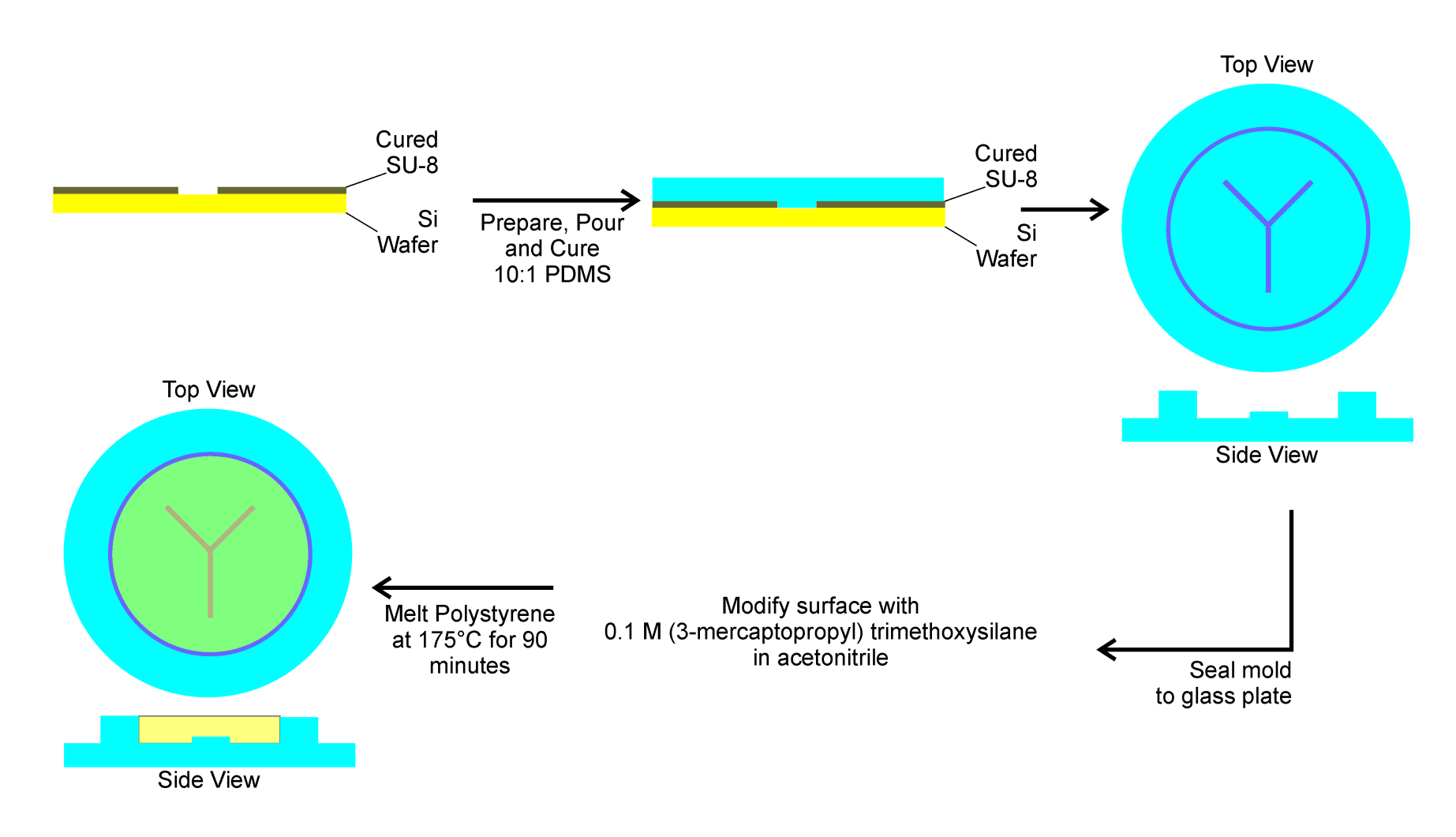


Figure 5.1: Rapid Prototyping in Polystyrene: A master is prepared with a recessed feature in SU-8 photoresist using the lithography techniques described in chapter 2. A PDMS replicate of this is made, and then modified as shown. Polystyrene is then melted into this mold, and removed. Using this technique, a polystyrene device can be fabricated from master to completion in one day.

which can then be cast in the melted polystyrene. This PDMS replicate is then sealed to a glass plate using a thin layer of uncured PDMS. A retaining ring for the melted polystyrene, fabricated from PDMS, is then sealed to the mold.

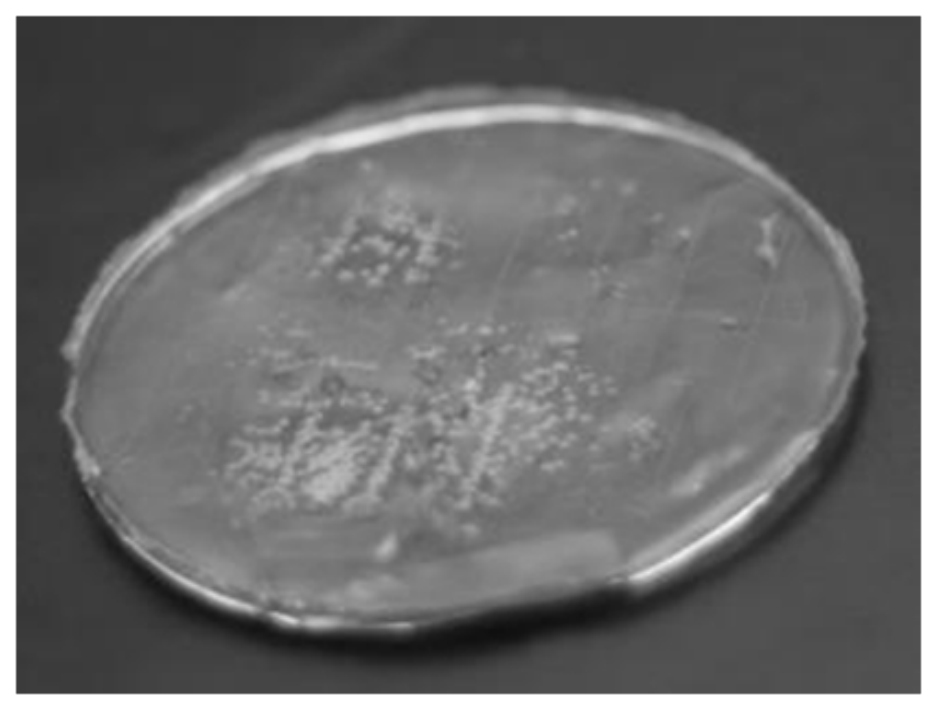
A surface modificiation is then performed by preparing a 0.1 M solution of (3-mer-captopropyl) trimethylsiloxane in acetonitrile, and filling the mold with this solution. The acetonitrile is allowed to evaporate, and then polystyrene from Petri dishes is melted into the mold by contact heating on a hotplate at 175 °C. The hotplate is then shut off, and the device is allowed to cool to room temperature. The polystyrene is then removed from the mold.

5.4.1.3 Current State/Progress

The most significant advance in fabricating these devices was the utilization of a surface modification step to reduce the repulsion of the melted polystyrene from the PDMS mold. As shown in figure 5.2, without the surface modification, bubbles are formed at the interface, which would prevent the utilization of the device. After modification however, the bubbles are eliminated, producing an improved replicate of the PDMS mold.

The heating protocol is important as well, as overheating can start thermal degradation of the polystyrene, resulting in yellowed features and high background fluorescence in the UV, which would be disadvantageous for several applications. Switching from convection oven heating to contact heating on a hotplate improved the clarity issues, along with eliminating the background fluorescence.

As mentioned above, these devices could be utilized to investigate cell-cell interactions between endothelium cells and RBCs, or potentially endothelial cells and platelets as previously described. ¹⁹ A first step towards performing these assays is the culture of endothelial cells on the device. Based on the importance of endothelium-derived nitric oxide shown in chapter 3, cell immobilization on polystyrene-derived devices could represent



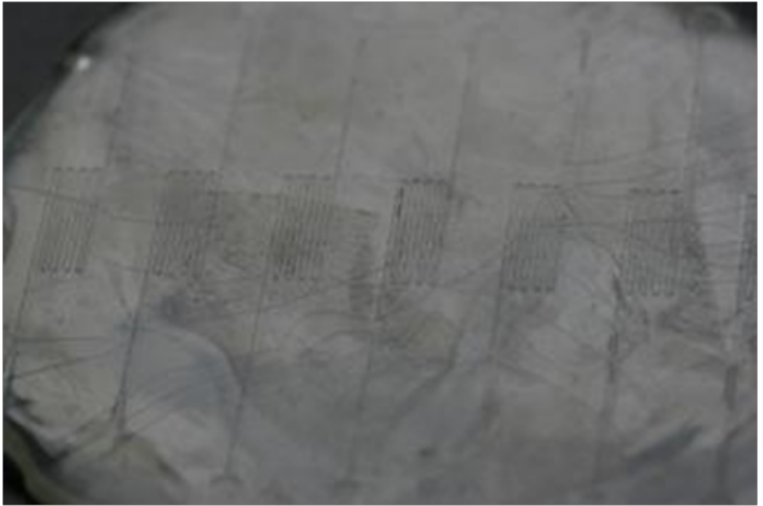


Figure 5.2: Surface Modification Eliminates Bubbles from Replicate: Shown above, is a polystyrene replicate fabricated from an unmodified PDMS mold. Shown below is a different replicate formed from a PDMS mold modified with 0.1 M (3-mercaptopropyl)trimethylsiloxane, which improves the interaction between the melted polystyrene and the PDMS mold.

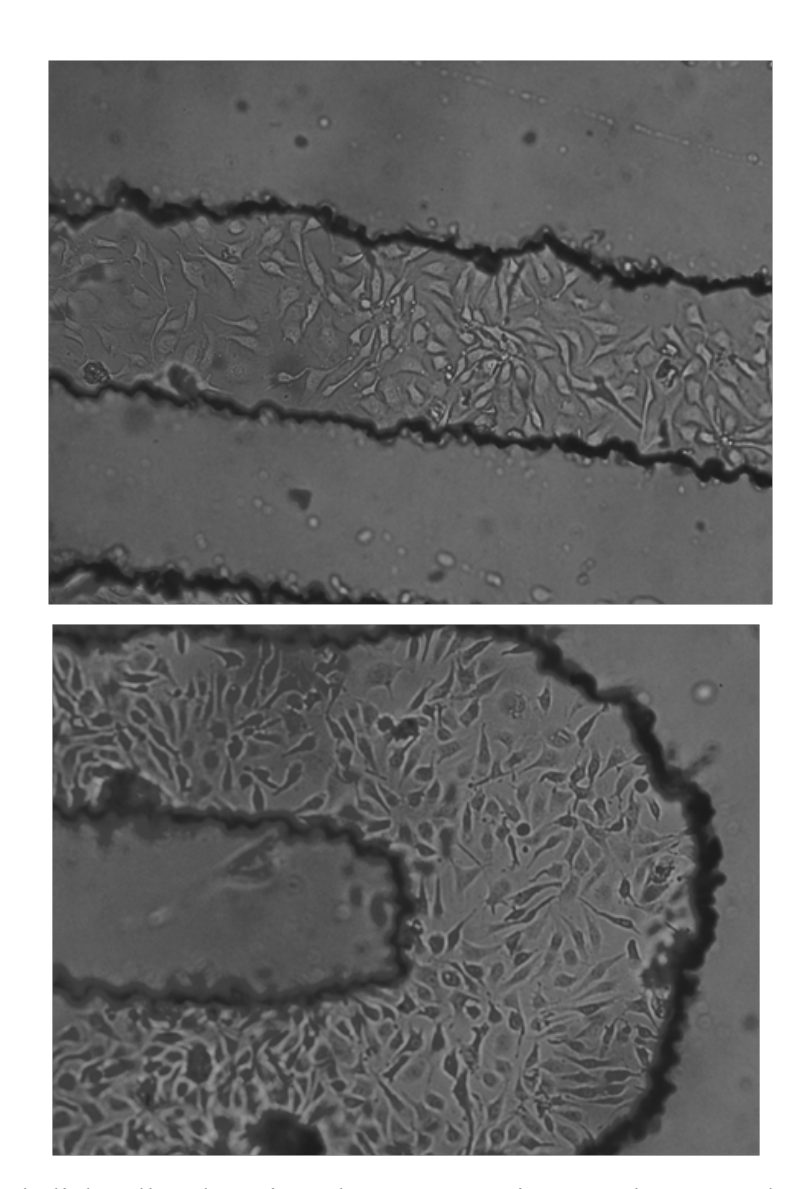


Figure 5.3: Endothelial Cell Culture in Polystyrene Device: A polystyrene device containing serpentine features is fabricated as described above. The channels are treated with 100 μ g/mL fibronectin for 3 hours, and then a cell solution obtained in the same manner as described in chapter 3 is pumped into the channels. The channels are re-seeded with the cell solution after 1 hour, and then media changed every hour for six hours.

a high throughput screening tool for compounds targeting the ATP mediated NO release mechanism.

Endothelial cell culture has been performed on these devices within serpentine channels that are arranged in the same geometry as a well plate as shown in figure 5.3. Cells are similar in appearance as those in a culture flask as shown in chapter 3, and studies are currently underway which are attempting to observe the cell-cell communication described above. Furthermore, because polystyrene is not oxygen permeable to the extent of PDMS, these polystyrene devices may also be applied to the oxygen sensor described in chapter 4.

5.4.2 PK/PD studies

In several conclusions throughout this dissertation it has been mentioned that the technology developed within can be utilized for drug screening applications. An important step in the process from drug candidate to approved medications however is the pharmacokinetics (PK) of a drug, the study of the amount of drug in a patient as a function of time, and the pharmacodynamics (PD) of a drug, which is the study of the effect of the drug on the body. These studies are currently conducted by in large-volume cell culture systems, or with *in vivo* models, both of which require a large quantity of material to conduct the studies.

With the ability to provide cellular function information, such as that shown in chapters 2 and 3, in a high throughput manner, it is plausible these microfluidic models could be used for PD studies. However because our models also incorporate a bloodstream mimic, the PK study investigating transport of a drug compound from a bloodstream, across an endothelium barrier, and perhaps to another cell type can be investigated in a high throughput manner, with the advantage of lower volume consumption with the microfluidic systems.

A first step however in the utilization of these models was to investigate the ability of several common pharmaceutical agents to partition across the polycarbonate membrane

system described in chapter 2. To perform these studies, various solutions of drug compounds were prepared, pumped through the microfluidic device described in chapter 2, and the well contents analyzed by quantitative LC-MS-MS for drug concentration.

5.4.2.2 Methods

Five compounds were investigated using the microfluidic device as described in chapter 2, and stock solutions are prepared. Levofloxacin and linezolid solutions are prepared by dissolving in each in water. Clopidogrel is dissolved in 0.1 M HCl, raltegravir is dissolved in DMSO, and efavirenz in 50% methanol/water. Standards between 1.0 and 7.0 μ M were prepared in PSS without bovine serum albumin and pumped through the microfluidic device for varying lengths of time. Analysis of the well contents after pumping was performed by removing 9.0 μ L from the well and dissolving it in 70 μ L of cold acetonitrile which contains ciprofloxacin as an internal standard. Any protein present in the solution would then precipitate out, and can be removed by centrifugation at 500 g for 10 minutes. The supernatant was then transferred to a polycarbonate PCR plate, and sealed with a RapidEPS seal by Bio Chromato (Fujisawa, Japan).

HPLC separation is then performed on a Supelco Ascentis Express C18 column that was 3 cm in length, has an ID of 2.1 mm, and was packed with 2.7 μ m particles (Sigma Aldrich). 10 μ L of the acetonitrile- dissolved sample is injected onto the column using an autosampler. LC separation was performed with the gradient described in figure 5.4

MS/MS analysis is performed first with electrospray ionization, then selection of a parent ion from each compound, which is then fragmented in a collision cell, and a daughter ion detected in a Quattro Micro mass spectrometer, using a process known as multiple

Compound	Parent Ion (Da)	Daughter Ion (Da)	Retention Time (min)
Linezolid	338.1	296.1	1.1
Levofloxacin	362.1	261.1	0.93
Clopidogrel	322.08	155	1.39
Efavirenz	316	168.1	1.37
Raltegravir	445.1	108.9	1.27
Ciprofloxacin (ISTD)	332.2	231	0.95

Table 5.1: Retention Time and Target Ions for MS/MS Analysis: Shown above are the target ions for analysis and the retention times on the described chromatographic system. Each compound is ionized and injected to the collision cell with an optimized ESI cone voltage and collisional energy. Internal standard calibration is performed to obtain concentrations in the wells.

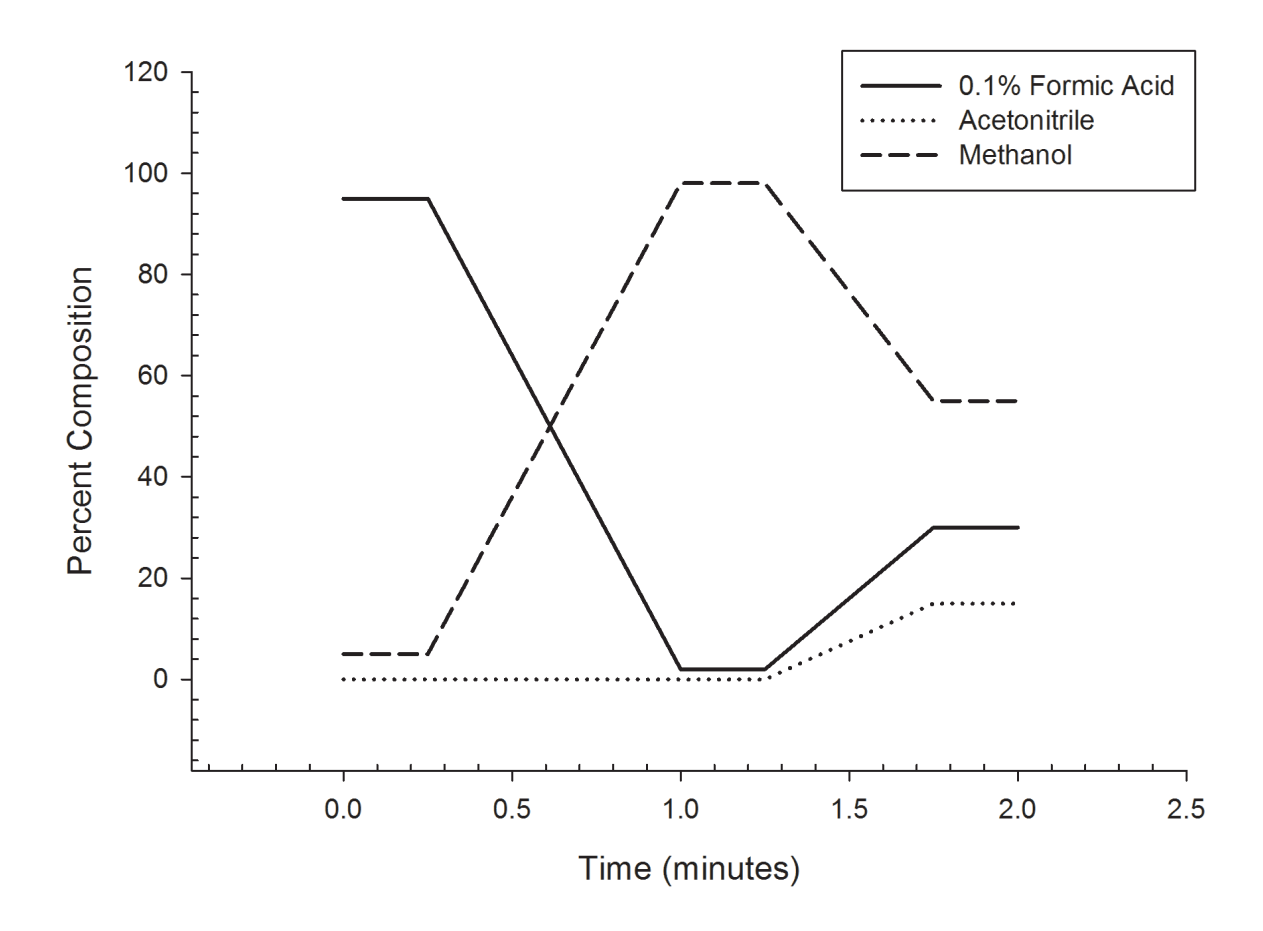


Figure 5.4: LC Gradient for LC-MS Analysis: This gradient was used in the chromatographic separation of the pharmaceutical compounds in the analysis investigating the compound transport across the polycarbonate membrane in the microfluidic device.

reaction monitoring (MRM). Table 5.1 summarizes the parent ions, daughter ions, and retention times for the compounds using the described system.

Linear calibration can be obtained using an internal standard method taking the ratio of the peak area of the sample compound to that of the internal standard. Without the use of specifically labeled internal standards, 5-10% RSDs of standards can be obtained with this method. This chromatographic system produces a linear range from a detection limit around 20 nM to an upper limit of 2000 nM for each compound, before column overloading (indicated by peak tailing) is observed in the chromatography. Samples are diluted to remain within this range when needed.

5.4.2.3 Results

Initially it was desirable to see if the compounds of interest are absorbed by PDMS, as has been considered. To investigate this possibility, PDMS well-based devices were prepared with and without polycarbonate membranes, and standards pipetted into these wells, to determine if the compounds are absorbed by the PDMS or the polycarbonate membrane. As shown in figures 5.5 through 5.10, linezolid, levofloxacin and raltegravir absorb minimally into PDMS, whereas clopidogrel and efavirenz absorb almost completely into PDMS. No difference is observed in any compound between the signal observed with and without the polycarbonate membrane, suggesting the polycarbonate is not responsible for this response.

A significant limitation of PDMS as a material for fabricating microfluidic systems is shown in figures 5.5 through 5.9; certain compounds will partition into it. In an attempt to reduce this effect, the devices were coated with bovine serum albumin (BSA), and were attempted here. However, no statistical difference was observed in the presence of BSA.

Efavirenz

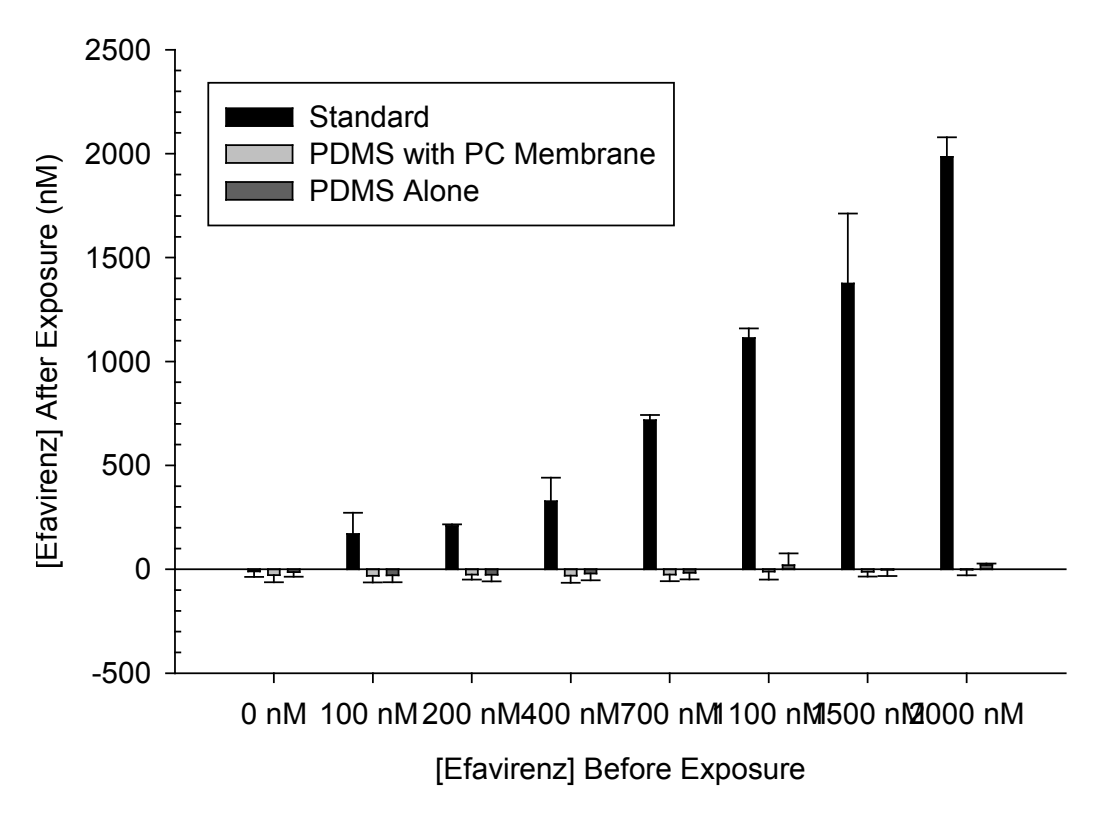


Figure 5.6: Efavirenz Absorbs Completely into PDMS: Shown here, Efavirenz absorbs completely into PDMS as none is detected in the wells after an incubation time of one hour. (n=4 devices, error bars area SD)

Linezolid

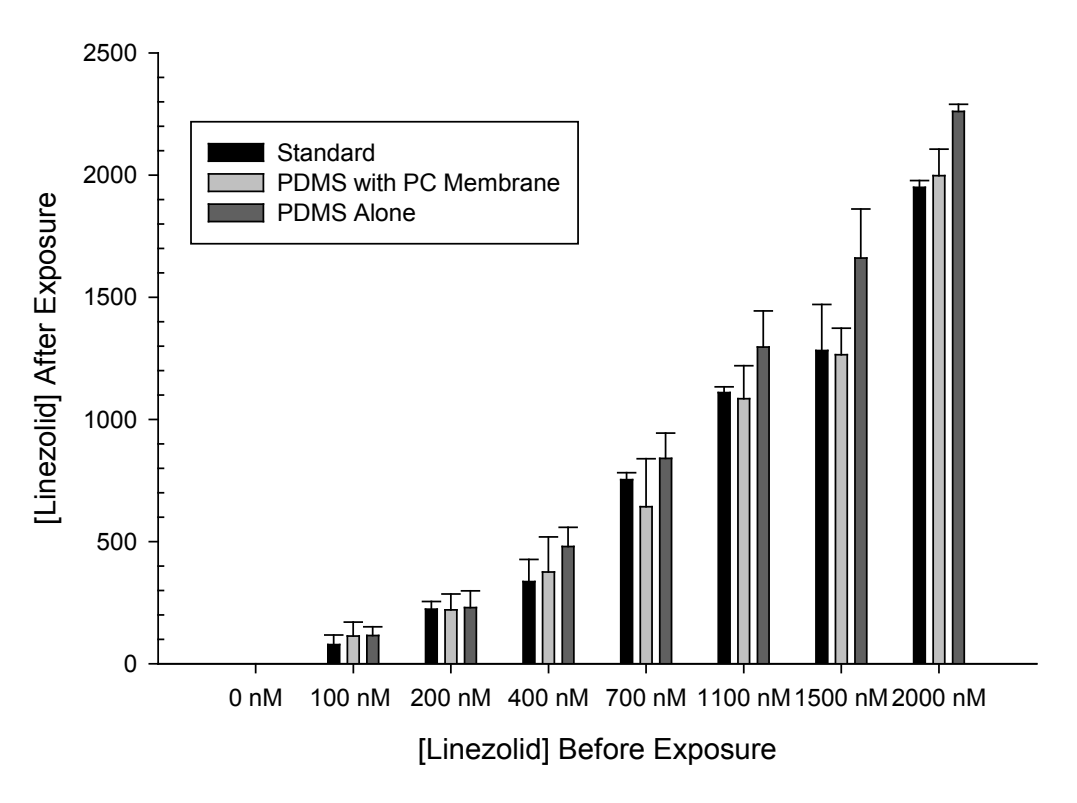


Figure 5.7: Linezolid Does Not Absorb Into PDMS. Shown here, linezolid does not absorb into PDMS. (n=4 devices, error bars area SD)

Levofloxacin

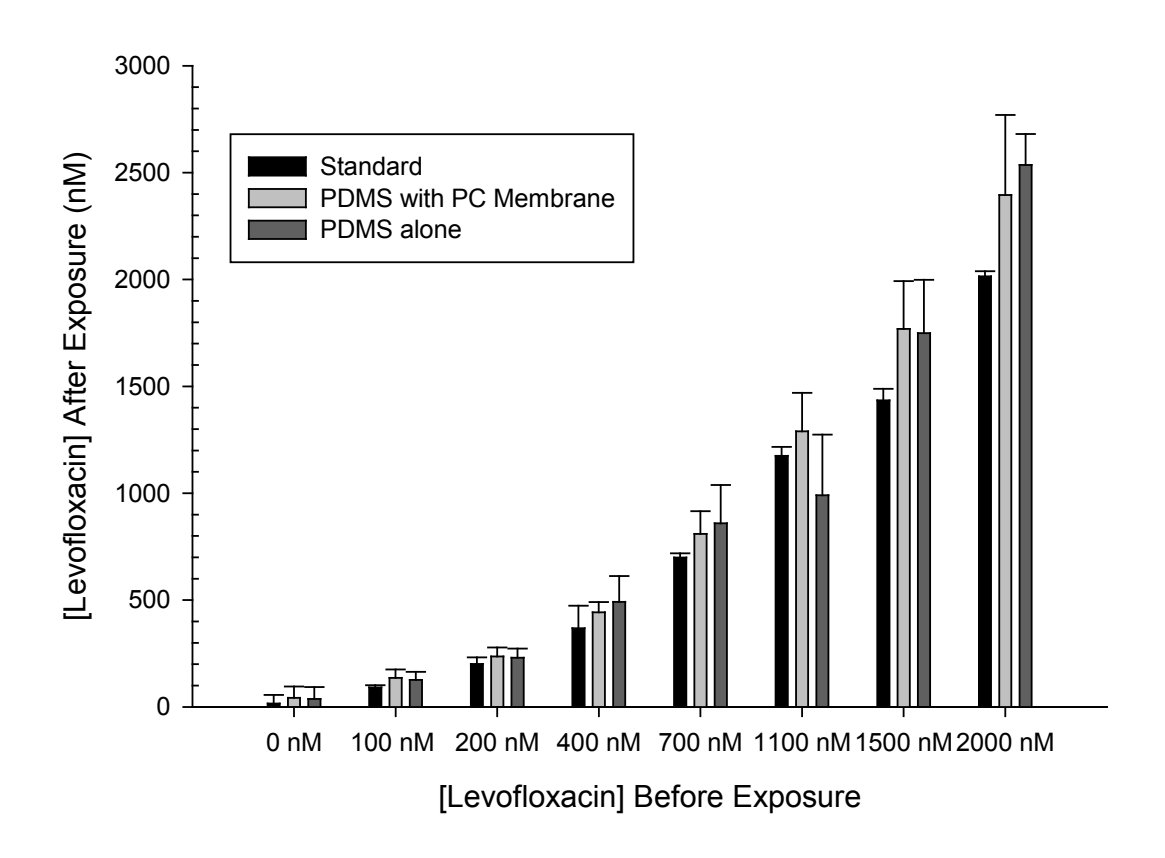


Figure 5.8: Levofloxacin Absorption into PDMS: Shown here, levofloxacin partitions minimally into PDMS. (n=4 devices, error bars area SD)

Therefore, the more promising solution would be to switch from PDMS devices, to those of another material, such as polystyrene as described above.

Of the remaining compounds that did not dissolve in the PDMS, it was still desirable to investigate the properties of their transport across the membrane by changing the length of time the solution was pumped, and the pore diameter of the polycarbonate track etched membrane. These experiments, the results of which are summarized in figure 5.9 through 5.12, show more compound is transported across the membrane for longer flow times, and for wider pore diameters, as would be expected.

These results suggest that while PDMS devices do allow for the potential investigation of some drug compounds in PK/PD studies, there are certain compounds which will not be able to be used for these investigations.

Current attempts to mediate this require moving from PDMS to polystyrene with these devices, but there is a challenge in that without the adhesive nature of PDMS to the polycarbonate membranes, it has been difficult to get the devices to seal properly. This has been mediated by obtaining polyester track etched membranes, fabricated in the same manner, but having the advantage of being solvent resistant. Therefore, the membranes can be soaked in toluene, allowed to dry briefly, and placed over polystyrene channels. This causes the membrane to adhere to the polystyrene.

A top well layer, fabricated in a similar pattern as that shown in chapter 2, can then be fabricated from a Petri dish, by drilling. This is then thermally sealed to the polystyrene channel layer with the polyester membrane adhered to it, with slight pressure in a convection oven at 100 °C. 1/16" coned ports (IDEX Health and Science/Upchurch Scientific) are then adhered to the device using JB Weld. Attempts at characterizing the feasibility of these devices are ongoing.

Linezolid 0.2 Micron Pore Diameter

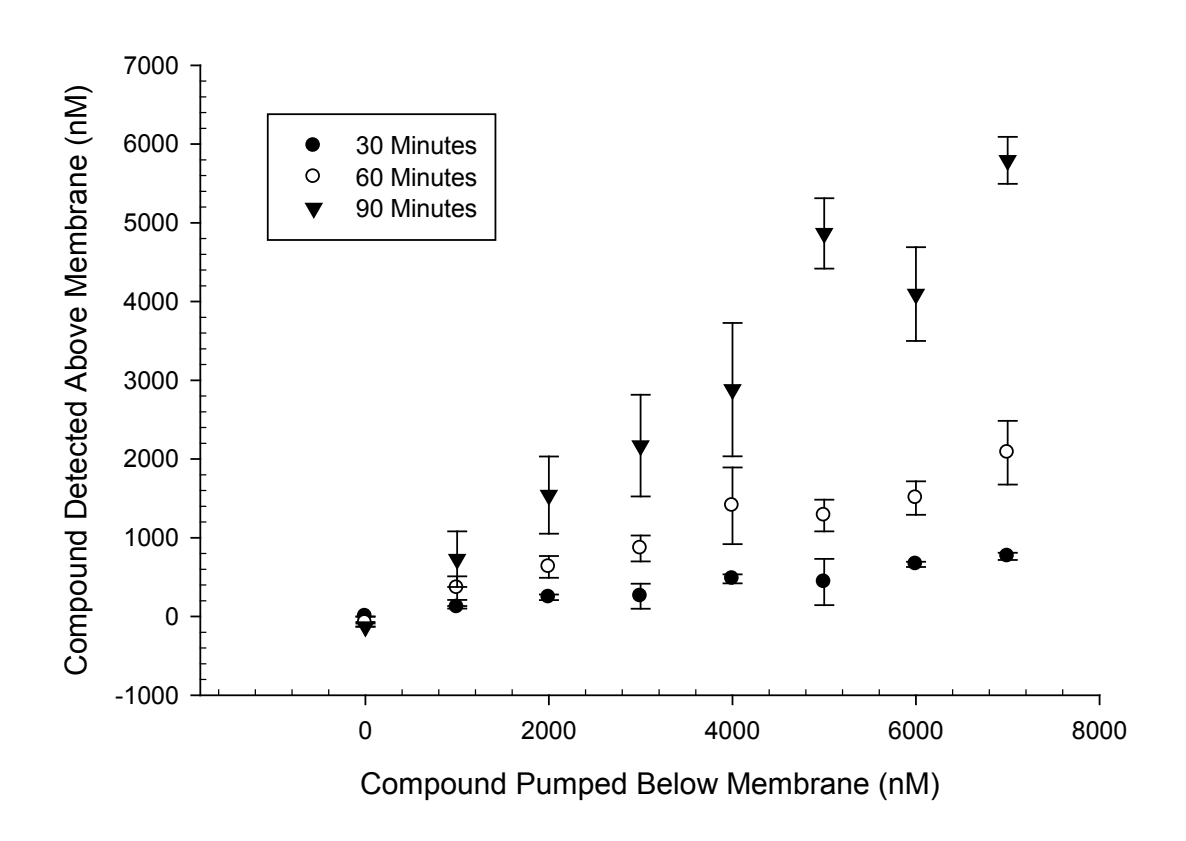


Figure 5.9: Linezolid Transport Across Membrane: As flow time increases, a greater concentration of linezolid can be detected above the membrane. (n=4 devices, error bars are standard deviation)

Raltegravir 0.2 micron pore diameter

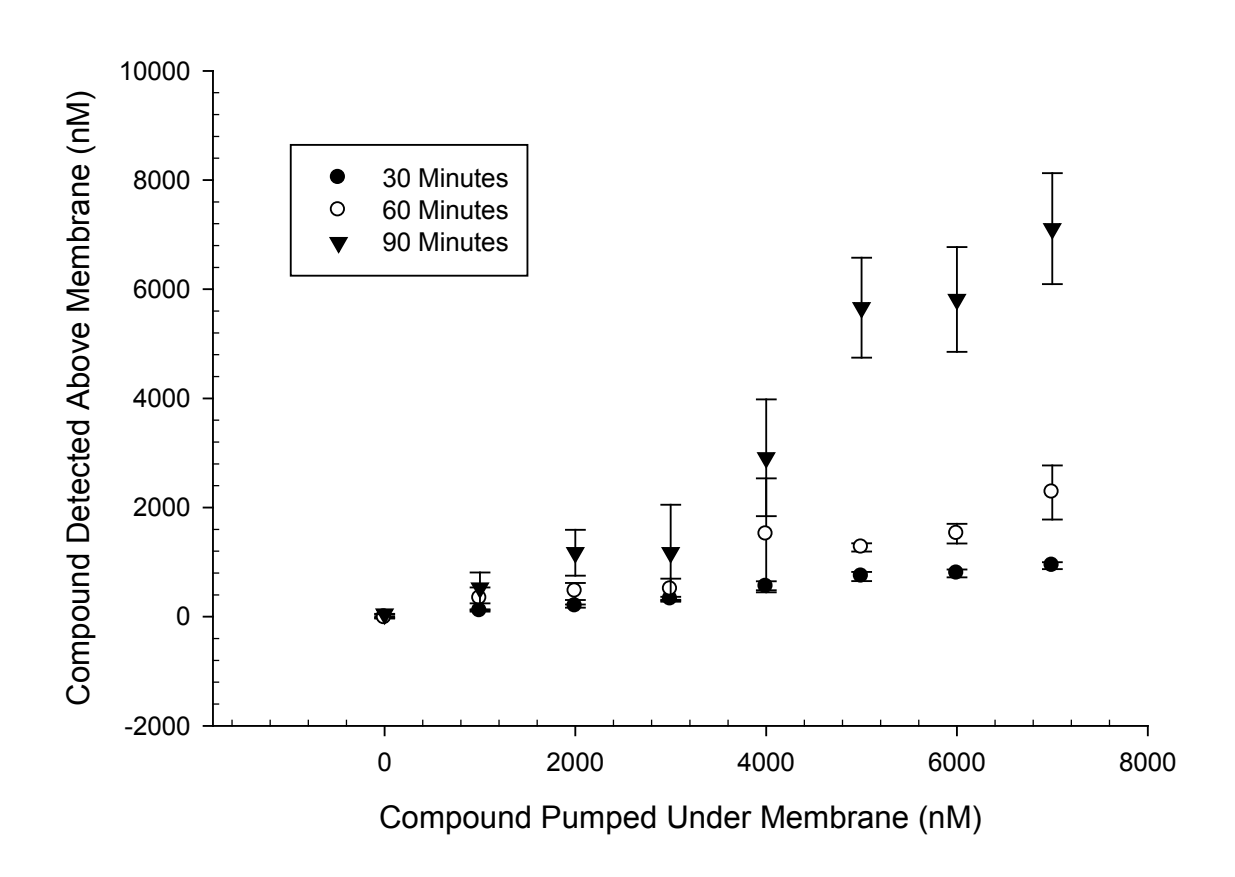


Figure 5.10: Raltegravir Transport Across Membrane: As flow time increases, a greater concentration of Raltegravir can be detected above the membrane. (n=4 devices, error bars are standard deviation)

Levofloxacin 0.2 Micron Pore Diameter

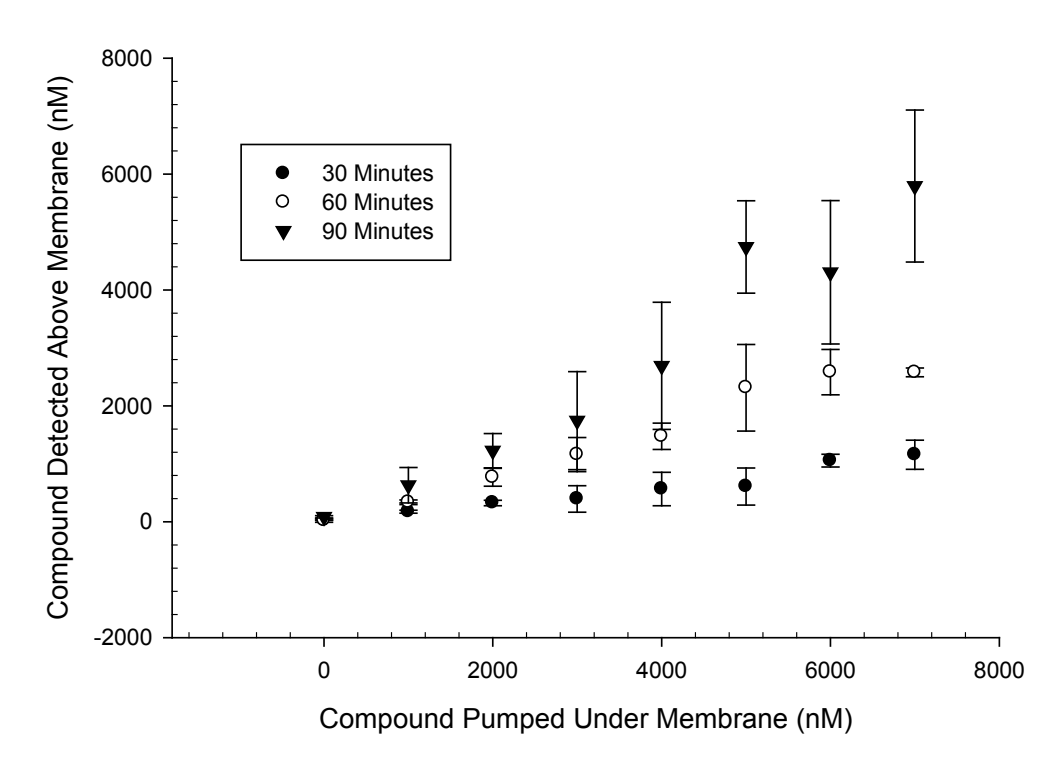


Figure 5.11: Raltegravir Transport Across Membrane: As flow time increases, a greater concentration of raltegravir can be detected above the membrane. (n=4 devices, error bars are standard deviation)

Clopidogrel 0.2 Micron Pore Diameter

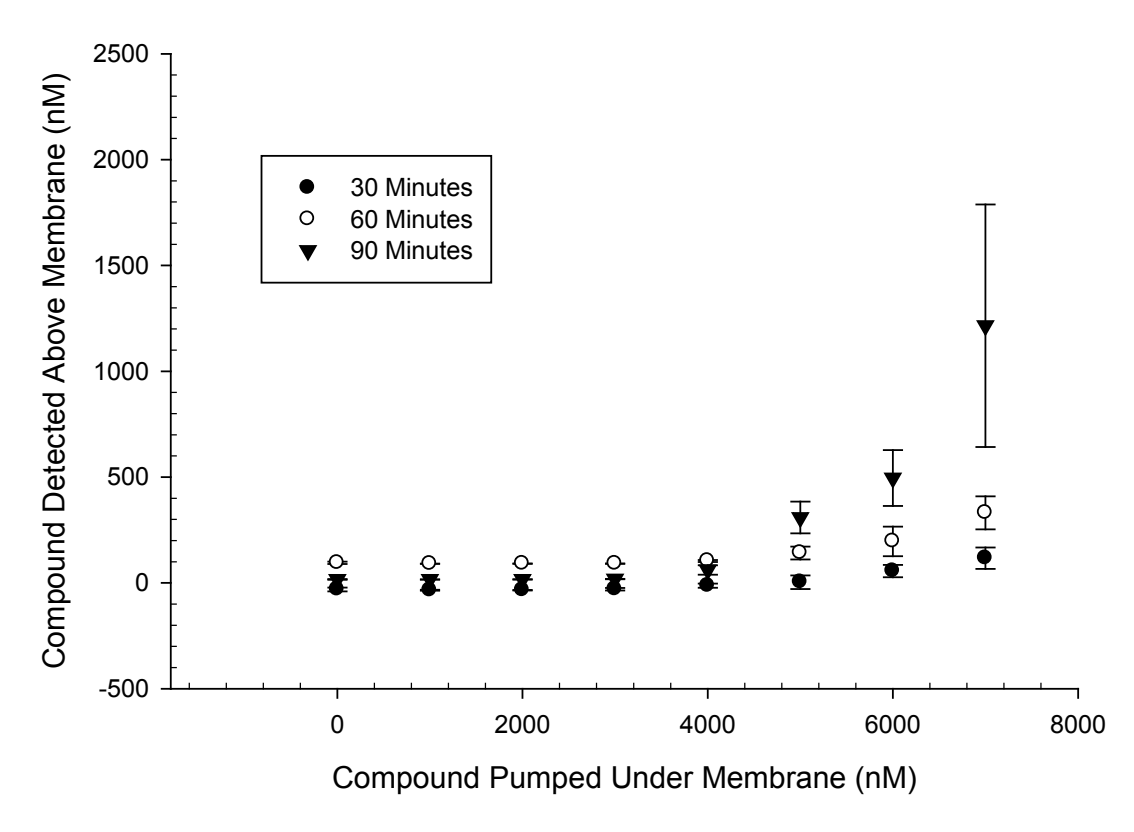


Figure 5.12: Clopidogrel Transport Across Membrane: Little transport of clopidogrel is observed until higher concentrations are pumped underneath the membrane, or longer flow times are used. This suggests the PDMS becomes saturated with clopidogrel, allowing it to flow through the membrane instead of absorbing. (n=4 devices, error bars are standard deviation)

REFERENCES

REFERENCES

- 1. Kim, W.-S.; Ye, X.; Rubakhin, S. S.; Sweedler, J. V., *Analytical Chemistry* **2006**, 78 (6), 1859-1865.
- 2. Ku, C.-J.; Karunarathne, W.; Kenyon, S.; Root, P.; Spence, D., *Analytical Chemistry* **2007**, *79* (6), 2421-2426.
- 3. Mainz, E. R.; Gunasekara, D. B.; Caruso, G.; Jensen, D. T.; Hulvey, M. K.; da Silva, J. A. F.; Metto, E. C.; Culbertson, A. H.; Culbertson, C. T.; Lunte, S. M., *Anal Methods-Uk* **2012**, *4* (2), 414-420.
- 4. Oblak, T. D.; Root, P.; Spence, D. M., Analytical Chemistry 2006, 78 (9), 3193-3197.
- 5. Sprague, R., S.; Olearczyk Jeffrey, J.; Spence Dana, M.; Stephenson Alan, H.; Sprung Robert, W.; Lonigro Andrew, J., *Am J Physiol Heart Circ Physiol* **2003**, *285* (2), H693-700.
- 6. Spence, D., M.; Torrence Nicholas, J.; Kovarik Michelle, L.; Martin, R. S., *The Analyst* **2004**, *129* (11), 995-1000.
- 7. Collins, S. L.; Edwards, M. A.; Kantak, K. M., *Psychopharmacology* **2001**, *154* (3), 261-273.
- 8. Tolan, N. V.; Genes, L. I.; Subasinghe, W.; Raththagala, M.; Spence, D. M., *Analytical Chemistry* **2009**, *81* (8), 3102-3108.
- 9. Stamler, J. S.; Jia, L.; Eu, J. P.; McMahon, T. J.; Demchenko, I. T.; Bonaventura, J.; Gernert, K.; Piantadosi, C. A., *Science* **1997**, *276* (5321), 2034-2037.
- 10. Gladwin, M. T.; Cosby, K.; Partovi, K.; Martyr, S.; Reiter, C.; Zalos, G.; Schechter, A. N.; Cannon, R. O., *Circulation* **2003**, *108* (17), 20-21.
- 11. Dietrich, H. H., Ellsworth, Mary L., Sprague, Randy S., Dacey, Ralph G. jr., *American Journal of Physiology-Heart Circ Physiol* **2000**, *278*, H1294-1298.
- 12. Kelm, M.; Feelisch, M.; Deussen, A.; Schrader, J.; Strauer, B. E., *Journal of Cardiovascular Pharmacology* **1991**, *17*, S95-S99.
- 13. Hakim, T. S.; Sugimori, K.; Camporesi, E. M.; Anderson, G., *Physiological Measurement* **1996**, *17* (4), 267-277.
- 14. Cosby, K.; Partovi, K. S.; Crawford, J. H.; Patel, R. P.; Reiter, C. D.; Martyr, S.; Yang, B. K.; Waclawiw, M. A.; Zalos, G.; Xu, X. L.; Huang, K. T.; Shields, H.; Kim-Shapiro, D. B.; Schechter, A. N.; Cannon, R. O.; Gladwin, M. T., *Nature Medicine* **2003**, *9* (12), 1498-1505.

- 15. Garcia, J. I.; Seabra, A. B.; Kennedy, R.; English, A. M., *Journal of Inorganic Biochemistry* **2010**, *104* (3), 289-296.
- 16. Cao, Z. L.; Bell, J. B.; Mohanty, J. G.; Nagababu, E.; Rifkind, J. M., *American Journal of Physiology-Heart and Circulatory Physiology* **2009**, 297 (4), H1494-H1503.
- 17. Faris, A.; Spence, D. M., *Analyst (Cambridge, U. K.)* **2008,** *133* (5), 678-682.
- 18. Meyer, J. A.; Froelich, J. M.; Reid, G. E.; Karunarathne, W. K. A.; Spence, D. M., *Diabetologia* **2008**, *51* (1), 175-82.
- 19. Ku, C. J.; Oblak, T. D.; Spence, D. M., *Analytical Chemistry* **2008**, *80* (19), 7543-7548.
- 20. Karunarathne, W.; Ku, C. J.; Spence, D. M., *Integr Biol* **2009**, *1* (11-12), 655-663.
- 21. Freedman, J. E.; Loscalzo, J.; Barnard, M. R.; Alpert, C.; Keaney, J. F.; Michelson, A. D., *The Journal of clinical investigation* **1997**, *100* (2), 350-6.
- 22. Mizutani, F.; Yabuki, S.; Sawaguchi, T.; Hirata, Y.; Sato, Y.; Iijima, S., Sensors and Actuators B-Chemical 2001, 76 (1-3), 489-493.
- 23. Vollmer, A. P.; Probstein, R. F.; Gilbert, R.; Thorsen, T., *Lab on a Chip* **2005**, *5* (10), 1059-1066.
- 24. Huh, D.; Matthews, B. D.; Mammoto, A.; Montoya-Zavala, M.; Hsin, H. Y.; Ingber, D. E., *Science* **2010**, *328* (5986), 1662-1668.
- 25. Huh, D.; Hamilton, G. A.; Ingber, D. E., *Trends Cell Biol* **2011**, *21* (12), 745-754.
- 26. Vogel, P. A.; Halpin, S. T.; Martin, R. S.; Spence, D. M., *Analytical Chemistry* **2011**, 83 (11), 4296-4301.
- 27. Choi, H.-G.; Boccazzi, P.; Sinskey, A. J.; Laibinis, P. E.; Jensen, K. F., *Polymer Preprints (American Chemical Society, Division of Polymer Chemistry)* **2004,** 45 (1), 106-107.
- 28. Park, D. S. W.; Hupert, M. L.; Witek, M. A.; You, B. H.; Datta, P.; Guy, J.; Lee, J. B.; Soper, S. A.; Nikitopoulos, D. E.; Murphy, M. C., *Biomedical Microdevices* **2008**, *10* (1), 21-33.
- 29. Ma, S. H.; Lepak, L. A.; Hussain, R. J.; Shain, W.; Shuler, M. L., *Lab Chip FIELD Full Journal Title:Lab on a Chip* **2005**, *5* (1), 74-85.
- 30. Gawron, A. J.; Martin, R. S.; Lunte, S. M., Eur. J. Pharm. Sci. **2001**, 14, 1-12.
- 31. Berthier, E.; Young, E. W.; Beebe, D., *Lab Chip* **2012**, *12* (7), 1224-37.
- 32. Duffy, D. C.; McDonald, J. C.; Schueller, O. J. A.; Whitesides, G. M., Analytical

Chemistry 1998, 70 (23), 4974-4984.

- 33. Shen, Y. K.; Lin, J. D.; Hong, R. H., *Polymer Engineering and Science* **2009**, 49 (1), 104-114.
- 34. Kim, D. S.; Lee, S. H.; Ahn, C. H.; Lee, J. Y.; Kwon, T. H., *Lab Chip* **2006**, *6* (6), 794-802.